FRACTIONAL ORDER FILTERING APPROACH TOWARDS ECG NON-STATIONARY BIOMEDICAL SIGNAL PROCESSING

Thesis Submitted

in the fulfillment of the requirements for the award of the degree

of

DOCTOR OF PHILOSOPHY

by

AMANDEEP KAUR

Registration No- 901706003

Under the supervision of

DR. SANJAY KUMAR	**DR. ALPANA AGARWAL**	**DR. RAVINDER AGARWAL**
ASSOCIATE PROFESSOR	PROFESSOR	PROFESSOR
ECED	ECED	EIED

DEPARTMENT OF ELECTRONICS AND COMMUNICATION ENGINEERING

THAPAR INSTITUTE OF ENGINEERING &TECHNOLOGY

Patiala-147004

April, 2024

DECLARATION

I hereby declare that the work which is being presented in thesis entitled "**Fractional order Filtering approach towards ECG Non-Stationary Biomedical Signal Processing**", in the partial fulfillment of the requirements for the award of the degree of **Doctor of Philosophy** submitted in the *Department of Electronics and Communication Engineering, Thapar Institute of Engineering and Technology, Patiala*, is an authentic record of my own research work carried out during a period of July, 2017 to February, 2023, under the supervision of Dr. Sanjay Kumar (Associate Professor, ECED), Dr. Alpana Agarwal (Professor, ECED) and Dr. Ravinder Agarwal (Professor, EIED), Thapar Institute of Engineering and Technology, Patiala. The matter presented in the thesis has not been submitted in part or full to any other University or Institute for the award of any degree in India or abroad.

Dated:

Amandeep Kaur

(901706003)

It is certified that the above statement made by the candidate is correct to the best of my knowledge and belief.

Dated:

Dr. Sanjay Kumar (Supervisor)	Dr. Alpana Agarwal (Supervisor)	Dr. Ravinder Agarwal (Supervisor)

CERTIFICATE

It is hereby certified that the thesis entitled "**Fractional order Filtering approach towards ECG Non-Stationary Biomedical Signal Processing**", submitted by Ms. Amandeep Kaur, a research scholar in the *Department of Electronics and Communication Engineering, Thapar Institute of Engineering and Technology, Patiala*, for the award of the degree of **Doctor of Philosophy**, is a record of bonafide research work carried out by her under our supervision and guidance. She has fulfilled the requirements for the submission of this thesis which has reached the requisite standard. The results embodied in this thesis have not been submitted to any other University or Institute for the award of any degree or diploma.

Dated:

Dr. Sanjay Kumar	**Dr. Alpana Agarwal**	**Dr. Ravinder Agarwal**
Associate Professor, ECED	Professor, ECED	Professor, EIED
Thapar Institute of Engineering and Technology, Patiala, Punjab-147004, India.	Thapar Institute of Engineering and Technology, Patiala, Punjab-147004, India.	Thapar Institute of Engineering and Technology, Patiala, Punjab-147004, India.

ACKNOWLEDGEMENTS

It gives me great pleasure to thank all the people who helped me directly or indirectly in completion of this dissertation. I want to begin by bowing before the Almighty God who made me capable in every aspect of life. I express my heartfelt gratitude to Him for always showering His blessings on me in all walks of my life.

My teachers, Dr. Sanjay Kumar, Dr. Alpana Agarwal and Dr. Ravinder Agarwal, who served as my supervisors, deserve my heartfelt gratitude for their sincere advice, support, and prodding to move forward. I am thankful to Dr. Sanjay Kumar for teaching me some of the best qualities that one needs in the course of life. He instilled the quality of discipline, presentation, writing research papers, to make eye-catching presentation, to be honest to oneself and to the profession. I am also grateful to him for enriching my spiritual beliefs that helped me get through difficult situations in life.

I would like to express my heart full indebtedness towards Dr. Ravinder Agarwal for always encouraging, motivating me and providing me with valuable feedback during our meetings.

I am also thankful to Dr. Alpana Agarwal, Professor, Head of ECED, for providing me with adequate infrastructure for carrying out the research work effectively. I would like to express my sincere thankfulness to my doctoral committee members Dr. Vinay Kumar, Dr. Manu Bansal and Dr. Shailendra Tiwari for always providing me with valuable feedback during the course of my PhD. I am thankful to ECED non-teaching staff members Mr. Vinod Bhatt, Mr. Vijay, and Mrs. Ramandeep Kaur for helping me with all the clerical work during the course. I am also thankful to Mr. Amanpreet Singh for his help in my course.

The entire course of this study would not have been completed without the love, support and encouragement of my family. I will be always be deeply indebted to my parents for raising me, believing in me, allowing me to do things in my way and

supporting me in every aspect of my life and prayed for my wellness every now and then. I am immensely proud to have younger brother Jaswinder Singh who helped me get through difficult times by listening to me and motivating me whenever needed.

During my PhD journey, I was blessed with my soulmate Mohandeep Singh Sidhu who has motivated me in this journey and helped me deal every situation with patience. I express my heartful gratitude to him for motivating me to keep my spirits high even in the hardest of the times. He believed in me more than I did and helped me in achieving various milestones in my research. He has always been my biggest cheerleader in every part of my success. This course of study would not have been possible without his support, guidance, and motivation.

I would also like to thank my best friend Gulshanpreet Kaur Josan and Sandeep Kaur for their unconditional care and support in every aspect of my life and career. I am grateful to my friends Ms. Aditi Bajaj and Ms. Anmol Gupta for their relentless support technically as well as emotionally who were there with me in my hardest of times and also, enjoyed every milestone together with me. I am grateful for the times I spent laughing and crying with my friends Ms. Aditi Bajaj, Ms. Anmol Gupta, Ms. Deepika Singh, Dr. Abhinav, Mr. Ankush and Mr. Ishan Chawla during the course of my study. I owe a deep sense of gratitude towards Ms. Anjana Bhatia and Dr. Bahl for always motivating and providing us with life lessons and make me feel like home.

Lastly, I would like to thank my parents and my parents-in-laws who stood by my side through every thick and thin of life I owe my sincere gratitude to them for helping me believe in my own self. I would also like to express my gratitude towards everyone who helped me in one way or another.

I would also like to acknowledge the Department of Science and Technology (DST) for making me the part of the research project sanctioned by Science and Engineering Research Board (SERB) and providing all the required support.

Amandeep Kaur

ABSTRACT

Due to the increase of desk-bound activities and sedentary lifestyle, cardiac diseases are increasing at an alarming rate especially in developing countries like India. According to the WHO data, one in four Indians died, because of cardiovascular diseases. Electrocardiogram (ECG) is the signal originated due to human heart activities. It is a record of the electrical commotion caused by depolarization and repolarization of the atria and ventricles of the heart muscles. ECGs are used to find anomalies in the heart beat which may be indicative of various cardiovascular diseases. Accurately detecting the anomalies in an ECG is the relevant issue of the medical field. Each beat of an ECG is composed of several pulses of different bandwidths (known as waves P, Q, R, S and T), and an iso-electric period which corresponds to the lapse of time between two consecutive beats. As the behaviour of an ECG waveform changes with time, so it is non-stationary, pseudo periodic in nature.

ECG is a powerful tool in determining the health and functioning of the heart. Faster detection and diagnosis of the cardiovascular conditions would aid physicians to provide appropriate treatment to the patients. Proper processing of an ECG signal and its accurate detection is very much essential as it determines the condition of the heart. The analysis of an ECG signal requires the information both in time and frequency, for clinical diagnosis. The non-stationarity of an ECG is often corrupted by low and high frequency noise components like power line interference (PLI), baseline wander, electromyogram, motion artifacts, etc. These different artifacts affect the morphology of the ECG waveform, thus making its analysis a difficult job.

There are many digital filtering techniques which are used in its processing in order to perform this task on computer-aided diagnosis. Finite Impulse Response (FIR) has been extensively used for ECG filtering. However, there seems to be an improvement for designing filter based upon self-convolution window concept. Hence, initial research

work in this thesis aims at establishing a new filter based on Hamming window referred as Hamming Self-Convolution window (HSCW) to remove various artifacts in an ECG waveform and further authenticate the efficacy of the proposed design through simulation results as compared to conventional window-based methods, such as Hamming and Kaiser window.

In the last decades, considerable focus has been paid by research community on the study of fractional-order digital differentiator (FODD). The FODD is concerned with estimating the fractional order derivatives of a signal or an unknown signal from its noisy observed data. It finds usage in fractional order control systems, signal processing, chaos and fractals, electrical networks, electromagnetic field theory. In signal processing, FODD proves to be an important mathematical tool that can give more peculiar characteristics as compared to the integer-order differentiator. Moreover, it provides an extra degree of freedom which helps in optimizing the performance based upon traditional integer-order calculus. Based on the concept of fractional order differentiation, the fractional order digital differentiator (FODD) could be designed for suitable signal processing applications. Therefore, Riesz fractional-order digital differentiator (RFODD) is explored in this thesis in context of ECG signal denoising and R-peak detection. ECG waveforms are analysed by varying fractional-order RFODD and their performance is estimated. The simulation studies conducted on MIT-BIH arrhythmia database (MIT-BIH-AD) indicates the superiority of the proposed method against well-established state-of-the-art methods.

After establishing an efficient method based on RFODD for pre-processing of an ECG signal, further research work aims at virtual-based implementation of the proposed fractional-order filter. For this, a classification system that includes the acquisition and pre-processing of real-time ECG signals, feature extraction, and classification of ECG beats into normal (subjects who have never had any heart ailment history) and abnormal (subjects who have had heart ailment history) classes using adaptive K nearest neighbor (ADkNN). The various real-time ECG subjects' waveforms acquired are analyzed in the proposed research. After preliminary processing based on RFODD, features are extracted and classification is performed. The performance parameters like sensitivity, positive predictivity, and accuracy of ADkNN are calculated in the proposed method. From the simulation studies conducted, it is seen that the proposed method performed well in terms of sensitivity, accuracy, and positive predictivity of the classifier.

Furthermore, to make a proposed classification system more generalized, robust and include more number of ECG beats classes, it is extended to the classification of MIT-BIH-AD. It is used to classify ECG beats of MIT-BIH-AD into six categories. The traditional methods for arrhythmia classification mainly includes intra-patient criterion that may not befit the inter-patient criterion. The research carried out in the thesis focuses both on intra and inter-patient criteria for classification. The simulation studies conducted on MIT-BIH-AD for classification proves that the obtained results in both criteria have outperformed other methods in the literature and the proposed work exhibits better results for minority class of MITBIH-AD in both the scheme.

Hence, the study carried out in this thesis has unfolded significant advantages of self-convolution window, fractional-order calculus for ECG processing applications and classification of real-time subjects and MIT-BIH-AD. Hence, the study opens up a new paradigm of research to include more number of classes for real-time ECG classification.

LIST OF ABBREVIATIONS

10-FCV	:	10-Fold Cross-Validation
A	:	Atrial Premature Contraction Beats
acc	:	Accuracy
ADkNN	:	Adaptive k Nearest Neighbor
AV	:	Atrioventricular
bpm	:	Beats per Minute
BW	:	Baseline Wander
DWT	:	Discrete Wavelet Transform
ECG	:	Electrocardiogram
EEG	:	Electroencephalogram
EEMD	:	Ensemble Empirical Mode Decomposition
EMD	:	Empirical Mode Decomposition
Err	:	Error Rate
FIR	:	Finite Impulse Response
FN	:	False Negative
FOC	:	Fractional-order Calculus
FOD	:	Fractional-order Differentiator
FODD	:	Fractional-order Digital Differentiator
FP	:	False Positive
FS	:	Fibonacci Series
HMLW	:	Half Main Lobe Width
HR	:	Heart Rate
HSCW	:	Hamming Self-Convolution Window
HSCW-BPF	:	HSCW Band-pass Filter
HSCW-HPF	:	HSCW High-pass Filter
HSCW-LPF	:	HSCW Low-pass Filter

ICA	:	Independent Component Analysis
IMFs	:	Intrinsic Mode Functions
KNN		K-Nearest Neighbor
L	:	Left Bundle Branch Block Beats
LA	:	Left Atrium
LV	:	Left Ventricle
MI	:	Myocardial Infarction
MIT-BIH-AD	:	Massachusetts Institute of Technology-Beth Israel Hospital Arrhythmia Database
ms	:	milliseconds
MSE	:	Means Square Error
MSLL	:	Maximum Side Lobe Level
mV	:	millivolts
N	:	Normal Beats
NI	:	National Instruments
NI-DAQ	:	National Instruments Data Acquisition
P	:	Paced Beats
PCA	:	Principal Component Analysis
PCs	:	Principal Components
PLI	:	Power-line Interference
PPe	:	Positive Predictivity
PVCs	:	Premature Ventricular Contractions
R	:	Right Bundle Branch Block Beats
RA	:	Right Atrium
RFODD	:	Riesz Fractional-order Digital Differentiator
RL	:	Riemann–Liouville
RV	:	Right Ventricle
SA	:	Sino-Atrial
SCW	:	Self-Convolution Windows
SE	:	Shannon Energy
Sen	:	Sensitivity
SG	:	Savitzky–Golay
SLFOR	:	Side Lobe Roll-off Factor

SLL	:	Side Lobe Level
SNR	:	Signal to Noise Ratio
ST	:	Stockwell Transform
SVM	:	Support Vector Machine
TD	:	Time-Domain
TFD	:	Time-Frequency Domain
TN	:	True Negative
TP	:	True Positive
TSCW	:	Triangular Self-Convolution Window
V	:	Premature Ventricular Contraction
WHO	:	World Health Organization
WT	:	Wavelet Transform

LIST OF FIGURES

Figure 1.1	:	A typical ECG signal of a male subject aged 24 years	2
Figure 1.2	:	Human Heart	3
Figure 1.3	:	Excitation pulse propagation through the heart	4
Figure 1.4	:	Propagation of ECG wave	5
Figure 2.1	:	Flowchart of the research work carried out in thesis	23
Figure 3.1	:	Magnitude frequency responses of HSCW, Kaiser, and Hamming window-based function	28
Figure 3.2	:	Block diagram of the proposed system for the identification of R-peak	28
Figure 3.3	:	Magnitude responses of HSCW, Kaiser, and Hamming window-based low pass filter	29
Figure 3.4	:	Magnitude responses of HSCW, Kaiser, and Hamming window-based high pass filters	30
Figure 3.5	:	**(a)** ECG record no. 107 indicates a complete heart-block situation, empty circles indicate the R-peaks to be detected **(b)** output from HSCW-BPF filter **(c)** the output of HSCW-BPF is squared for better localization and filled circles depict the detected R-peaks.	32
Figure 3.6	:	**(a)** The R-peak to be detected is highlighted by an empty circle ECG (record 203) from MIT-BIH-AD that has changing QRS morphology and **(b)** the output of the HSCW-BPF filter **(c)** the output of HSCW-BPF is squared for better localization and filled circles depict the detected R-peaks.	33
Figure 3.7	:	**(a)** ECG record no. 222 from MIT-BIH-AD has baseline drift **(b)** the HSCW-BPF filter output **(c)** the output of HSCW-BPF is squared for better localization and filled circles depict the detected R-peaks.	33

Figure 3.8	:	Comparison of FN counts for various MIT-BIH-AD records for three window-based filters – Hamming, Kaiser, and the proposed method (HSCW-BPF)	37
Figure 3.9	:	Comparison of FP count for various records of MIT-BIH-AD for three window-based filters – Hamming, Kaiser, and the proposed method (HSCW-BPF)	38
Figure 3.10	:	Comparison of error rate (%) for records of MIT-BIH-AD for three window-based filters – Hamming, Kaiser, and the proposed method (HSCW-BPF)	38
Figure 4.1	:	Block representation of the proposed algorithm (here p is the fractional-order)	46
Figure 4.2	:	Flow chart of the *proposed* threshold technique for R-peak detection	49
Figure 4.3	:	ECG **Record no. 104** with burst noise at various fractional orders (p)	51
Figure 4.4	:	Zoomed plot of the encircled section of Figure 4.3	52
Figure 4.5	:	**(a)** ECG **record no. 107** indicating high T-peak amplitude **(b)** band-pass filtering **(c)** Riesz derivative **(d)** smooth ECG waveform.	55
Figure 4.6	:	**(a)** depicts burst noise in **record no. 200 (b)** Riesz derivative of the signal enhancing high-frequency QRS complex **(c)** smooth ECG waveform for R-peak detection	55
Figure 4.7	:	**(a)** Plot of ECG waveform of **record 116** depicting inverted R-peaks **(b)** Riesz derivative of the same waveform attenuating the low-frequency T peaks while enhancing the high-frequency inverted R-waves and **(c)** The averaging filter smooths the ECG waveform for detection of R-peaks	56
Figure 4.8	:	**(a) Record no. 203** representing the varying RR interval **(b)** Riesz-based derivative magnifying high-frequency QRS complex **(c)** The even ECG wave smoothened by a moving average filter for correct R-peaks delineation	57
Figure 4.9	:	**(a)** The other plot of **record no. 203** exhibits changing QRS morphology **(b)** Riesz derivative amplifies the high-	57

		frequency component irrespective of the morphology **(c)** smooth ECG beat of the same segment for efficient QRS detection	
Figure 4.10	:	**(a)** ECG record number 100 from MIT-BIH-AD **(b)** ECG record number 100 corrupted with EMG noise from MIT-BIH Noise Stress database **(c)** R-peak detected using the proposed method	60
Figure 4.11	:	Comparison of the number of records which has 100% sensitivity (Sen) and positive predictivity (PPe) from the literature with the *proposed method.*	61
Figure 4.12	:	Comparison of the number of records having a zero error rate in various algorithms from the literature with the *proposed method.*	61
Figure 5.1	:	ECG Electrodes	67
Figure 5.2a	:	AD8232 integrated signal conditioning block	67
Figure 5.2b	:	AD8232 Module	68
Figure 5.3	:	NI-myDAQ	69
Figure 5.4	:	LM 2596	69
Figure 5.5a	:	ECG signal acquisition process in the lab	70
Figure 5.5b	:	ECG signal acquisition	70
Figure 5.6	:	Block diagram of the proposed work	71
Figure 5.7	:	Riesz derivative of two distinct ECG beats	72
Figure 5.8a	:	ECG beat belonging to two class type	73
Figure 5.8b	:	Fibonacci series signal generated from Figure 5.8a	74
Figure 5.9	:	Features used for classification	75
Figure 5.10	:	(a) Real-time ECG waveform of subject 1 (b) band-pass filtering (c) Riesz-based derivative signal	79
Figure 5.11	:	(a) Real-time ECG signal of subject 2 (b) Riesz-based derivative signal	80
Figure 5.12	:	(a) ECG waveform of subject 3 (b) Riesz-based derivative signal	80
Figure 5.13	:	(a) ECG waveform of subject 3 (b) Riesz-based derivative signal	81

Figure 5.14	:	Two classes' FS Shannon energy in a boxplot diagram	82
Figure 5.15	:	Plot of classification rate verse number of principal Component	83
Figure 5.16	:	Classification Results	84
Figure 6.1	:	Block diagram for MIT-BIH-AD classification	91
Figure 6.2	:	Riesz derivative of six different type of ECG beats	92
Figure 6.3a	:	Six different type of ECG beats	94
Figure 6.3b	:	FS signal acquired from Figure 6.3a.	94
Figure 6.4	:	Boxplot representation of the Shannon energy of FS of six classes.	98
Figure 6.5	:	Plot indicating classification for intra-patient scheme versus the number of PC	100
Figure 6.6	:	Plot indicating classification rate for inter-patient scheme versus the number of PC	100
Figure 6.7	:	Classification evaluation parameters for intra-patient criterion	101
Figure 6.8	:	Classification evaluation parameters for inter-patient criterion.	102

LIST OF TABLES

Table 3.1	:	The impulse response of linear phase filters	30
Table 3.2	:	Experimental results of the proposed approach using HSCW-BPF	35
Table 3.3	:	Experimental studies using Hamming window function	36
Table 3.4	:	Experimental studies using Kaiser window function	36
Table 3.5	:	Comparison of the results with other well-known algorithms	39
Table 3.6	:	Comparison of the FN count for MIT-BIH-AD records	39
Table 3.7	:	Comparison of the FP count for MIT-BIH-AD	39
Table 4.1	:	Various parameter performances of different ECG records at different fractional orders (p)	53
Table 4.2	:	Test findings of the proposed approach	58
Table 4.3	:	Experimental results of EMG corrupted ECG records	60
Table 4.4	:	Comparison of various performance parameters results with the established algorithms	62
Table 4.5	:	Comparison of the total number of FN and FP	62
Table 5.1	:	Confusion Matrix	83
Table 5.2	:	ECG classification results for two classes	84
Table 5.3	:	Comparison with the literature	84
Table 6.1a	:	Dissection of beats for 10-FCV approach for intra-patient criterion	89
Table 6.1b	:	Dissection of beats based on 10-FCV approach for the inter-patient criterion	90
Table 6.1c	:	Dissection of ECG record for inter-patient criterion based on10-FCV approach for the training and testing set	90
Table 6.2	:	Features employed for arrhythmia classification	95

Table 6.3a	:	Calculation guide for N beat class's TP, TN, FN, and FP	98
Table 6.3b	:	Performance evaluation parameters for Classifier	99
Table 6.4	:	ECG arrhythmia classification results for six classes for intra-patient criterion	101
Table 6.5	:	ECG arrhythmia classification results for six classes for inter-patient criterion.	102
Table 6.6	:	Comparison of the ECG arrhythmia classification	104

TABLE OF CONTENTS

Declaration **iii**

Certificate **v**

Acknowledgements **vii**

Abstract **ix**

List of Abbreviations **xiii**

List of Figures **xvii**

List of Tables **xxi**

Table of Contents **xxiii**

1. Introduction **1**

1.1 Overview of Electrocardiogram (ECG) 1

1.2 Anatomy of the Human Heart 3

1.3 ECG Signal Processing 6

1.4 Contribution to Research Work 7

1.5 Organization of Thesis 9

2. Literature Survey **11**

2.1 Preliminaries of Digital Differentiators and Filters 11

2.1.1 ECG filtering based on digital differentiators and filters 12

2.2 Self Convolution Window (SCW) Method 13

2.2.1 Application of SCW 13

2.3 Preliminaries of Fractional-Order Calculus (FOC) 14

2.3.1 Riesz based fractional-order digital differentiator (RFODD) 16

2.3.2 Application of RFODD 16

2.4 LabVIEW-based Virtual Implementation of ECG signal Acquisition and Classification 16
2.5 Classification of ECG signal 18
2.6 Motivation 20
2.6.1 Research Gaps 21
2.6.2 Objectives 21
2.7 Research Methodology 22

3. ECG R-peak Detection employing Self Convolution Window-based Filters 25
3.1 Concept of Self Convolution Window 25
3.1.1 Hamming self-convolution window function (HSCW) 26
3.1.2 Comparison of magnitude frequency response of HSCW with classical windows 27
3.2 HSCW Band-Pass (HSCW-BPF) Approach 28
3.3 ECG R-peak Detection 31
3.3.1 Illustration of R-peak detection from MIT-BIH-AD 31
3.3.2 Quantitative analysis of MIT-BIH-AD 34
3.4 Comparison with state-of-the-art Methods 36
3.5 Conclusion 40

4. ECG R-peak Detection using Riesz Fractional-Order Digital Differentiator 43
4.1 Concept of Fractional-order Differentiator (FOD) 43
4.2 Riesz Fractional-Order Digital Differentiator (RFODD) 44
4.3 RFODD in ECG Signal Processing 46
4.3.1 Selection of optimal fractional-order parameter 50
4.3.2 Illustration of R-peak detection from MIT-BIH-AD 54
4.3.3 Quantitative analysis of MIT-BIH arrhythmia database 58
4.4 Performance of Proposed Method when EMG noise is added 59
4.5 Comparison with state-of-the-art methods 60
4.6 Conclusion 62

5. Virtual Instrumentation-based Implementation of the proposed Fractional-order Filter **65**

5.1 Selection of Subjects 66

5.2 Proposed Virtual Instrumentation-based Design for ECG Signal Acquisition 66

5.2.1 Electrodes 66

5.2.2 AD8232 Module 67

5.2.3 NI myDAQ Device 68

5.2.4 LM 2596 69

5.3 Data Acquisition 70

5.4 Feature Extraction of Real-time ECG Subjects 71

5.4.1 Approach I 72

5.4.2 Approach II 72

5.4.2.1 Fibonacci series (FS) 73

5.4.2.2 Additional time-domain features (Additional TD features) 74

5.4.2.3 Time-frequency domain features (TFD features) 74

5.4.3 Principal Component Analysis (PCA) 75

5.4.4 Adaptive K- Nearest Neighbor (ADkNN) 76

5.5 Results and Discussion 79

5.5.1 R-peak Detection 79

5.5.2 Classification of real-time ECG subjects 81

5.5.2.1 Feature selection using PCA 83

5.5.2.2 Classification results 83

5.6 Conclusions 85

6. ECG Beat Classification using MIT-BIH-AD **87**

6.1 Overview of Classification 88

6.2 Selection of ECG beats of MIT-BIH-AD for various Classes 88

6.3 Feature Extraction of ECG beat of MIT-BIH-AD 90

6.3.1 Approach I 92

6.3.2 Approach II 93

6.3.2.1 Fibonacci series 93

6.3.2.2 Additional time-domain (TD) characteris1tics 94
6.3.2.3 Time-frequency domain (TFD) characteristics 95
6.3.3 Principal Component Analysis (PCA) 96
6.3.4 Adaptive K nearest neighbor (ADkNN) 96
6.4 Results and Discussion 97
6.4.1 Feature selection using PCA 99
6.4.2 Simulation results for the intra-patient scheme 101
6.4.3 Simulation results for the inter-patient scheme 102
6.5 Comparison with state-of-the-art Methods 103
6.6 Conclusions 103

7. Conclusion and Future Work 107
7.1 Conclusion 107
7.2 Future Work 109
References 111
List of Publications 121

CHAPTER 1

INTRODUCTION

Science and everyday life cannot be and should not be separated. Science is about knowing: Engineering is about doing.

-Anonymous

WILLEM EINTHOVEN, a Dutch Physician, invented the clinical electrocardiograph 1903, ushering in a new age in medical diagnostic methods that included the introduction of electronics to the field of health care. Since then, computers and electronics have been essential parts of biomedical signal analysis systems. The Electrocardiogram (ECG) is arguably the most well-known, widely accepted, and often-used biological signal for the diagnosis and analysis of heart diseases by cardiologists. ECG signals have a wide array of applications in the biomedical domain in determining the functioning of the heart. This chapter reviews ECG in brief, the anatomy of the human heart, the basic pre-processing of ECG signal, its R-peak detection, feature extraction, and finally classification of ECG beats for diagnosis and prognosis of heart diseases by physicians.

1.1 Overview of Electrocardiogram (ECG)

The ECG is the electrical record of the contractile action of the human heart. It can be easily recorded with surface electrodes on the limbs or chest. The rhythm of the heart is determined in beats per minute (bpm) by counting the immediately recognizable waves. ECG signal is quasi-periodic in nature. It consists of a variety of waveforms, including P-wave, T-wave, the QRS complex, *etc.* A typical ECG signal is shown in Figure 1.1. P-wave is a small amplitude wave of 80 milliseconds (ms) duration followed by the PQ segment which is also 80 ms in length [1]. The QRS complex is a rapid signal pulse and has an R-peak with a large amplitude [2]. The general ST segment is flat and is usually 100-120 ms in length. T-wave appearing in the ECG signal after the ST segment is also

a low amplitude wave and extends over 120 to 160 ms [1]. These waves correspond to the depolarization and repolarization mechanism related to the conduction activity of the heart.

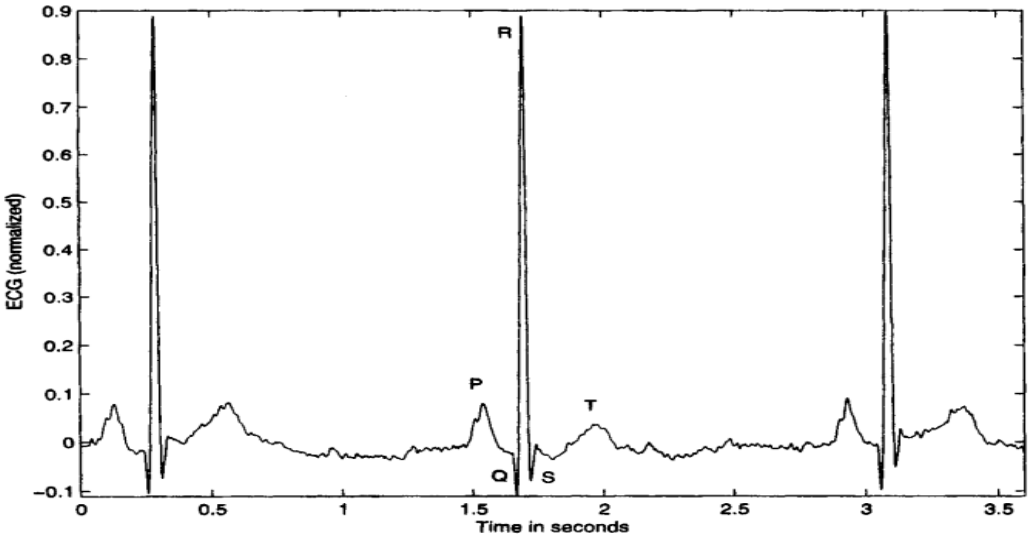

Figure 1.1 A typical ECG signal of a male subject aged 24 years [1]

Each healthy ECG beat has a sinus rhythm which reflects information about ECG waves and segments. Based on these ECG recordings, its waves, and intervals have fixed durations for a normal healthy beat. If the ECG beat's wave and segment don't fall within the durations mentioned above, it is said to be an abnormal beat, otherwise, it is a healthy beat, *e.g.,* in the case of a healthy ECG beat, the ST segment is generally iso-electric in nature but it may be depressed or increased in myocardial ischemia or infarction case. Conduction abnormalities of the heart have an impact on the QRS waveshape; for instance, the right bundle-branch block results in a patient's QRS complex being enlarged and sometimes jagged. So, this wider-than-normal QRS complex differs significantly from the typical QRS complex of a healthy ECG beat [1].

Premature Ventricular Contractions (PVCs), caused by ectopic foci on the ventricles, disrupt the normal ECG rhythm and can result in ventricular dissociation and fibrillation. The latter is a condition in which the ventricles contract irregularly independent of the atria, which can be fatal. PVC wave shapes are considerably different from those of the normal beats of the same person due to the distinct conduction pathways of the ectopic impulses and the associated anomalous contraction events [1]. Therefore, the processing and analysis of ECG waveform is a crucial part of the identification of

heart disorders. The detection of cardiac ailments at an early stage followed by proper treatment can save a lot of lives.

1.2 Anatomy of the Human Heart

The heart is an organ, almost the size of our fist, which pumps oxygenated blood to all parts of the body and deoxygenated blood to the lungs. It has four chambers as depicted in Figure. 1.2. Two atria on the top collect the blood and two ventricles on the bottom pumps out the blood. The resting or filling phase of a heart chamber is referred to as diastole and the contracting or pumping phase is referred to as systole [1]. The superior and inferior vena cava sends contaminated blood to the Right Atrium (RA), often known as the auricle. The tricuspid valve allows blood to go from the right atrium to the Right Ventricle (RV) during atrial contraction. The pulmonary valve pumps out the contaminated blood from the right ventricle during ventricular systole to the lungs for purifying (oxygenation).

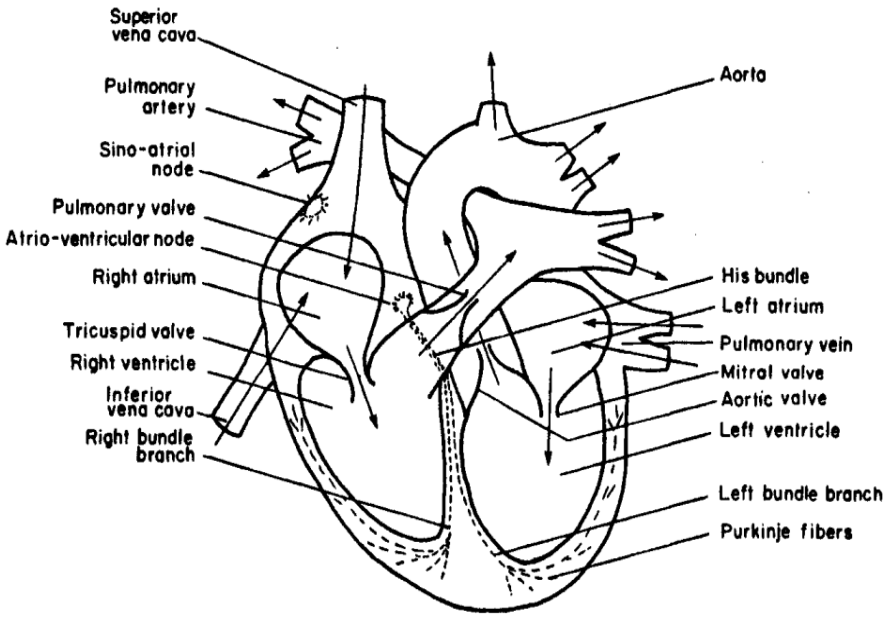

Figure 1.2 Human Heart [1]

Purified blood from the lungs enters the Left Atrium (LA), where it travels through the mitral valve during atrial contraction to the Left Ventricle (LV). The largest and most significant heart chamber is the left ventricle. Among the heart chambers, the left ventricle contracts hardest since it must pump out the oxygenated blood against the

pressure of the rest of the circulatory system of the body, blood passes through the aortic valve and the aorta. Given the increased significance of the contraction of the ventricles, the names systole and diastole are assigned to the ventricles by default.

The Heart Rate (HR) or cardiac rhythm is regulated by specialized pacemaker cells that form the Sino-Atrial (SA) node, which is situated at the junction of the right atrium and the superior vena cava [1]. Impulses from the autonomous and central nervous systems regulate the SA node's firing rate, causing the neurotransmitters acetylcholine (for vagal stimulation, which lowers heart rate) or epinephrine to be released (for sympathetic stimulation, causing an increase in the heart rate). The average heart rate while at rest is around 70 Beats per Minute (bpm). When compared to before a condition termed bradycardia may be indicated by unusually low heart rates during activity that is below 60 bpm. The instantaneous HR may spike as high as 200 bpm during severe exercise or sporting activity. Tachycardia is a high resting heart rate that can be caused by illness, disease, or cardiac anomalies.

The electrical system of the heart: A specialized conduction system that is fundamental to and exclusive to the heart, as well as coordinated electrical events, play significant roles in the heart's regular contractile action. The basic, inbuilt cardiac pacemaker that initiates its train of action potentials is the SA node. The SA node's action potential spreads through the rest of the heart causing a specific pattern of excitement and contraction as depicted in Figure 1.3.

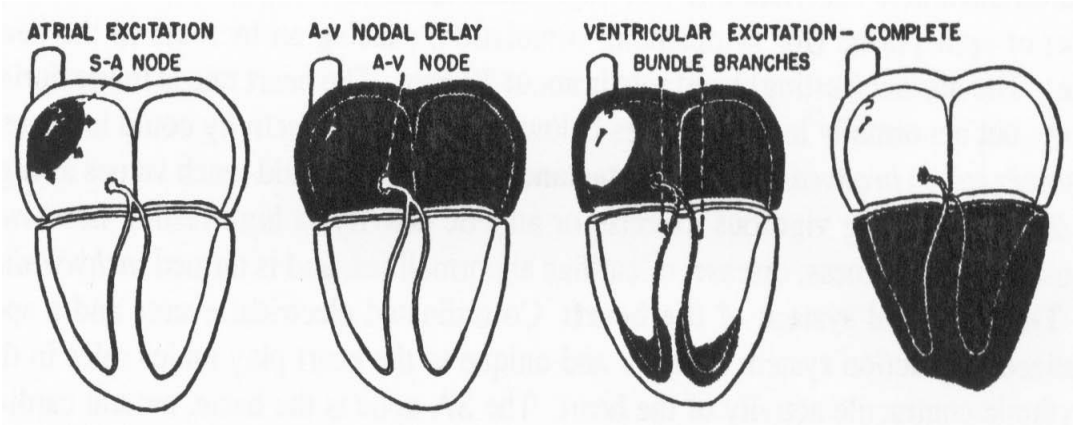

Figure 1.3 Excitation pulse propagation through the heart [1].

A cardiac cycle has the following waves and events [3].

a) The SA nodes fires.

b) At relatively slow rates, electrical activity moves through the atrial muscles, causing the atria to slowly depolarize (contract). The consequence is the P wave in the ECG as shown in Figure. 1.4. The P wave is a slow, low-amplitude wave with an amplitude of around 0.1 to 0.2 millivolts (mV) and a length of about 60 to 80 milliseconds (ms) due to the slow contraction of the atria and their tiny size.

c) The excitation wave experiences a propagation delay at the Atrioventricular (AV) which results in an iso-electric segment of duration 60–80 ms appearing after the P wave in the ECG, named the PQ segment. The pause helps in finishing the process of moving blood from the atria to the ventricles.

d) The stimulus is rapidly transmitted to the ventricles by the His bundle, bundle branches, and Purkinje system of specialized conduction fibers.

e) The wave of stimulus rapidly depolarizes (contracts) the ventricles as it moves up the heart from the apex. As a result, the ECG's QRS wave develops, which is a strong biphasic or triphasic wave with an amplitude of roughly 1 mV and a duration of 80 ms as depicted in Figure 1.4.

f) Ventricular muscle cells have an action potential duration of 300–350 ms, which is comparatively long as seen in Figure 1.4. The plateau portion results in an isoelectric period, known as the ST segment, lasting between 100 and 120 ms after the QRS.

g) The slow T wave, with an amplitude of 0.1-0.3 mV and a length of 120-160 ms, is produced by the ventricles repolarizing (relaxing) as displayed in Figure 1.4.

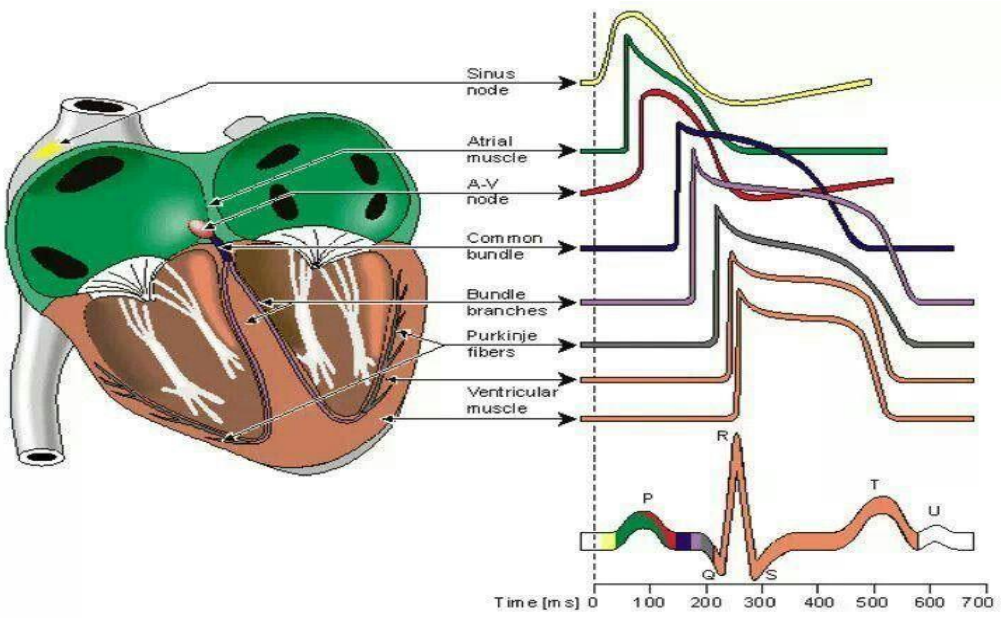

Figure 1.4 Propagation of ECG wave [4]

Any deviation from the normal ECG sinus rhythm caused by early or delayed depolarization or repolarization of the atria and ventricles changes the shape of the QRS, which is further linked to one or more cardiac disorders. Therefore, ECG is regarded as a crucial diagnostic instrument for monitoring cardiovascular problems.

1.3 ECG Signal Processing

Pre-processing of raw ECG signals helps to remove various narrow-band and wide-band interferences. The power-line interference constitutes narrow-band interference and electrode pop-up or contact noise, patient electrode motion artifacts, and baseline wandering constitutes wide-band interference. The commonly used method to eliminate noise in ECG is the application of Finite Impulse Response (FIR) filters [5]. These methods perform well for attenuating the noise of the known frequency bands (for example noise arising from electrical work). The problem with this technique is that the noise frequency is not always known, this can be solved by employing filters for various frequency bands. However, extensive use of low and high-pass filters will distort the morphology of the signal [6]. Moreover, they have other limitations like ringing effects [7,8].

The research focus on study of the concept of Self-Convolution Windows (SCW) which has a smaller side lobe level and has application in minimizing the error caused by spectral leakage in the power system [9]. The problem with this approach is also that it does not perform well when noise is from an unknown frequency band and extensive use of filters will distort the morphology and the information is lost.

Recently, Fractional-order Calculus (FOC) has been the center of attention in research communities due to its remarkable performance in engineering and science domains. The inquisitiveness for the introduction of fractional derivatives in the signal processing field is prompted by its astonishing performances and robustness attained in control theory. FOC has achieved powerful recognition due to its significant advantage over integer-order counterparts [10]. A lot of attention has been paid to the design of Fractional-order Digital Differentiator (FODD) that can perform non-integer order differentiation. FOC is the generalization of the integer-order calculus i.e.,$D^{\alpha}f(x) = d^{\alpha}f(x)/dx^{\alpha}$, where α represents the real number. It is a mathematical tool that provides peculiar details about the signals [11]. FOC is grabbing a lot of attention lately, some of the reasons are mentioned below:

a) The majority of real-time signals, like speech and music, etc., have spectra that don't change by multiples of 20 dB/decade either way. FOC offers a significant amount of flexibility, which has proven to be useful for modeling and identification research [12].
b) Fractional zero-phase FIR filters successfully minimized the phase distortion and significantly improved the signal information retention while denoising the signal [10]. The FOC-based design preserves the signal information more than its integer counterpart model.

There is a growing list of applications demonstrating the immense success of FOC in the field of signal processing. However, very few studies have been conducted that use FODD for biomedical signal processing. Therefore, the goal of this research work was to examine the applicability with a particular emphasis on their potential to enhance valuable data and remove artifacts.

1.4 Contribution to Research Work

According to a recent World Health Organization (WHO) report, heart diseases have emerged as an increasing threat since the turn of the century. Cardiac ailments pose a serious threat to humanity, particularly in developing nations like India. 82% of all deaths reported annually around the world are from developing nations [13]. ECG is a non-invasive tool used as the parameter for assesing the cardiac activity for many decades. It is the record of the electrical commotion caused by depolarization and repolarization of the atria and ventricles of the heart muscles. Arrhythmia, often known as irregular heartbeats, is a frequent kind of cardiac illness that is brought on by the human heart's electrical conduction system and affects the regularity of the heartbeat. The death rate varies for gender and race. Obesity, diabetes, smoking, and a sedentary lifestyle all contribute to the sharp rise in heart-related fatalities in the modern period. Therefore, experts from all around the world are looking into the detection and classification of a heartbeat into normal and abnormal heartbeats.

The automatic computer-based diagnosis of cardiac ailments at an early stage followed by proper treatment can save a lot of lives. Almost all automatic methods concentrate on the detection of R-peak. Clinically speaking, accurate detection of the R-

peak is extremely important. It forms the basis for other feature extraction in the time domain. A self-convolution window based on Hamming window is used to design a Hamming self-convolution window (HSCW) filter which possesses a lower side-lobe level and narrow main-lobe width as compared to well-known windows in literature. It helps in denoising and then R-peak detection in ECG waveform in various situations like high T-wave amplitude, and changing QRS morphology. It has outperformed the results of the state-of-the-art methods for R-peak delineation.

The FOC method provides an extra degree of freedom which helps in optimizing the performance of the methods based on integer-order calculus [14]. Also, it is used to remove artifacts and cancel noise from ECG signals since a fractional-order differentiator has shown provide more peculiar details about signals than an integer-order counterpart. R-peaks in ECG signal are detected using Riesz Fractional-order Digital Differentiator (RFODD) based on the differencing method. ECG waveforms from the Massachusetts Institute of Technology-Beth Israel Hospital Arrhythmia Database (MIT-BIH-AD) even when corrupted with EMG noise from the MIT-BIH Noise Stress database, the proposed method proved to be effective in the delineation of R-peaks.

Following this pre-processing, an attempt is made to develop a real-time classification method to classify real subject ECG beats. The virtual instrumentation method based on LabVIEW is designed for acquiring real-time ECG data. Thus, a complete classification method is proposed which comprises data acquisition, pre-processing, feature extraction, and classification of ECG beats into normal (subjects who have never had any heart ailment history) and abnormal (subjects who have had heart ailment history) classes. The experimental studies have achieved excellent results for real-time ECG subjects. In this research, new and novel features are used based on fractional order and the Fibonacci series. The Adaptive k Nearest Neighbor (ADkNN) is explored for the classification.

After performing classification on real subject ECG beats, the proposed method is extended on MIT-BIH-AD to make a system more robust and to include more classes of ECG beat. It is used to classify ECG beats of MIT-BIH-AD into six categories. In the proposed method, both intra and inter-patient criteria for classification are used. The suggested work also performs well for the minority class of MIT-BIH-AD.

1.5 Organization of Thesis

The research work carried out in this dissertation is organized into seven chapters, as follows:

Chapter 2: Literature Survey

This chapter offers a thorough study of the literature survey for the research work. It presents the preliminaries of integer-order calculus, self-convolution window, FOC, Riesz Fractional-order Digital Differentiator (RFODD), classification of ECG beats, and ECG signal acquisition process. Furthermore, the motivation behind the research work, research gaps, objectives, and research methodology are also discussed in this chapter.

Chapter 3: ECG R-peak Detection employing Self-Convolution Window-based Filters

This chapter demonstrates a new kind of ECG denoising algorithm based on the SCW concept. The SCW based on Hamming window referred to as Hamming Self-Convolution Window (HSCW) is used to design a new kind of filter, which removes various artifacts in ECG waveform. The HSCW filter performance for R-peak delineation in ECG waveform is then compared to well-established window-based filters, for example, Hamming and Kaiser-based filters. This algorithm is validated on the MIT-BIH-AD and the results are presented. ECG waveform from MIT-BIH-AD is taken into account to illustrate the effectiveness of the proposed method in comparison to other window-based filters.

Chapter 4: ECG R-peak Detection using Riesz Fractional-Order Digital Differentiator

Following the advantage of FOC over integer order, RFODD based on the differencing method is applied to ECG signal denoising and R-peak detection in this chapter. ECG waveforms are analyzed by varying fractional order of RFODD and their performance is calculated. The proposed method is tested on the MIT-BIH-AD. The approach is effective in detecting R-peak in ECG waveform even when ECG data is corrupted with EMG noise. Several ECG waveforms from MIT-BIH-AD are taken into consideration to demonstrate the efficiency of the suggested method in R-peak delineation in various situations.

Chapter 5: Virtual Instrumentation-based Implementation of the Proposed Fractional-order Filter

The virtual instrumentation-based method for real-time ECG signal acquisition is designed in this chapter. The work proposes a classification system that includes the acquisition and pre-processing of real-time ECG signals, feature extraction, and classification of ECG beats into normal (subjects who have never had any heart ailment history) and abnormal (subjects who have had heart ailment history) classes using adaptive K nearest neighbor (ADkNN). The various real-time ECG subjects' waveforms are analyzed. The performance parameters like sensitivity, positive predictivity, and accuracy of ADkNN are presented. The proposed method performed well in terms of sensitivity, accuracy, and positive predictivity.

Chapter 6: ECG beat Classification using MIT-BIH-AD

This chapter demonstrates an ECG classification method that performs well in a real-world scenario. The research work analyzes intra- and inter-patient approaches in ECG beat classification. After ECG data pre-processing, features are extracted, and a dimensionality reduction algorithm is used to reduce the size of the feature vector. The ADkNN learning algorithm is investigated. The ECG beat is classified into six categories using ADkNN. The performance parameters that are paid attention to are sensitivity, positive predictivity, and accuracy of the ADkNN and compared with the state-of-the-art methods. The simulation results and discussion of the ECG beat classification into six types add to the chapter's completion.

Chapter 7: Conclusion and Future Work

This chapter summarises the main contribution of the research carried out in this thesis and suggests a few directions for future research.

CHAPTER 2

LITERATURE SURVEY

Literature survey is not just a chronological catalogue but an evaluation, integrating the previous research together.

-Anonymous

THIS CHAPTER PROVIDES THE IN-DEPTH STUDY of various ECG pre-processing and classification techniques. Further, this chapter elaborates the work that has already been reported in the literature to consolidate the research carried out in this thesis. Additionally, this chapter presents the motivation behind the research work including gaps and objectives of research as well as a research methodology.

2.1 Preliminaries of Digital Differentiators and Filters

Differentiators or differentiating filters are used in many digital systems to determine the signal's time-derivative. They are employed in almost all applications of sciences and engineering. For instance, it is employed in communication, control and radar systems, audio and video processing applications, and other fields of engineering [15]. The most crucial components in the digital signal processing are digital filters [16]. Digital filters remove the unwanted signal of certain frequencies from the incoming signal to obtain the desired signal of specific frequencies. The filtering of data is the oldest discipline in the field of digital signal processing. For the past decades, several techniques have been proposed for filtering ECG signals using digital filters and they are mentioned in the next section.

2.1.1 ECG filtering based on digital differentiators and filters

The implementation of recursive digital filters of finite impulse response (FIR) is the simplest and most extensively used method for minimising noise in ECG data [6]. The other widely used filter is infinite impulse response or Butterworth filters [5]. An adaptive recurrent filter structure was developed for noise reduction and arrhythmia identification in ambulatory ECG by obtaining the impulse response of normal QRS complex [17].

Razzaq *et al*. [18] suggested a system, which proposes an adaptive noise rejection filter that detects and removes power-line interference (PLI). The system can determine the frequency of PLI and its harmonics without additional reference input. The suggested system functions well in a non-stationary environment and is built on a recursive state space model. The system is capable of self-adjusting its tracking frequency for very exact filtration of PLI and its harmonics.

Phukpattaranont *et al*. [19] proposed the QRS detection algorithm using quadratic filters to enhance QRS signal-to-noise ratio (SNR). The noteworthy enhancement in QRS SNR is obtained even in challenging situations including low amplitude QRS complexes corrupted with baseline drift and abnormal morphologies. The performance of this algorithm is evaluated on MIT-BIH-AD.

Vullings *et al*. [20] proposed Kalman filter with adaptive noise-covariance estimation and tested the model on various ECG signals to determine whether the filter is able of boosting the SNR of these signals while maintaining clinically relevant morphological variations in the ECG at the same time. To operate, the filter successively estimates the measurement and process noise covariances to estimate the Kalman gain and update the estimated ECG complexes.

FIR filter performs well in attenuating the noise of the known frequency bands. The problem arises when the noise frequency is not unknown, this can be solved by employing filters for various frequency bands. The extensive use of low and high-pass filters will distort the morphology of the ECG signal [6]. Moreover, FIR filters have limitations like ringing effects [8].

2.2 Self-Convolution Window (SCW) Method

Numerous signal processing and communication research fields have successfully employed the concept of windows. A thorough review of different window functions was very nicely presented in [21]. The generation of a new window class is presented in [22, 23] obtained by multiple time convolution of weighted cosine windows that has flat-top main lobe and high side lobe attenuation and is able of reducing long-range leakage. The quasi-synchronous window is presented in [24] which exhibits a lower side lobe obtained by convolving the same or different classical windows, which tends to reduce the long-range leakage, and gives a more accurate measurement of many electrical quantities.

Zhang *et al*. [25] presented the self-convolution window which has high accuracy in examining the harmonic analysis of the periodic signal in comparison to the classical windows. Errors generated by spectral leakage of harmonic parameters are significantly reduced when a *p*th-order convolution window is employed.

Wen et al. [9] employed the triangular self-convolution window (TSCW) to attain the desired side lobe level for harmonic analysis of the power system. Compared to the conventional triangular window, this has a low peak side lobe level, a high side lobe roll-off rate, and a simple spectral representation.

Krishna *et al.* [26] demonstrated a significant reduction in the side lobe level using various self-convolution windows (for instance, -13.27 to -26.53 dB in the case of rectangular and - 45.53 to - 90.98 dB in the case of the triangular window, respectively).

Rai *et al*. [27] used TSCW which yielded good results as the measurement error is reduced when predicting the supply voltage harmonics. It has also aided in the detection of weak harmonics in the power system. TSCW can compress the spectral leakage due to the narrow main lobe and rapid side lobe decay.

2.2.1 Application of SCW

The application of the self-convolution window is listed as follows:

a) Convolution window reduces long-range leakage, and yields more accurate measurement of many electrical quantities [24].

b) Errors generated by spectral leakage of harmonic parameters are significantly reduced when a *p*th-order convolution window is employed [25].
c) It also helps in detecting weak harmonics in power systems [9].
d) TSCW can compress the spectral leakage due to the narrow main lobe and rapid side lobe decay [27].

However, over the past few years, the research has been shifted towards investigating the fractional-order calculus (FOC) as it has received a lot of attention due to motivations in various engineering and science fields. FOC provides an extra degree of freedom to alter the characteristics of integer-order calculus and hence, proves to be efficient in providing peculiar details as compared to their integer-order calculus.

2.3 Preliminaries of Fractional-order Calculus (FOC)

The processing and analysis of ECG data use various joint time-frequency tools such as wavelet transform (WT), [28-35] and Stockwell transforms (ST) [36-39]. FOC has received a lot of attention in recent years due to motivations in various engineering and science fields. The good performances and robustness of fractional derivatives attained in control theory have sparked the curiosity for the introduction to the signal processing area. Designing digital fractional order differentiators or filters for noise reduction, crucial information augmentation and fractal signal generation are the focus of FOC application. Based on the idea of fractional-order differentiation [40, 41], the fractional-order differentiator (FOD) might be created for applications in designed for image processing [42, 43], control systems [44] signal processing [45-47] and also in ECG signal processing applications.

Ferdi applied FOC to ECG signals, emphasizing the ability of the former to remove noise, enhance useful information and generate fractal signals [48]. The important pre-processing step for wave identification in biological signals is low-pass differentiation. It does the following (a) converts wave edges that are rising and falling into positive and negative pulses, (b) converts peaks and troughs into zero crossings, and (c) filters out DC components and high-frequency noises [49].

Ferdi [50] also proposed a non-causal finite impulse response (FIR) filter which is created by combining differentiation and a high-frequency noise filter, and the

coefficients of this filter depends on the fractional order. The filter is useful for wave detection of biomedical signals that are distorted by high-frequency noises like ECG and electroencephalogram (EEG). The high-frequency noise components are successfully reduced by this improved filter while the characteristics of the original signal are preserved.

Ferdi *et al*. [51] used FOD for the detection of R-peaks in ECG. The differentiator is followed by nonlinear transformation to amplify peaks corresponding to R peaks with high slopes. When the algorithm is tested against the MIT-BIH Arrhythmia database (MIT-BIH-AD), the failed detection rate is 0.37%.

Benmalek *et al*. [52] employed an algorithm which uses fractional-order differentiation and integration-based algorithms to detect the R-peaks by eliminating P and T waves and other artifacts present in ECG. To highlight QRS complexes, nonlinear transformation is applied to the signal. When evaluated on the MIT-BIH-AD, this algorithm sensitivity, positive predictivity, and error rate are 99.86%, 99.86%, and 0.28% respectively.

Jain *et al*. [53] proposed ECG denoising which uses Savitzky–Golay (SG) filtering, Riemann–Liouville (RL) fractional integral and empirical mode decomposition (EMD) approach. Decomposition of ECG waveform into intrinsic mode functions (IMFs). These IMFs are distorted with various artifacts and noises of high and low frequencies. By applying RL and SG filtering on IMFs corrupted with high-frequency and low-frequency noises, respectively, denoises the signal. Denoised ECG signal is reconstructed with the help of noise-free IMFs and signal-dominant IMFs. The MIT-BIH-AD is used to assess the methodology, and it performs better in terms of signal-to-noise ratio (SNR) and mean square error (MSE).

Wang *et al*. [10] proposed fractional zero-phase FIR filters based on Liouville–Weyl and Weyl–Liouville fractional compound integral, which have successfully decreased phase distortion and improved the trade-off between signal denoising and signal information retention. The approach has better experimental and quantitative results when evaluated on ECG records from MIT-BIH-AD by adding disturbance and random noise to it [10].

Wang *et al.* [54] suggested a parallel-type fractional zero-phase filtering based on Grunwald–Letnikov (GL) differ-integrators for ECG denoising. Moreover, the signal information is adequately retained during the denoising process.

2.3.1 Riesz-based fractional-order digital differentiator (RFODD)

The ideal frequency response of conventional FOD is given by:

$$H_d(w) = (jw)^p \tag{2.1}$$

where p is a real number. Although conventional FOD with the ideal response in (2.1) has been successfully used in various signal processing applications, this phase shift is unwanted and a zero-phase shift ideal response of FOD is needed which is given below:

$$G_d(w) = |w|^p \tag{2.2}$$

Three methods i.e., differencing method, Tustin's method, and the discrete cosine method is used to design RFODD [55].

2.3.2 Application of RFODD

a) Image sharpening application is demonstrated in [55] to show the effectiveness of the RFODD
b) The zero-phase Riesz FOD is more suitable than the constant-phase conventional FOD in digital color image sharpening applications [55].

2.4 LabVIEW-based Virtual Implementation of ECG signal Acquisition and Classification

One of the most important tasks for real-time system or model is the acquisition of ECG signals. There are many data acquisition devices and software packages accessible, but National Instruments (NI) LabVIEW is the most popular and dominant [56-58] because the acquisition and analysis of acquired signals are controlled by built-in procedures in LabVIEW. Furthermore, the latter is capable of easily creating a user interface [56].

Lascu *et al.* [56] suggested ECG signal acquisition method by cascading a low pass filter with a cut-off frequency of 40 Hz with a moving average filter. For the

acquisition process, a PCI-6023E card was used. Sharma *et al*. [57] proposed a system that acquires ECG signals in real time and identifies any cardiac abnormalities. It identifies whether or not a specific wave in an ECG signal is in range by using light-emitting diodes (LEDs). The system included myDAQ device, a Vernier adaptor, and an ECG sensor combined with ECG electrodes to gather data from the subjects, which was then analyzed in LabVIEW. Ten subjects were randomly selected for testing [57]. A design of an analog front end for the reliable acquisition of ECG signals is proposed. The design has taken into account the nature of ECG signal as well as the necessity to make the circuit portable and low-cost [58].

Singh *et al.* [59] developed a device based on Einthoven's triangle and it employed Lead II configuration to acquire ECG data. A three-lead portable system used an AD620 instrumentation amplifier in the ECG amplifier circuit, apprehended by a signal conditioning circuit with the operational amplifier. The acquired analog signal is converted into digital using a NI-DAQ card. Further, the processing is carried out in LabVIEW using its in-built libraries of digital filtering techniques to remove noise from the obtained data. The algorithm is developed to compute heart rate and examine arrhythmia.

A low pass and notch filter with a cut-off frequency of 150 Hz and 60 Hz respectively is used [60]. Lead II ECG data is acquired using the AduC831 DAQ system combined with J Free Chart. To investigate the impact of interventions or pathophysiological variations between groups, a single lead may be sufficient. Even though 12 lead ECG recordings are ubiquitous, preclinical investigations frequently call for single lead ECG recordings, maybe they are simpler to use and more practical to record [61].

Dhande [62] built a ECG monitoring system, which comprised sensor electrodes, filters, and amplifiers to capture ECG signals. The acquired ECG signal using this model is first amplified and then passed through low-pass and high-pass filters to obtain the signal of the desired range of frequencies. The results are confirmed through spice simulations and PCB layout. NI DAQ is used for interfacing the analog and digital parts of the model. LabVIEW is used for further processing and analysis of its temporal parameters to calculate heart rate and for the classification of beats into tachycardia, bradycardia and normal.

Wavelet transform (WT) is used to denoise ECG signal in LabVIEW as it is a very perceptive way to decipher its information, thus leaving no room for information loss. Therefore, it helps in diagnosing cardiac disease or ailments more efficiently. Real-time ECG signals can be easily read on a computer/laptop with the help of the LabVIEW toolkit by employing NI-DAQ [63].

Zaidi *et al*. [64] proposed an approach that is implemented on the LabVIEW Biomedical toolkit to perform ECG processing and extract features like heart rate, QRS width, PR interval, QT interval, and RR interval. Normal sinus rhythm, atrial fibrillation, paroxysmal atrial fibrillation, and the supraventricular tachycardia dataset are used in this research for analysis and convincing results are obtained.

This research consists of a device, which employs AD8232 as an instrumentation amplifier, followed by LM741 used for signal conditioning. DAQ card performs as an Analog Digital Converter (ADC) [59]. Using LabVIEW and the biomedical toolkit, ECG features are extracted. In this proposed approach, a telemedicine application is included which allows the doctor to examine their subjects/patients remotely [65].

Shafi *et al*. [66] developed a low-cost ECG monitoring system based on piezoelectric sensors and NI-DAQ cards. The heart rate is computed using piezoelectric sensors and preprocessing and analysis are done using LabVIEW. The online MIT-BIH database is imported into a biomedical toolkit for analysis and its features are extracted [67].

Ay *et al.* [68] developed a real-time ECG system using NI-DAQ and ECG module AD8232. ECG of 12 subjects is recorded in relaxed and after-running conditions. Out of 12 subjects, six are smokers and the rest are a non-smoker. The experimental results are recorded for graphical and statistical analysis.

2.5 Classification of ECG signal

The essential step in the process of image and signal classification is the extraction of the feature. The raw ECG signal and transformed ECG signal are used to procure features. Features can be morphological, statistical or both. The most common ECG feature is called RR interval and it is defined as the time interval between two consecutive R-peaks of the ECG record [7, 69]. Additional features are based on various heartbeat intervals

and segments and ECG morphology [70]. The numerous algorithms are proposed in [70-72] to determine the fiducial points in ECG and to calculate the values of several heartbeat intervals since healthy heartbeat intervals lie within a specified range. Independent component analysis (ICA) is the alternative statistical method for extracting features [73]. ECG signal was decomposed into a weighted sum of basic components (mutually statistically independent) using ICA.

Sarfraz *et al*. [74] developed a new feature set of ECG beat which includes morphological features and ICA extracted features. A new quality-aware ECG beat classification technique that can minimises false alarms and ensures class-specific accuracies for each of the four classes of heartbeats in noisy ECG recordings [75].

Life-threatening illness patients need ongoing medical attention. They are often admitted to intensive care units (ICU), any abnormal ECG signals or arrhythmia will be constantly watched, and critical patients will receive prompt medical assistance. False arrhythmia alarms, however, make it difficult to monitor patients. Therefore, the goal of this study is to forecast false alarms brought on by arrhythmic ECG signals. For every testing scenario, the suggested approach was able to produce accuracy levels above 80% [76]. The transformed domain is a crucial method for feature extraction. Discrete wavelet transform (DWT), S-Transform (ST), and Empirical mode decomposition (EMD) are the methods most frequently employed. Due to its ability to extract distinguishing information for ECG classification, wavelet was frequently used.

Martis *et al.* [77] employed the dimensionality reduction algorithms principal component analysis (PCA), linear discriminant analysis (LDA), and independent component analysis (ICA) on fourth-level detail and approximation coefficients of DWT independently and six features from both sub-bands were extracted and fed to classifiers [77]. A approach is proposed in [78] which combines ST and DWT-based features to extract ST-based features.

Rajesh *et al.* [79] employed two approaches: EMD and ensemble empirical mode decomposition (EEMD). ECG beat is broken down into intrinsic mode functions (IMF) using these two methods. Using the acquired IMFs from the two techniques separately, four features were extracted and fed to the classifiers for ECG classification. Even in noisy environments, this approach demonstrated its capacity to distinguish between

various heartbeats. As for ECG beat classification, any multi-class classifier is used. The frequently employed models are support vector machine (SVM) [80, 81], artificial neural network (ANN) [82-85], K-nearest neighbor (KNN), deep neural network [86, 87], and Convolutional Neural network [88, 89].

IMFs-based features obtained in [79] are fed to a sequential minimal optimization-support vector machine (SMO-SVM). A method for an ensemble of SVMs is proposed in [81]. This approach performed better than the single SVM model when the same feature set was used. A method for ventricular premature beats detection is described which explores the signals acquired from the arterial and the venous pressure sensors, located in the extracorporeal blood circuit of a hemodialysis machine. A set of simple features is extracted, and linear discriminant analysis is performed to classify beats as either normal or ventricular premature. Performance is evaluated on signals from nine hemodialysis treatments, using leave-one-out cross-validation [90]. In [91], the author fine-tunes the SVM classifier and performed feature selection using a particle swarm optimization (PSO) algorithm. The other classifiers employed are hidden Markov model (HMM) [92], multilayer perceptron neural network (MLPNN) [78], evolutionary neural network [93], self-organizing maps (SOMs) [94] and random forest [95], and so on to build classification models.

2.6 Motivation

As inferred from the study of available literature in the research community, a significant amount of research work has been carried out in integer-order ECG signal processing. The insightful concept of FOC has been applied to numerous applications in engineering disciplines. FOC method provides an extra degree of freedom, which helps in optimizing the performance of the methods based on integer-order calculus. So, an interest urged to incorporate the concept of FOC in ECG signal processing applications. Further, there is a need for realistic classification, which can perform data acquisition, pre-processing, feature extraction, and classification of ECG beats. The model must perform better for the minority classes as well and achieve good parameters such as accuracy, sensitivity, and positive predictivity. Thus intriguingly, based on the relevant facts and the rich literature, an effort is made to identify the gaps in the study and to design the statement of problems for the proposed work.

2.6.1 Research gaps

Based on the survey conducted, some of the research gaps that have been identified are as follows:

a) It is well-known that many physical phenomena can be precisely and successfully described using fractional derivatives, whereas these phenomena can be roughly captured by the traditional integer-order derivative-based approaches. Moreover, fractional derivatives depend on the entire history of the function whereas integer-order derivatives depend solely on the local behaviour of the function. There is a scope of research motivation to employ fractional derivatives in biomedical signal processing.
b) The exact estimation of the QRS complex is still a challenge due to various artifacts present in the signal, thus affecting the morphology and detection adversely, so further improvements are still an important goal of current research.
c) There is still a place to propose a better feature extraction approach for automatic ECG signal detection and classification, which will outperform conventional techniques.
d) The current research has attained good accuracies but it primarily focuses on an *intra-patient criterion or beat-based scheme.* Nevertheless, in a practical scenario, the training set would be from different subjects and the testing set would be from completely different subjects (*inter-patient criterion or record-based scheme*).
e) The approaches currently in use work poorly for imbalanced datasets since they achieved poor results in terms of sensitivity and positive predictivity for small-size classes in the dataset.

2.6.2 Objectives

Based on the basic principles, literature survey conducted and the insight developed regarding FOC, the following objectives have been put forward:

a) To develop an efficient algorithm based on novel fractional order filtering for ECG signal processing.
b) Virtual instrumentation-based implementation of the proposed fractional order filter.

c) To extract ECG features and perform classification based on the proposed filtering techniques.
d) To evaluate the proposed developed system.

2.7 Research Methodology

The key to achieving the aforementioned research goals is to thoroughly review the body of prevalent literature to garner the information that will help in comprehending the core ideas of the subject being studied. Figure 2.1 displays a flowchart of the work done for this thesis. Initially, comprehensive studies regarding digital differentiators and filters are conducted. Furthermore, the fundamentals and concepts of SCW, its applications, and design methods are studied to gain significant perspective about their implementation for signal or ECG signal processing applications. This in-depth analysis led to the formulation of a new filter based on Hamming window referred to as Hamming self-convolution window-based filter. The applicability of the proposed filter is validated through various illustrations of ECG signal processing.

The research work emphasizes the advantages of FOC over integer order in signal processing applications. A method based on Riesz fractional-order digital differentiator is proposed for ECG signal processing. The significance of the proposed fractional method is justified through various illustrations of ECG signals. Then a classification system is proposed which includes the data acquisition, pre-processing of real-time ECG subjects, feature extraction and classification of ECG beats into normal (subjects who never had cardiac ailment history) and abnormal (subjects who had cardiac ailment history) classes. The efficacy of the proposed method is evaluated both qualitatively and quantitatively by taking standard ECG data, *i.e.,* MIT-BIH-AD into account. The effectiveness of the proposed method is compared against well-established state-of-the-art methods in the literature. All the results are supported by simulation. The simulations are performed by using software version 2013, 2021a of MATLAB on a personal computer, LabVIEW 2016 with Intel Core i5, and 3.40 GHz CPU processor with 8 GB of RAM.

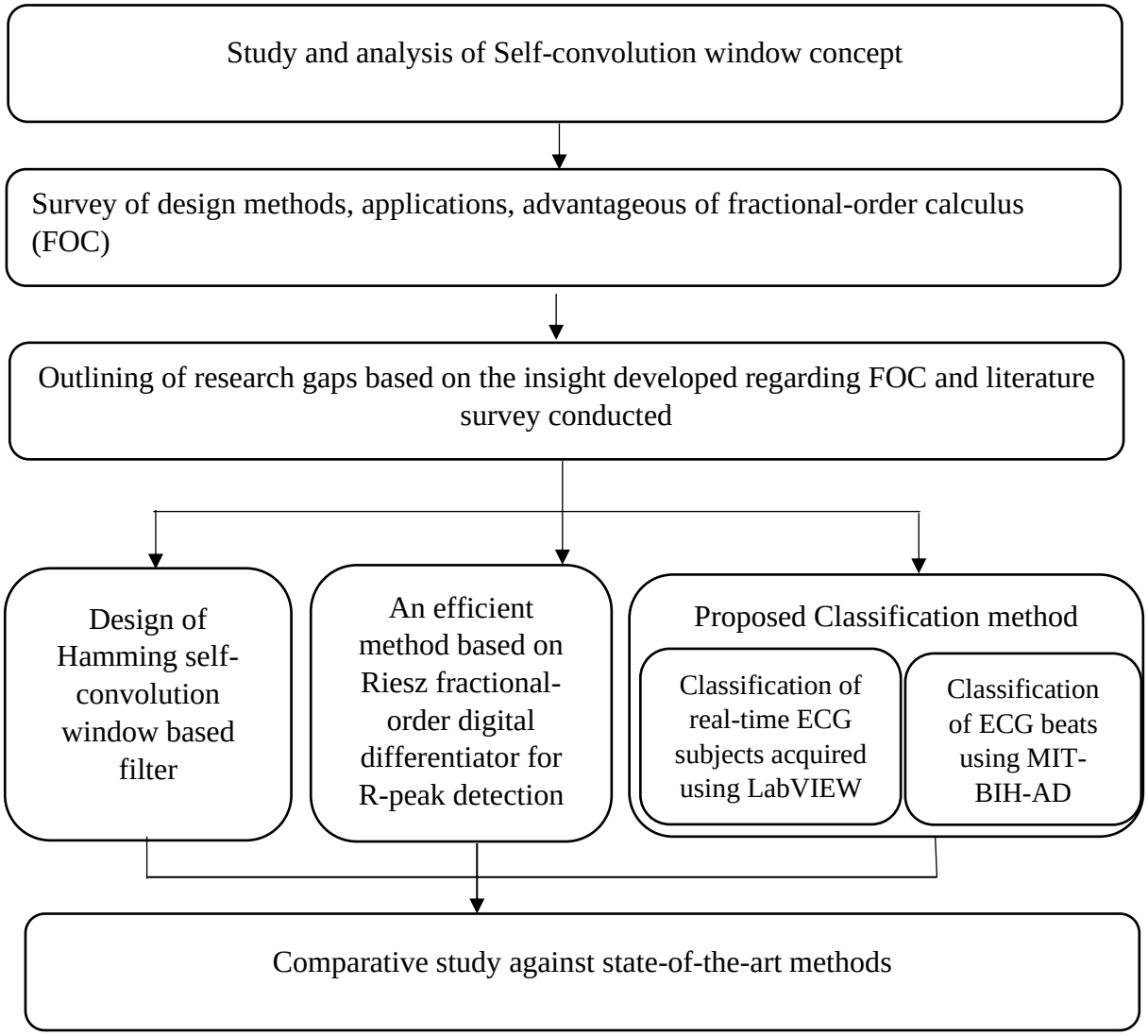

Figure 2.1 Flowchart of the research work carried out in the thesis.

CHAPTER 3

ECG R-PEAK DETECTION EMPLOYING SELF CONVOLUTION WINDOW-BASED FILTERS

ELECTROCARDIOGRAM (ECG) signal processing and analysis is becoming more and more popular as it is beneficial in the diagnosis and predicts the health of the human heart and it is the foundation for clinically automatic machine estimation. R-peak is the most crucial component in ECG beat and is frequently used to examine normal and abnormal subjects (patients). The most challenging domain of biomedical research over the past few decades has been R-peak detection in ECG. The QRS complex in an ECG has a higher frequency than other waves (P, T, U-wave), so most algorithms estimate the QRS complex by either filtering or suppressing lower frequency waves, including numerous artifacts like baseline wander, power line interference, and electromyograph noises.

FIR filtering is commonly used in signal processing [6], but it has limitations like ringing effects. This research work demonstrates a new kind of filter based on the *Self-Convolution Window* (SCW) concept. Filters based on SCW have proved to possess a narrow main lobe and lower side lobe [28]. They are effective in suppressing the ripples in the stop-band. Therefore, a new kind of ECG denoising algorithm based on SCW is proposed.

3.1 Concept of Self-Convolution Window

Windows functions used for signal processing applications are well explained in [21, 96]. The self-convolution window functions concept has been used in this study for accurate biomedical signal processing applications. A novel type of filter for ECG denoising and R-peak detection is designed using the *Hamming Self-Convolution Window* (HSCW),

which has a lower side-lobe level and narrow main lobe width compared to traditional and well-known window functions.

The rectangular convolution window [9, 26] and triangular convolution window [9] have demonstrated that the self-convolution family of windows performs better in terms of performance criteria like Side Lobe Level (SLL), Side Lobe Roll-off Factor (SLFOR) than traditional window function. The following window functions parameters is used to evaluate it [8, 97]:

a) **Maximum Side Lobe Level (MSLL):** This measure of peak side lobe ripple value is derived from the log magnitude plot of the transformed window.
b) **Half Main Lobe Width (HMLW):** The frequency at which the main Lobe descends to the peak ripple value of the side lobes.
c) **Side Lobe Roll-off Factor (SLFOR):** It is called an asymptotic decay rate. At higher frequencies, the window with the quick side lobe decay attenuates.

It is demonstrated in [26] that the rectangular window and its self-convolution counterpart window SLL is decreased from -13.27 dB to -26.53 dB. Likewise, there is a reduction of SLL from -45.53 to -90.98 when the triangular window and its convolution are taken. It is revealed that the SLL of the convolution level is less as compared to its convolution counterpart [26]. Wen *et al*. [9] present that the triangular self-convolution window (TSCW) for the second and fourth-order, self-convolution window's SLL is -52 dB and -104 dB respectively, whereas for triangular window has SLL of -26.448 dB.

3.1.1 Hamming self-convolution window function (HSCW)

The time domain Hamming window of length b is defined as [8, 98]:

$$w(t) = \begin{cases} k + (k-1)\ \cos\left(\frac{2\pi t}{b}\right) & |t| \leq b \\ 0 & otherwise \end{cases} \tag{3.1}$$

where $k = 0.54$. The m^{th} order HSCW is created, by the self-convolution window method [9, 26], by the $(m-1)$ self-convolutions of m instances of Hamming window, where m is the number of Hamming windows, also known as the window order or the order of HSCW.

If $w(t)$ is the time domain representation of the window, then the m^{th} order self-convolution window is given as [9, 26]:

$$w_m(t) = w(t) * w(t) * \cdots * w(t) \tag{3.2}$$

where $*$ represents the convolution operation. Applying Fourier transformation (FT) to (3.2) results in the following expression [26]:

$$W_m(\omega) = (W(\omega))^m \tag{3.3}$$

On applying FT to (3.1), one obtains the expression of Fourier frequency domain Hamming window as [26]:

$$W(\omega) = \left(\frac{(k-1)\omega^2}{\omega^2 - \left(2\pi/a\right)^2} - k\right) 2a\ sinc(a\omega) \tag{3.4}$$

where $sinc(\cdot)$ denotes sinc function, defined as $sinc(p) = \sin(\pi p)/\pi p$. Taking the order of HSCW $m = 2$, (3.3) and (3.4) is simplified as [26]:

$$W_2(\omega) = \left(\frac{(k-1)\omega^2}{\omega^2 - \left(2\pi/a\right)^2} - k\right)^2 4a^2 sinc^2(a\omega) \tag{3.5}$$

3.1.2 Comparison of the magnitude frequency response of HSCW with classical windows

The magnitude frequency responses of HSCW, Hamming, and Kaiser window (for $\beta = 6$) of length M are depicted in Figure 3.1. The Hamming window is described in the preceding section, and [8, 98] provides a thorough illustration of it. The definition of the Kaiser window is given below [8, 98]:

$$\mathrm{w(t)} = \begin{cases} \dfrac{\mathrm{I_0}\left[\beta\sqrt{1-\left(\frac{\mathrm{t}}{\mathrm{a}}\right)^2}\right]}{\mathrm{I_0(\beta)}}, & |\mathrm{t}| \le \mathrm{a} \\ 0, & \text{elsewhere} \end{cases} \tag{3.6}$$

where β is the variable parameter, $\mathrm{I_0(x)}$ is the Zero-order modified Bessel Function of the first kind defined as:

$$\mathrm{I_0(x)} = 1 + \sum_{\mathrm{i}=0}^{\infty}\left[\frac{1}{\mathrm{i!}}\left(\frac{\mathrm{x}}{2}\right)^{\mathrm{i}}\right]^2 \tag{3.7}$$

According to Figure 3.1, HSCW has a smaller SLL and a narrow main lobe width than Hamming and Kaiser windows. SLL for the conventional Hamming and Kaiser window is -44 dB and -46 dB respectively, however, it is significantly improved in HSCW as it is reduced to -93.90 dB.

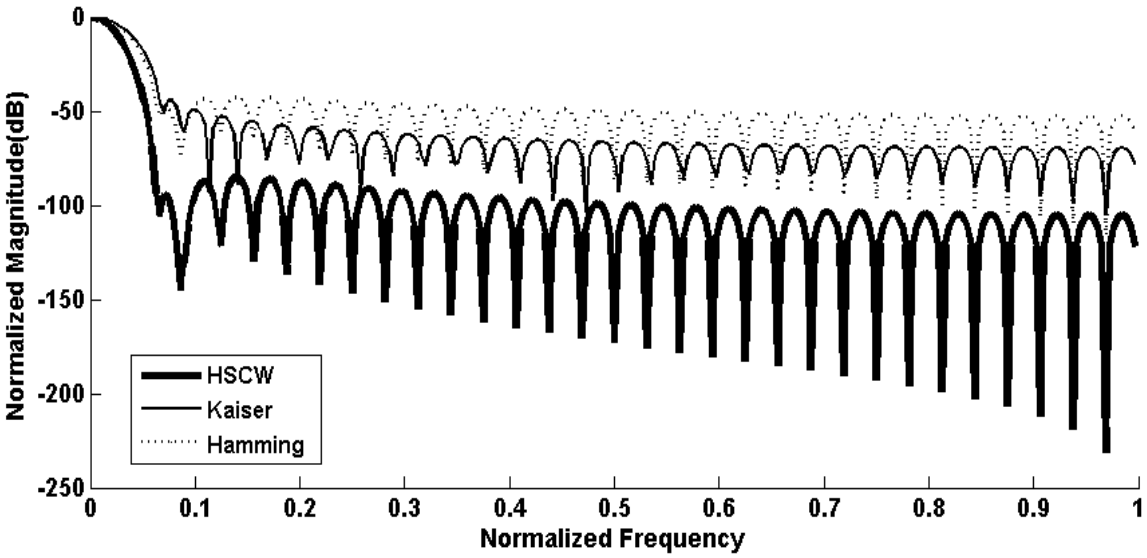

Figure 3.1 Magnitude frequency responses of HSCW, Kaiser, and Hamming window-based function

3.2. HSCW Band-Pass Filtering (HSCW-BPF) Approach

Figure 3.2 shows the proposed approach for the identification of R-peak in ECG data. The MIT-BIH-AD is used as input to the proposed filter based on the HSCW function. The HSCW Band-pass Filter (HSCW-BPF), which consists of the HSCW low-pass filter (HSCW-LPF) and HSCW high-pass filter (HSCW-HPF) is used to pre-process the raw ECG data. The output of HSCW-BPF is squared and a thresholding operation is applied to detect R-peak.

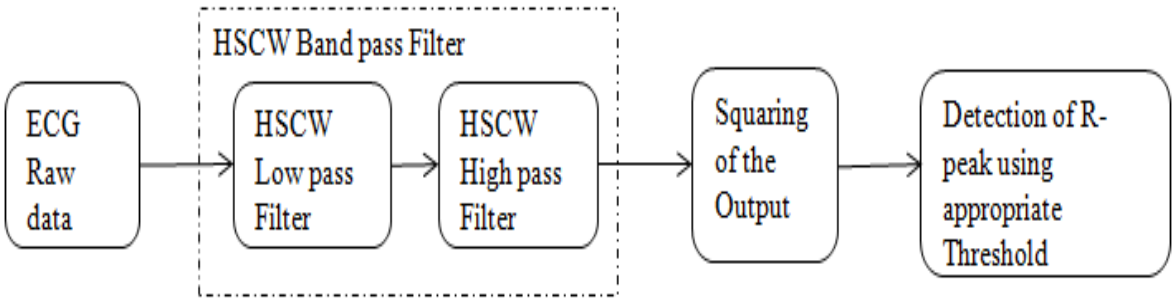

Figure 3.2 Block diagram of the proposed system for the identification of R-peak

The HSCW-BPF is used in the proposed method to implement HSCW-based filtering. This is accomplished by cascading the HSCW low-pass filter with the HSCW high-pass filter. The QRS complex of ECG has a frequency band of 5-15 Hz [99]. The cut-off frequencies of both the proposed filters are selected accordingly. The cut-off

frequency of HSCW-LPF and HSCW-HPF is selected to 15 Hz and 5 Hz respectively. Each record of ECG is sampled at the same frequency and the sampling frequency is 360 Hz. Figure 3.3 and Figure 3.4 respectively, display the magnitude response of HSCW-LPF and HSCW-HPF.

The stop-band attenuation and transition width are the two principal distinguishing features of a filter. The frequency range that permits the transition between a filter's pass-band and stop-band is known as the transition width. The truncation of the infinite impulse response of a filter with a window function leads to ringing effects due to Gibbs phenomenon [8, 98]. The ripples in the stop-band result in poorer attenuation of frequencies of the signal lying in the stop-band. So, the filter should have lesser stop-band ripples to have better cancellation of frequencies in the stop-band. Comparing HSCW-LPF and HSCW-HPF to traditional Kaiser and Hamming windows, stop-band ripples are remarkably small. Thus, the proposed filters have better stop-band attenuation than the classical Kaiser and Hamming window-based filters.

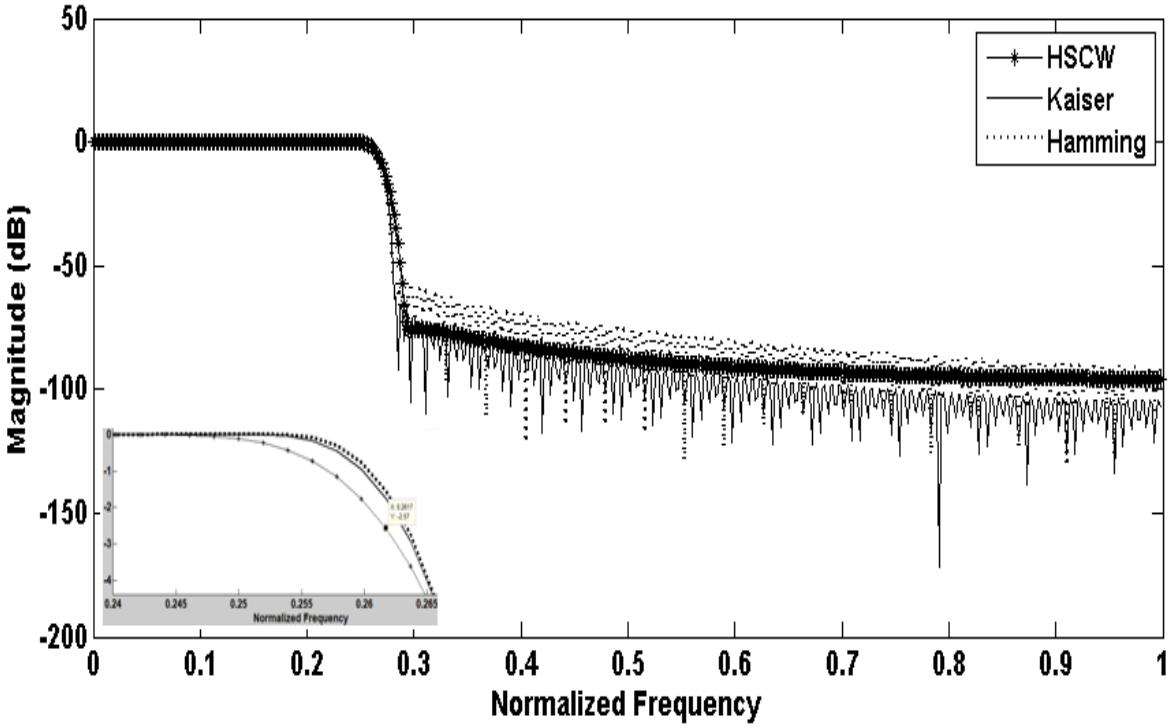

Figure 3.3 Magnitude responses of HSCW, Kaiser, and Hamming window-based low pass filter

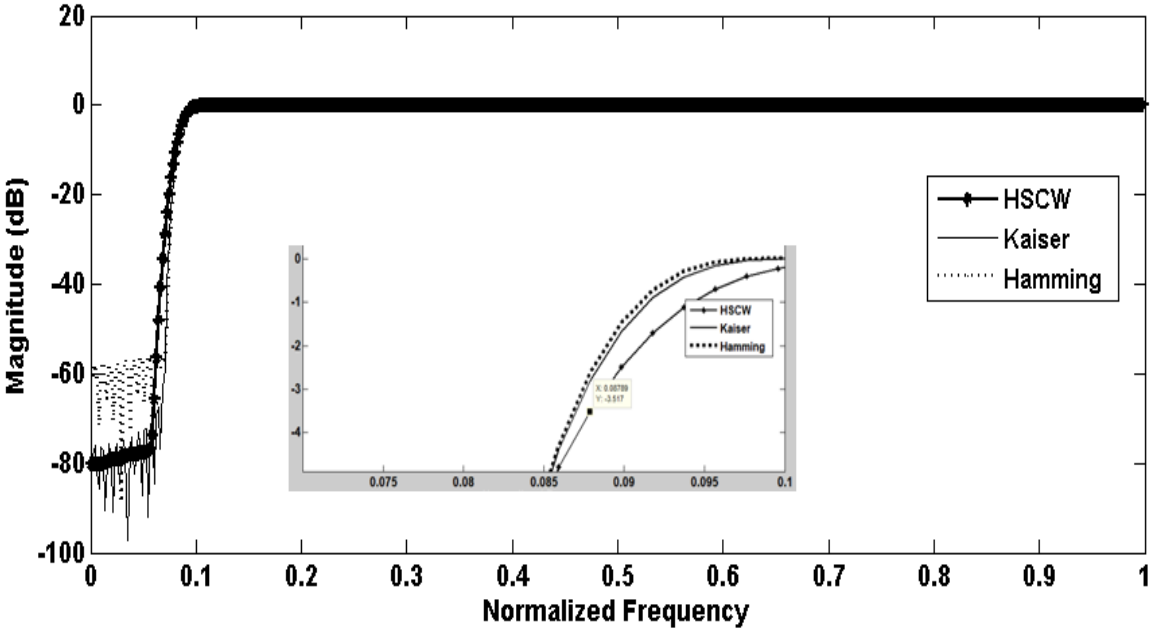

Figure 3.4 Magnitude responses of HSCW, Kaiser, and Hamming window-based high pass filters

The following steps are used to obtain Hamming self-convolution window FIR filters:

a) The cut-off frequency is determined
b) The impulse response $h_d(n)$ of the ideal filter is chosen based on Table 3.1
c) The side lobes of the window function have an equal impact on the stop-band δ_s and pass-band δ_p ripple. The minimum stop-band attenuation is chosen as 20log [min $\{\delta_s, \delta_p\}$]
d) The impulse response is truncated using the Hamming self-convolution window

Table 3.1 The impulse response of linear phase filters [98]

Filter	**Impulse response (h[n],n≠ α)**	**h[α]**
Low-pass	$\frac{\sin(\omega_c(n-\alpha))}{\pi(n-\alpha)}$	$\frac{\omega_c}{\pi}$
High-pass	$-\frac{\sin(\omega_c(n-\alpha))}{\pi(n-\alpha)}$	$1-\frac{\omega_c}{\pi}$

The HSCW-BPF filter eliminates the artifacts present at various frequencies. As raw ECG has artifacts at higher and lower frequencies. The dominant higher-frequency artifacts are power line interference (50-60 Hz) and electrosurgical noises [99]. These are removed by the suggested low-pass HSCW filter. The baseline wanders with a frequency

range of 0-2.5 Hz and consists of lower frequency artifacts. The suggested high-pass HSCW filter eliminates the baseline drift, which can occasionally cause abrupt changes in the ECG amplitude.

3.3 ECG R-peak Detection

The obtained artifacts free ECG waveform is squared to improve R-peaks' localization and their prominence to other small amplitude peaks. The highest peak in ECG waveform can be used to identify the R-peak. The detection must take care to prevent considering the two highest peaks that occur within 0.25 seconds as two separate peaks [100]. This ensures that the pseudo-R-beats are removed. The adjustment of the dynamic threshold to estimate the R-peaks, which are crucial to the detection process, is the other important factor. The correct threshold selection is essential since there will be a discernible amplitude difference level between R-peaks and non-R-peaks. The various thresholds in the range of $((0.3 \text{ to } 0.4) \times \max \text{R} - \text{peak amplitude})$ [31] and the optimal are chosen.

The likelihood of a false negative (FN) increases if the threshold is higher than necessary, while the false positive (FP) frequency ses if the threshold is lower. To accurately detect R-peak, the threshold is carefully chosen.

3.3.1 Illustration of R-peak detection from MIT-BIH-AD

The following simulations of MIT-BIH-AD records are displayed:

Record No. 107

It displays the complete heart block. R-peak detection is challenging in this circumstance as R-peaks are followed by high-amplitude T-waves. A brief section of record 107 (500-4500 samples) is chosen to contain paced beats to demonstrate the efficiency of the HSCW-BPF filter in R-peak detection. The HSCW-BPF filter has accurately recognized the R-peak by suppressing the T-wave as depicted in Figure 3.5(b). The successful delineation of R-peaks is represented in Figure 3.5(c).

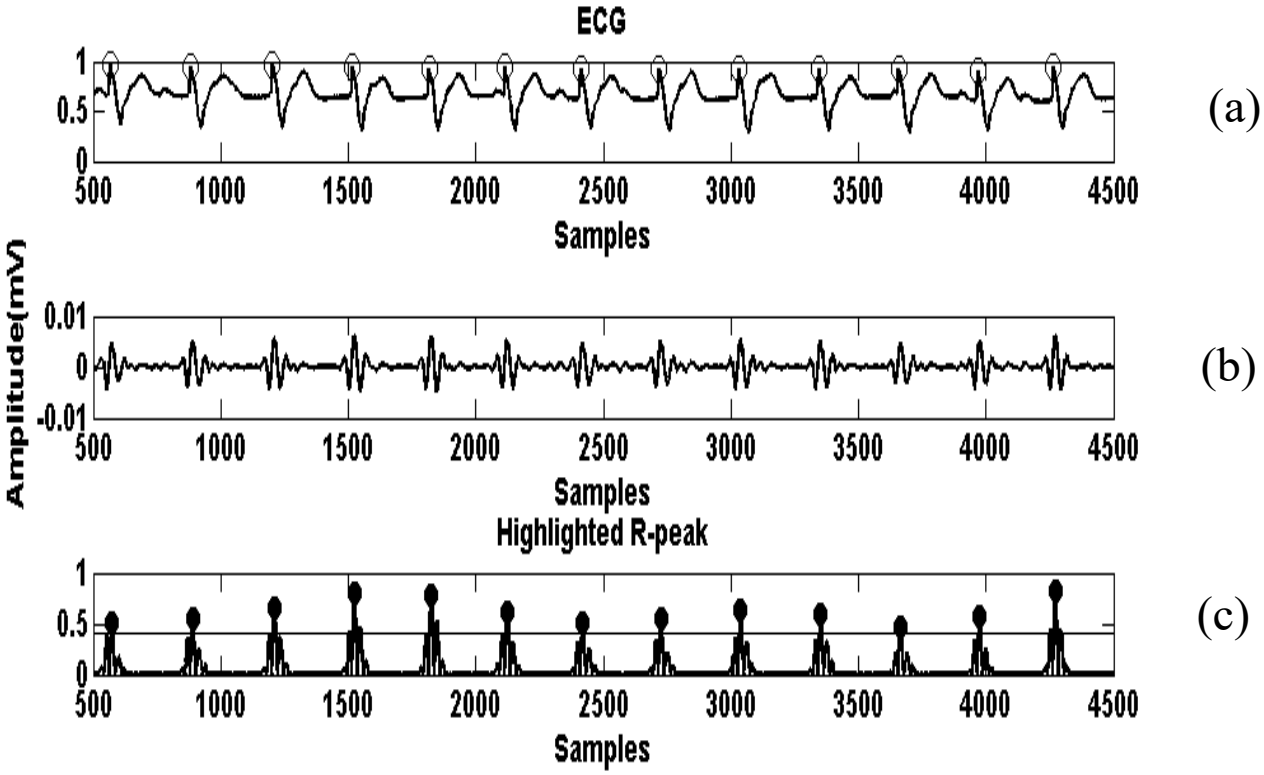

Figure 3.5 (a) ECG record no. 107 indicates a complete heart-block situation, (ranging from 1.38 to 12.50 seconds) empty circles indicate the R-peaks to be detected **(b)** output from HSCW-BPF filter **(c)** the output of HSCW-BPF is squared for better localization and filled circles depict the detected R-peaks.

Record No. 203

This record belongs to a male 43 years old. A segment of this record from 217055-219055 samples (591-606 seconds) is taken into consideration as it has highly changing QRS morphology (Figure 3.6(a)) due to axis shift with the influence of artifacts like muscle artifacts and baseline shifts and PVC (premature ventricular contraction) beats followed by tall T waves. All these artifacts and patterns attenuated the QRS morphology. As depicted in Figure 3.6, the HSCW-BPF filter has efficiently eliminated all these patterns while also eminently detecting R-peaks in the changing QRS morphology situation (Figure 3.6(c)).

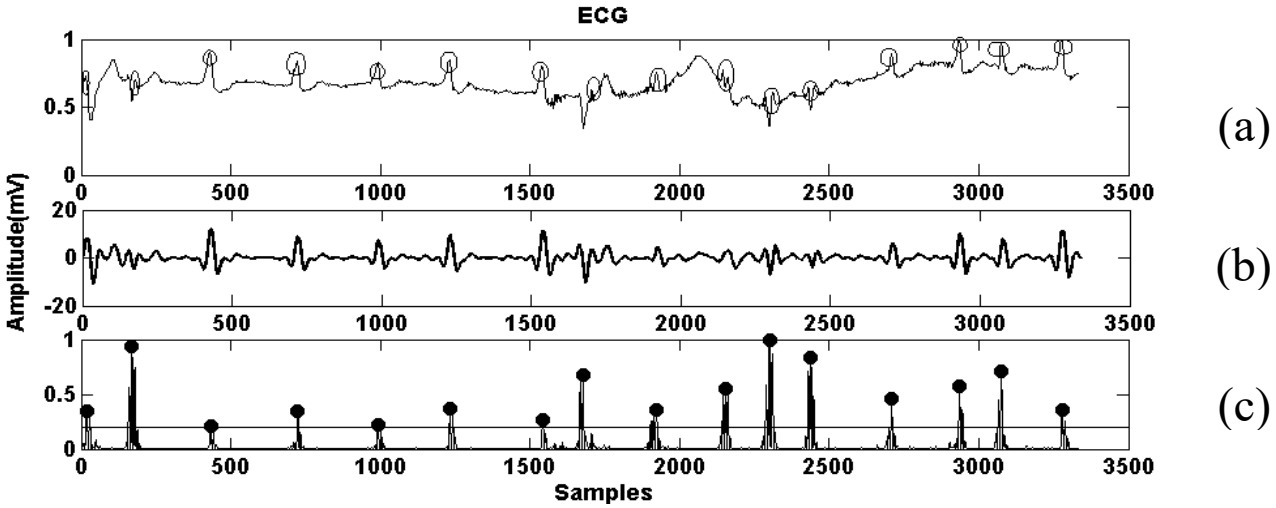

Figure 3.6 (a) The R-peak to be detected is highlighted by an empty circle ECG (record 203 ranging from 0 to 9.72 seconds) from MIT-BIH-AD that has changing QRS morphology and **(b)** the output of the HSCW-BPF filter **(c)** the output of HSCW-BPF is squared for better localization and filled circles depict the detected R-peaks.

Record No. 222

The most frequent artifact in ECG with low-frequency ranges such as 0-2.5 Hz is baseline drift. It is primarily caused during respiration and exercise. The baseline drift in ECG (1102-1112 seconds of record 222) is depicted in Figure 3.7(a). The HSCW-BPF effectively removes the baseline drift as depicted in Figure 3.7(b) and Figure 3.7(c) highlights the detected R-peaks.

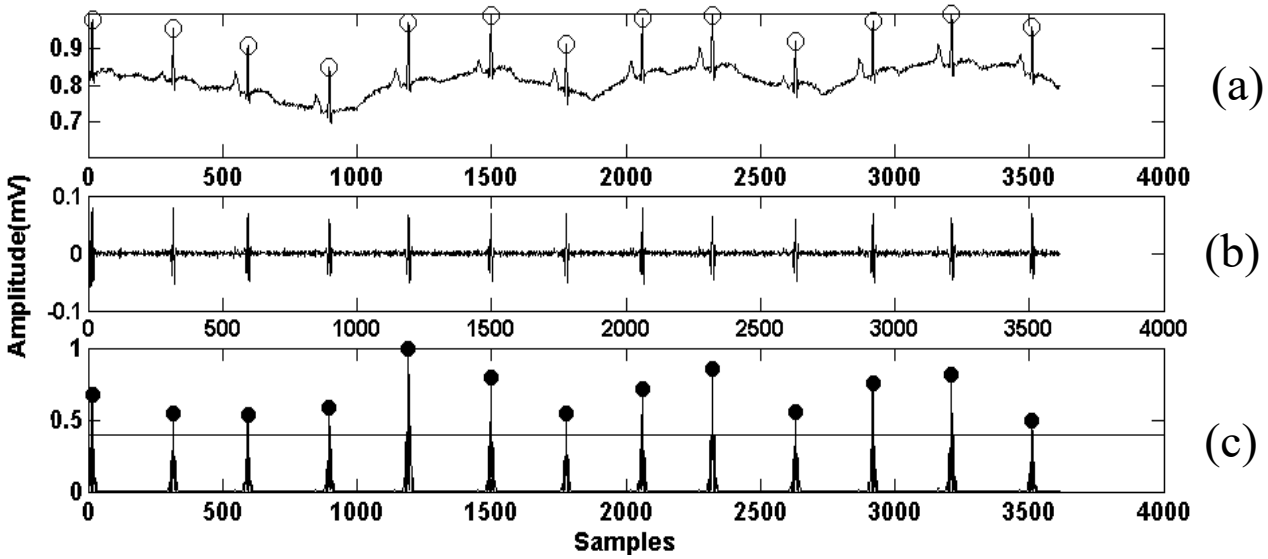

Figure 3.7 (a) ECG record no. 222 from MIT-BIH-AD has baseline drift ranging from 9.72 to 11.12 seconds **(b)** the HSCW-BPF filter output **(c)** the output of HSCW-BPF is squared for better localization and filled circles depict the detected R-peaks.

The illustration from MIT-BIH-AD clearly illustrates through the visual interpretation that the proposed method is effective in detecting R-peaks in various situations like changing QRS morphology, baseline drift, and in high amplitude T-wave.

3.3.2 Quantitative Analysis of MIT-BIH-AD

To perform the quantitative analysis, the work is tested on MIT-BIH-AD, and performance parameters such as sensitivity (*Sen*), positive predictivity (*PPe*), and error rate (Err) are computed. Sensitivity refers to test's ability to designate a subject as positive. The more is the value of sensitivity less is the number of False Negative and thus few cases of disease are missed. Positive predictivity is the proportion of cases giving positive test results who are already patients. It is the ratio of patients truly diagnosed as positive to all those who had positive test results. Accuracy represents how close a measurement comes to its true value.

They are defined as:

$$Sen = \frac{TP}{TP+FN} \tag{3.8}$$

$$PPe = \frac{TP}{TP+FP} \tag{3.9}$$

$$Err = \frac{FP+FN}{total\ detected\ beats} \tag{3.10}$$

where TP is the overall number of accurate R-peak identified in the record when compared to the annotation of each ECG signal record. By using the annotation as a reference, FN represents the overall number of missed R-peak. Additionally, FP is the total number of incorrectly identified R-peak or extra R-peaks identified as R-peaks. The proposed approach accuracy is determined by using Error (*Err*). A beat is regarded as a true beat if it occurs within the 100 ms range of the annotated time for each record, else it is regarded as a false beat [101].

The experimental findings for several of the MIT-BIH-AD records are tabulated in Table 3.2. The experimental results revealed a sensitivity of 99.93%, positive predictivity of 99.95%, and an error rate of 0.117% greater than any of the results obtained by algorithms that were published in the research literature [19, 31, 99, 102, 103]. The rest of the records all have an error rate lower than 1%, except for record number 201, which has an error rate of more than 1%. For the following records 100, 102, 113, 115-

117, 122-124, 212, 213, 217-221, 223, 230-232, the error rate is 0%, and the average values for TP, FN, and FP are 109416, 76 and 53 respectively.

Table 3.2 Experimental results of the proposed approach using HSCW-BPF

Record No.	**Actual beats**	**Detected beats**	**TP**	**FN**	**FP**	***Sen* (%)**	***PPe* (%)**	**Err (%)**
100	2273	2273	2273	0	0	100	100	0
101	1865	1865	1863	2	2	99.89	99.89	0.21
102	2187	2187	2187	0	0	100	100	0
103	2084	2081	2079	5	0	99.76	100	0.24
104	2229	2221	2215	14	6	99.37	99.72	0.9
105	2572	2571	2567	5	4	99.8	99.84	0.35
106	2027	2026	2025	2	1	99.90	99.95	0.14
107	2137	2137	2136	1	1	99.95	99.95	0.093
108	1763	1765	1763	0	2	100	99.88	0.11
109	2532	2531	2531	1	0	99.96	100	0.039
111	2124	2125	2124	0	1	100	99.95	0.047
112	2539	2540	2539	0	1	100	99.96	0.039
113	1795	1795	1795	0	0	100	100	0
114	1879	1880	1879	0	1	100	99.94	0.053
115	1953	1951	1951	0	0	100	100	0
116	2412	2412	2412	0	0	100	100	0
117	1535	1535	1535	0	0	100	100	0
118	2278	2279	2278	0	1	100	99.95	0.043
119	1987	1988	1987	0	1	100	99.94	0.0503
121	1863	1861	1861	2	0	99.89	100	0.107
122	2476	2476	2476	0	0	100	100	0
123	1518	1518	1518	0	0	100	100	0
124	1619	1619	1619	0	0	100	100	0
200	2601	2602	2601	0	1	100	99.96	0.038
201	1963	1960	1951	12	9	99.38	99.54	1.07
202	2136	2135	2135	1	0	99.95	100	0.046
203	2980	2979	2975	5	4	99.83	99.86	0.302
205	2656	2651	2650	6	0	99.77	100	0.22
207	1860	1857	1855	5	2	99.73	99.89	0.37
208	2955	2955	2952	3	3	99.89	99.89	0.203
209	3005	3006	3005	0	1	100	99.96	0.033
210	2650	2650	2649	1	1	99.96	99.96	0.075
212	2748	2748	2748	0	0	100	100	0
213	3251	3251	3251	0	0	100	100	0
214	2262	2261	2261	1	0	99.95	100	0.044
215	3363	3363	3359	4	4	99.88	99.88	0.237
217	2208	2208	2208	0	0	100	100	0
219	2154	2154	2154	0	0	100	100	0
220	2048	2048	2048	0	0	100	100	0
221	2427	2427	2427	0	0	100	100	0
222	2483	2484	2483	0	1	100	99.95	0.0402

223	2605	2605	2605	0	0	100	100	0
228	2053	2052	2049	4	3	99.8	99.85	0.341
230	2256	2256	2256	0	0	100	100	0
231	1571	1571	1571	0	0	100	100	0
232	1780	1780	1780	0	0	100	100	0
233	3079	3079	3077	2	2	99.93	99.93	0.12
234	2753	2754	2753	0	1	100	99.96	0.036
Total	109494	109472	109416	76	53	**99.93**	**99.95**	**0.117**

3.4 Comparison with state-of-the-art Methods

The performance of HSCW-BPF is assessed using MIT-BIH-AD and compared with the classical window-based bandpass filters using 15 records of MIT-BIH-AD. The experimental work for Hamming and Kaiser window-based filters for the detection of R-peak are presented in Tables 3.3 and 3.4, respectively.

Table 3.3 Experimental studies using Hamming window function

Record No.	**Actual beats**	**Detected Beats**	**TP**	**FN**	**FP**	***Sen* (%)**	***PPe* (%)**	***Err* (%)**
100	2273	2273	2273	0	0	100	100	0
101	1865	1865	1862	3	3	99.83	99.83	0.32
102	2187	2185	2185	0	2	100	99.90	0.091
103	2084	2081	2077	7	4	99.66	99.80	0.52
104	2229	2221	2214	15	7	99.32	99.68	0.99
105	2572	2573	2561	11	12	99.57	99.53	0.89
106	2027	2021	2019	8	2	99.6	99.9	0.49
107	2137	2136	2131	5	5	99.76	99.76	0.46
108	1763	1760	1743	20	17	98.86	99.03	2.10
109	2532	2533	2530	2	2	99.92	99.92	0.15
111	2124	2121	2121	3	0	99.85	100	0.14
112	2539	2541	2538	1	3	99.96	99.88	0.15
113	1795	1795	1795	0	0	100	100	0
114	1879	1879	1877	2	2	99.89	99.89	0.21
115	1953	1953	1953	0	0	100	100	0
Total	31959	31937	31879	77	59	99.75	99.81	0.42

Table 3.4 Experimental studies using Kaiser window function

Record No.	**Actual Beats**	**Detected Beats**	**TP**	**FN**	**FP**	***Sen* (%)**	***PPe* (%)**	***Err* (%)**
100	2273	2273	2273	0	0	100	100	0
101	1865	1863	1861	2	2	99.89	99.89	0.21
102	2187	2185	2185	0	0	100	100	0
103	2084	2081	2076	5	5	99.75	99.75	0.48
104	2229	2221	2213	16	8	99.28	99.63	1.08

105	2572	2567	2566	4	5	99.8	99.8	0.35
106	2027	2026	2022	4	4	99.8	99.8	0.39
107	2137	2136	2136	1	1	99.9	99.95	0.093
108	1763	1761	1745	18	16	98.97	99.09	1.93
109	2532	2530	2529	3	1	99.88	99.96	0.15
111	2124	2121	2121	3	0	99.85	100	0.14
112	2539	2541	2539	2	2	99.92	99.92	0.15
113	1795	1795	1795	0	0	100	100	0
114	1879	1879	1876	3	3	99.84	99.84	0.31
115	1953	1953	1953	0	0	100	100	0
Total	31959	31932	31890	61	47	99.8	99.85	0.33

Tables 3.2, 3.3, and 3.4 shows that the proposed method produces a lesser number of FN and FP for records 104, 106, 108, 109, 111, 112, and 114 than the Hamming and Kaiser windows-based bandpass filters. Records number (100-115) have an average error of 0.35% for HSCW-BPF, 2.10% for Hamming, and 1.93% for Kaiser. The records from 100-115 have *Err* below 0.5% for HSCW-BPF while in Hamming-based band pass filter records 103, 104, 105, and 108, and Kaiser-based bandpass filters records 104 and 108 have *Err* above 0.5%. The comparative bar graph for the number of FP, FN, and *Err* among these three window-based filters is displayed in Figure 3.8, Figure 3.9, and Figure 3.10 respectively for easier comprehension. Thus, it is evident that the proposed method achieved better performance in terms of reduced FP, FN, and *Err* than traditional window-based bandpass filters Hamming and Kaiser.

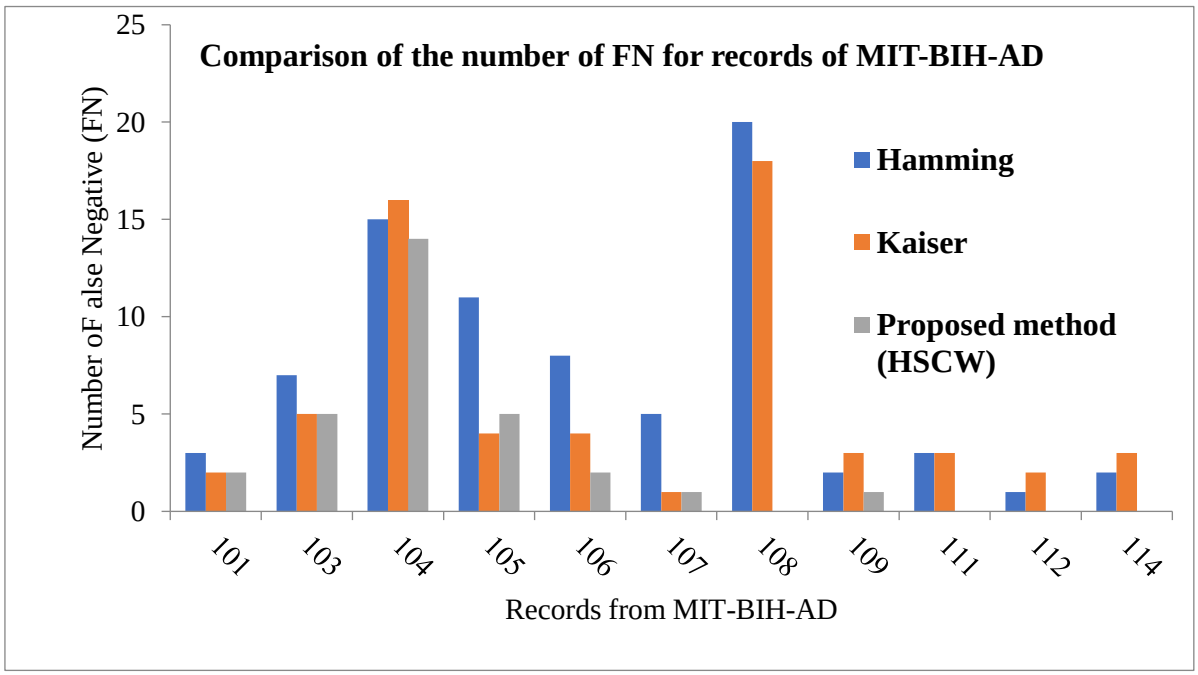

Figure 3.8 Comparison of FN counts for various MIT-BIH-AD records for three window-based filters – Hamming, Kaiser, and the proposed method (HSCW-BPF)

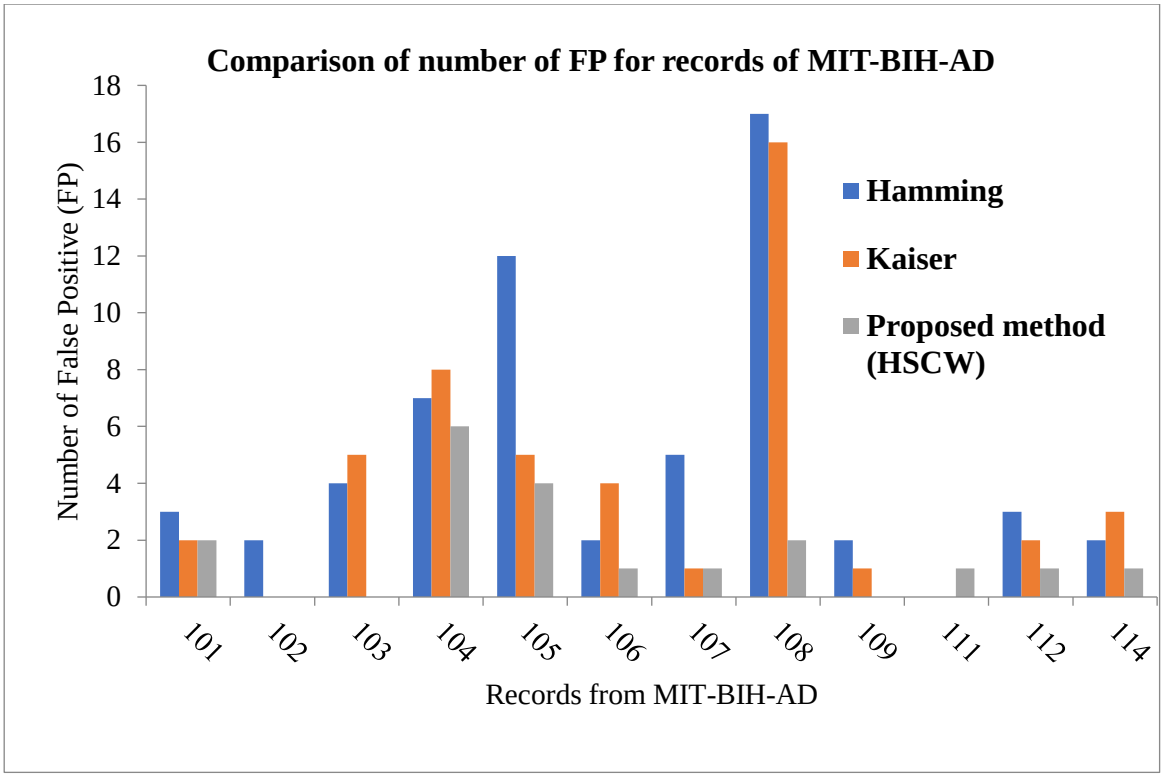

Figure 3.9 Comparison of FP count for various records of MIT-BIH-AD for three window-based filters – Hamming, Kaiser, and the proposed method (HSCW-BPF)

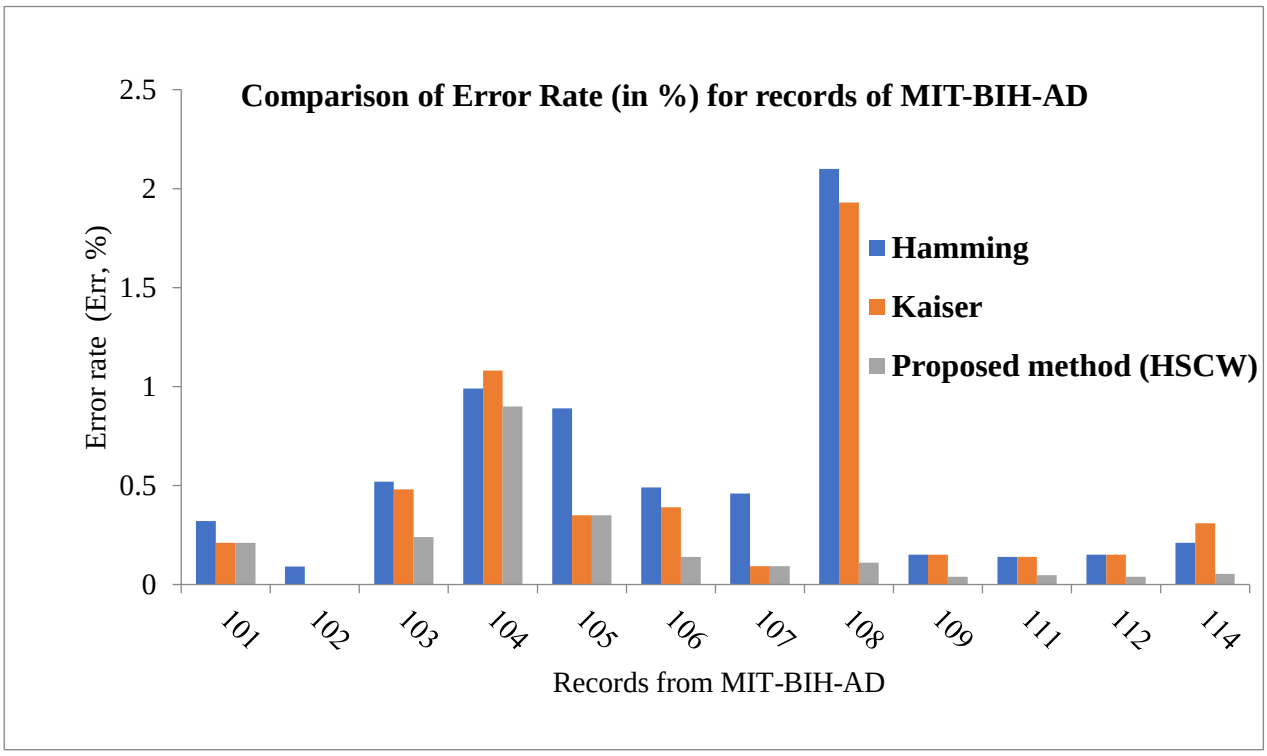

Figure 3.10 Comparison of error rate (%) for records of MIT-BIH-AD for three window-based filters – Hamming, Kaiser, and the proposed method (HSCW-BPF)

Record no. 203 in literature [19, 31, 99, 102, 103] has high FN and FP whereas the HSCW-BPF filter has decreased them to 5 and 4, respectively. Similarly, it has lower FN, FP, and *Err* than the literature [19, 31, 99, 102, 103] for records-108, 116, 210, 232. Table 3.5 compares the HSCW-BPF with well-known algorithms from the literature. Tables 3.6 and 3.7 respectively, depict the comparison of FN and FP of the proposed method with the earlier work mentioned in the literature [19, 31, 99, 102].

Table 3.5 Comparison of the results with other well-known algorithms

Methods	**Sensitivity (%)**	**Positive predictivity (%)**	**Error rate (%)**
Zidelmal *et al.* (2012) [31]	99.64	99.82	0.54
Sabherwal *et al*. (2017) [99]	99.9	99.9	0.16
Tompkins (1985) [103]	99.75	99.54	0.71
Phukpattaranont *et al.*(2015) [19]	99.88	99.81	0.38
Sharma *et al.* (2017) [102]	99.9	99.88	0.23
Proposed algorithm	**99.93**	**99.95**	**0.117**

Table 3.6 Comparison of the FN count for MIT-BIH-AD records

Records	**105**	**108**	**116**	**203**	**208**	**210**	**222**
Zidelmal *et al.* (2012) [31]	44	35	15	36	12	23	2
Sabherwal *et al.* (2017) [99]	4	0	6	21	2	5	5
Phukpattaranont *et al.* (2015) [19]	11	53	19	22	15	11	11
Sharma *et al.* (2017) [102]	15	7	20	30	17	0	0
Proposed algorithm	**5**	**0**	**0**	**5**	**3**	**1**	**0**

Table 3.7 Comparison of the FP count for MT-BIH-AD record

Record	**105**	**108**	**116**	**203**	**210**	**222**	**228**	**232**
Zidelmal *et al.* (2012) [31]	15	25	4	25	18	2	27	0
Sabherwal *et al.* (2017) [99]	8	0	4	11	6	6	7	15
Phukpattaranont *et al.* (2015) [19]	28	19	2	35	7	13	16	1
Sharma *et al.* (2017) [102]	32	10	2	12	3	1	22	8
Proposed algorithm	**4**	**2**	**0**	**4**	**1**	**1**	**3**	**0**

The suggested approach significantly improves performance metrics such as sensitivity, positive predictivity, and error rate for the detection of R-peaks, thus ranking it among the most efficient R-peaks detectors. It is evident in rich literature [19, 31, 99, 102, 103] that the error rate has been significantly reduced. Additionally, the proposed method has outperformed the outcomes of well-known window-based filters (Hamming and Kaiser) in terms of decreased false negatives, false positives, and error rates. The results of the experimental research demonstrate that the suggested method outperforms

other complex ECG patterns, such as those with high T-wave amplitude, high-grade noise, muscle artifacts and changing QRS morphology, and varying R-R intervals. The algorithm is also suitable for both normal and abnormal subjects.

3.5 Conclusion

A new and innovative method for R-peak detection is proposed for ECG biomedical signals. The suggested Self-Convolution Window-based FIR Filter is an amalgamation of two concepts, *i.e.,* convolution window and FIR filters. A new and novel R-peak detection technique is developed based on the proposed window concept. It is demonstrated above that the self-convolution window achieved narrow main lobe width and peak side lobe level of -93.90 dB which is significantly less than the traditional window functions in literature.

The self-convolution window has proved to possess fewer ripples in the stop-band as compared to well-known conventional window functions. Following this interpretation, the proposed algorithm employs Hamming Self-Convolution Window (HSCW**)** based band-pass filter for denoising ECG signals. The proposed work is used to eradicate the dominant artifacts like baseline wandering using high-pass HSCW filters and power line interference using low-pass HSCW filters. Thus, R-peak is detected in complete heart block situations, noisy ECG, and changing QRS morphology records.

The performance evaluation of the suggested algorithm when tested on the MIT-BIH-AD has produced superior results than those found in the existing literature, in terms of sensitivity, positive predictivity, and error rate, and the obtained values are 99.93%, 99.95%, and 0.117% respectively. The proposed approach detects R-peak with high efficiency and is robust to noise. The acquired results are better than those of published studies that demonstrate the superiority of the HSCW-BPF filter traditional Hamming and Kaiser window-based bandpass filters in identifying R-peaks.

Thus, the HSCW-BPF filtering applied to the ECG signals appears to be effective and outperforms the other well-known techniques. The suggested work can be expanded further to the convolution of different window functions.

The following are the primary characetristics that distinguish the proposed technique from recognised techniques:

- The self-convolution window concept is applied for the first time in biomedical signal for potential clinical purposes.
- The proposed filter based on the self-convolution window concept suppresses the ripples in the stop band effectively as the window based on the proposed approach has narrow main lobe width and very low side lobe level.
- It has reliably detected R-peaks in various complex patterns with a low false negative, false positive and error rate.

CHAPTER 4

ECG R-PEAK DETECTION USING RIESZ FRACTIONAL ORDER DIGITAL DIFFERENTIATOR

FRACTIONAL ORDER CALCULUS (FOC) has received significant attention in recent decades due to its widespread applications in physics and engineering. Fractional derivatives' successful applications and robustness in control theory have sparked interest in their introduction to the signal processing fields [52]. FOC applications are studied by designing digital fractional order differentiators or filters for noise reductions, critical information augmentation, and fractal signal synthesis [49].

Fractional-order differentiator proves to provide more peculiar details about the signal than its integer-order counterpart [10]. The concept of fractional-order calculus is employed for noise cancellation and artifact removal in ECG signals as it has the natural ability to reduce noise and boost valuable information [10]. This chapter aims to propose an efficient algorithm using Riesz fractional-order digital differentiator (RFODD) based on the differencing method for detecting R-peaks, which is a crucial criterion for evaluating cardiac problems. ECG waveforms are analyzed on various fractional orders of RFODD, and the results are validated through simulations and performance metrics.

4.1 Concept of Fractional-order Differentiator (FOD)

The main aim of the FOD design problem is to focus on designing a digital filter in such a way that its actual frequency response is similar to the ideal response of the former. The ideal frequency response of traditional FOD is represented by [55]

$$H_d(\omega) = (j\omega)^p \tag{4.1}$$

where p is a real number. Several signal processing applications have used FOD with an ideal response in (4.1). The frequency response of FOD in (4.1) has a j^p phase shift in the filter output, which is undesirable in some applications. As a result, the zero-phase shift response of FOD is given below [55]:

$$G_d(\omega) = |\omega|^p \tag{4.2}$$

The aforementioned FOD is referred to as Riesz FOD as it is related to the Riesz potential [55]. Considering the ideal response $G_d(\omega)$ in (4.2), the inverse continuous-time inverse Fourier Transform (FT) of the Riesz kernel, which depends on the fractional-order p is represented as [55]:

$$K_p(t) = \frac{1}{2\Gamma(-p)\cos(p\pi/2)} |t|^{-p-1} \tag{4.3}$$

where Γ denotes gamma function. The p^{th} order Riesz fractional derivative of function $x(t)$ based on the above kernel function is defined as follows:

$$D^p x(t) = x(t) * K_p(t) \tag{4.4}$$

where $*$ denotes the convolution operator. If $X(\omega)$ is the continuous-time FT of $x(t)$, the following frequency-domain relation is obtained

$$FT[D^p x(t)] = |\omega|^p X(\omega) \tag{4.5}$$

Thus, the ideal frequency response of Riesz FOD with zero phase shift is $G_d(\omega) = (\omega)^p$, as compared to traditional FOD based on Caputo and Riemann-Liouville fractional derivatives, which have a frequency response $H_d(\omega) = (j\omega)^p$ with a phase shift j^p [55]. The benefit of zero-phase filtering is that it lessens phase distortion [10] and aids in precisely locating R-peaks in the ECG waveform.

4.2 Riesz Fractional Order Digital Differentiator (RFODD)

The frequency response $G(e^{j\omega})$ of the zero-phase shift digital filter transfer function is abbreviated by $G(z)$, which fits the ideal response $G_d(\omega)$. The relation is represented in (4.6) between the ideal responses $G_d(\omega)$ and $H_d(\omega)$. The RFODD transfer function $G(z)$ can be acquired from the traditional FOD $H(z)$ whose frequency response approximates $H_d(\omega)$ [55] as given as:

$$G_d(\omega) = \frac{H_d(\omega)+H_d(-\omega)}{2\cos(p\pi/2)} \tag{4.6}$$

The frequency response $G_d(\omega)$ of RFODD is only the scaling even part of frequency response $H_d(\omega)$ of the conventional FOD. The scaling constant is $1/\cos(p\pi/2)$. The filter $G(z)$ will fit $G_d(\omega)$ well, if the frequency response of FOD $H(z)$ approximates $H_d(\omega)$ well. In (4.7), filter $G(z)$ is presented as [55]

$$G(z) = \frac{1}{2\cos(p\pi/2)}\left(H(z) + H(z^{-1})\right) \tag{4.7}$$

Following, the objective is to design RFODD using the differencing method. The transfer function to design conventional FOD is presented by [55]

$$\begin{aligned} H(z) &= (1-z^{-1})^p \\ &= \sum_{k=0}^{\infty}(-1)^k C_k^p z^{-k} \end{aligned} \tag{4.8}$$

where coefficients C_k^p is defined as [55]

$$\begin{aligned} C_k^p &= \frac{\Gamma(p+1)}{\Gamma(k+1)\Gamma(p-k+1)} \\ &= \begin{cases} 1, & k=0 \\ \frac{p(p-1)(p-2)\cdots(p-k+1)}{1.2.3\cdots k}, & k\geq 1 \end{cases} \end{aligned} \tag{4.9}$$

Substituting (4.8) into (4.7), the transfer function of RFODD is acquired as

$$\begin{aligned} G(z) &= \frac{1}{2\cos(p\pi/2)}\left((1-z^{-1})^p + (1-z)^p\right) \\ &= \frac{1}{2\cos(p\pi/2)}\left(\sum_{k=0}^{\infty}(-1)^k C_k^p z^{-k} + \sum_{k=0}^{\infty}(-1)^k C_k^p z^k\right) \\ &= g(0) + \sum_{k=1}^{\infty} g(k)(z^{-k} + z^k) \end{aligned} \tag{4.10}$$

where coefficients $g(k)$ is given by [55]

$$g(k) = \begin{cases} \frac{(-1)^k C_k^p}{2\cos(p\pi/2)}, k \geq 1 \\ \frac{1}{\cos(p\pi/2)}, k = 0 \end{cases} \tag{4.11}$$

Substituting $z = e^{j\omega}$ in (4.10)

$$\begin{aligned} G\left(e^{j\omega}\right) &= \frac{1}{2\cos(p\pi/2)}\left(\left(1-e^{-j\omega}\right)^p + (1-e^{j\omega})^p\right) \\ &= \frac{1}{2\cos(p\pi/2)}\left(e^{-\omega p/2}\left(e^{j(\omega/2)} - e^{-j(\omega/2)}\right)^p\right) + (e^{\omega p/2}(e^{-j(\omega/2)} + \\ & e^{j(\omega/2)})^p) \end{aligned}$$

$$= \begin{cases} \frac{1}{2\cos(p\pi/2)}\left(j^p e^{-\omega p/2} + (-j)^p e^{\omega p/2}\right)(2\sin(\frac{\omega}{2}))^p, \omega \geq 0 \\ \frac{1}{2\cos(p\pi/2)}\left((-j)^p e^{-\omega p/2} + j^p e^{\omega p/2}\right)(2\sin(\frac{-\omega}{2}))^p, \omega < 0 \end{cases}$$

$$= \frac{\cos((p/2)(\pi - |\omega|))}{\cos(p\pi/2)}(2\sin(\frac{|\omega|}{2}))^p \quad (4.12)$$

When frequency ω is small, then $G\left(e^{j\omega}\right) = |\omega|^p$ holds. Thus, $G(z)$ fits the ideal response $G_d(\omega)$ at the low-frequency band. The phase of $G(e^{j\omega})$ is zero, therefore, no phase distortion occurred due to FOD $G(z)$ in (4.10) [55].

It is clear from the literature that fractional-order calculus preserves the signal's detail more effectively than integer-order calculus [10, 16]. Additionally, RFODD has zero phase shift, it efficiently minimizes the phase distortion and aids in locating R-peaks in ECG waveforms at exact locations, which in turn proves to be helpful in automatic R-peak detectors.

4.3 RFODD in ECG Signal Processing

Figure 4.1 depicts the algorithm suggested for the delineation of R-peaks in the ECG waveform using RFODD. ECG waveforms are taken from the MIT-BIH-AD [40] to assess the effectiveness of the proposed approach. The MIT-BIH-AD has 48 records of half-an-hour fragments of two-channel ambulatory, *i.e.*, each record consisting of upper and lower leads. One of the leads prominently displays the QRS complex [31]. Thus, the upper lead is employed by default. Therefore, only one channel with a prominent QRS signal is chosen. Each ECG record is converted to digital form at 360 Hz with an 11-bit resolution and a 10 mV range [104]. ECG is pre-processed with the band-pass filter and the output is passed through RFODD, to acquire the fractional derivative of the signal. The R-peaks in the QRS complex of ECG are further detected using novel thresholding.

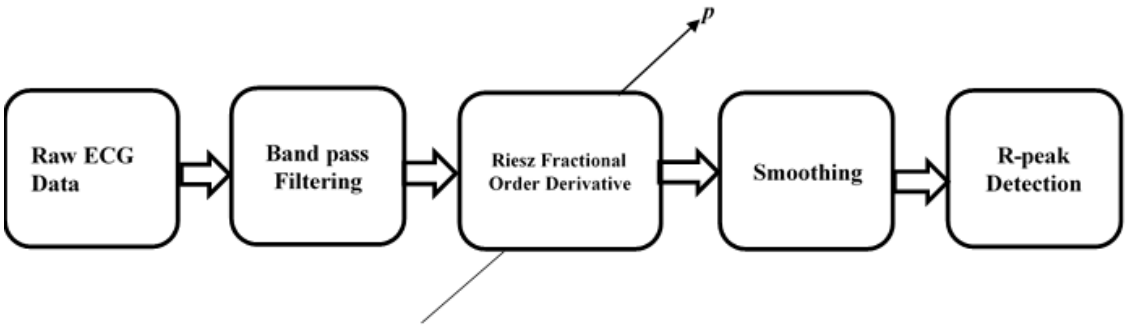

Figure 4.1 Block representation of the proposed algorithm (here *p* is the fractional-order)

ECG waveforms are often altered in real-world situations, with numerous types of noises and artifacts such as power line interference and electromyogram because of motion artifacts and muscle contraction, baseline wanders owing to respiration, instrumentation noise, etc. Some of these distortions significantly alter the ECG morphology, therefore making the analysis a tough task especially when computer-aided algorithms are employed.

The MIT-BIH-AD ECG signals have high-frequency noises (power line interference, electromyogram due to motion artifacts) and low-frequency noises (baseline wander), to eliminate these noises, band-pass filtering is employed. The Butterworth filter is used because it has a maximum flat frequency response in the pass band. The band-pass filter has a lower and higher cut-off frequency of 5 Hz and 25 Hz (QRS complex has a frequency band 5-25 Hz [99]. The artifacts like power line interference (50Hz) and baseline wander (nearly 1 Hz) are eliminated.

Afterward, the aim is to accentuate the QRS complex in ECG. The high frequency of the signal is enhanced by the derivative [99]. To emphasize the high frequency, which is the defining property of the QRS complex [99], and to attenuate the lower frequency P and T waves, the Riesz-based derivative is generated for the clean ECG (de-noised ECG) signal. The amplification of R-peak in the *suggested* Riesz-based fractional differentiation step has removed the necessity for a squaring operation or Shannon energy envelope which would otherwise have increased the computing cost and time. During this signal differentiation operation, the high-frequency noises (which have spectral content identical to that of the QRS complex of ECG) are also enhanced, but the moving window average filter eliminates these [99]. A moving average filter is then applied to the transformed signal after this step [30]. It is a window-based averaging filter that functions as a low-pass filter and is given below

$$y(n) = \frac{1}{N}[x\big(n-(N-1)\big) + x\big(n-(N-2)\big) + \cdots x(n)] \tag{4.13}$$

where N is the length of the selected window. The selection of a suitable window length is crucial for achieving better performance. Mostly, the width of the moving average filter window is often set to be equal to the duration of the QRS complex. If the window chosen is narrow, then numerous peaks for a single QRS complex are created. It results in false detection (FP) of R-peaks if the right thresholding approach is not adopted for its detection. If the window chosen is very wide, then it takes additional T-peaks in

integration. Due to the enormous number of samples, the amplitude of the envelope in the processed signal is diminished and the signal's shape is not extracted accurately and some R-peaks are not identified (FN).

The QRS complex in ECG signals lasts for about 100 ms [30]. The MIT-BIH-AD ECG signal sampling rate is 360 Hz [20]. As the consequence, the window size $(100 \times 10^{-6} \times 360)$ [30] is chosen as 36 samples, which is roughly the duration of the QRS complex. The impact of different window sizes i.e. narrow (10 samples), equals to QRS duration (36 samples) and wide (100 samples) moving average filter is illustrated in [30] i.e. narrow and wide window of moving average filter will raise FP and false-negative FN respectively. Therefore, 36 samples, which are nearly equivalent to the QRS span are chosen as the size of the window.

The flow diagram for the thresholding technique, which is used to detect R-peaks on the smooth ECG waveform $y(n)$ is illustrated in Figure 4.2. The technique consists of three processes: (i) QRS localization, (ii) Discarding multiple peak detection, and (iii) finding the missed peak in search-back.

a) Set a threshold $th = 0.3 \times \max(y)$, if $y \geq th$ then location $n \rightarrow QRS$, else location $n \rightarrow not\ QRS$. As the QRS sample lasts for 36 samples or 100 ms, two peaks that occur within that time frame should be treated as the same peak [104, 105].
b) It must make sure that two of the highest peaks occurring during the refractory period (200ms or 72 samples) are treated as two different peaks to prevent duplicate detections of R-peaks. To prevent pseudo-R-peaks, one of them is excluded [100]. The absolute refractory period is the interval between the termination of the QRS complex and the start of the T-wave (an additional stimulus cannot trigger a new action potential, regardless of the intensity of the stimulus). The relative refractory time follows the absolute refractory period (a strong stimulation may trigger a new action potential). The latter occurs at the apex of the T-wave. Thus, ventricular depolarization is prevented in this situation due to a physiological constraint. So, one peak is eliminated.
c) To find missing peaks, peaks are sought with a new threshold (th1) that is 0.25 times the original threshold if no peak is found within or close to an average RR interval (RR avg., which is the time between two consecutive R-peaks). The

newly identified peak with $th1$ should be 200ms from the previously detected peak with th. The search back method is used once again to find missing peaks with threshold *th1* if the newly identified peak and the previously detected peak do not have peaks within or close to an average RR interval. Until all of the missed peaks are found, this process is repeated.

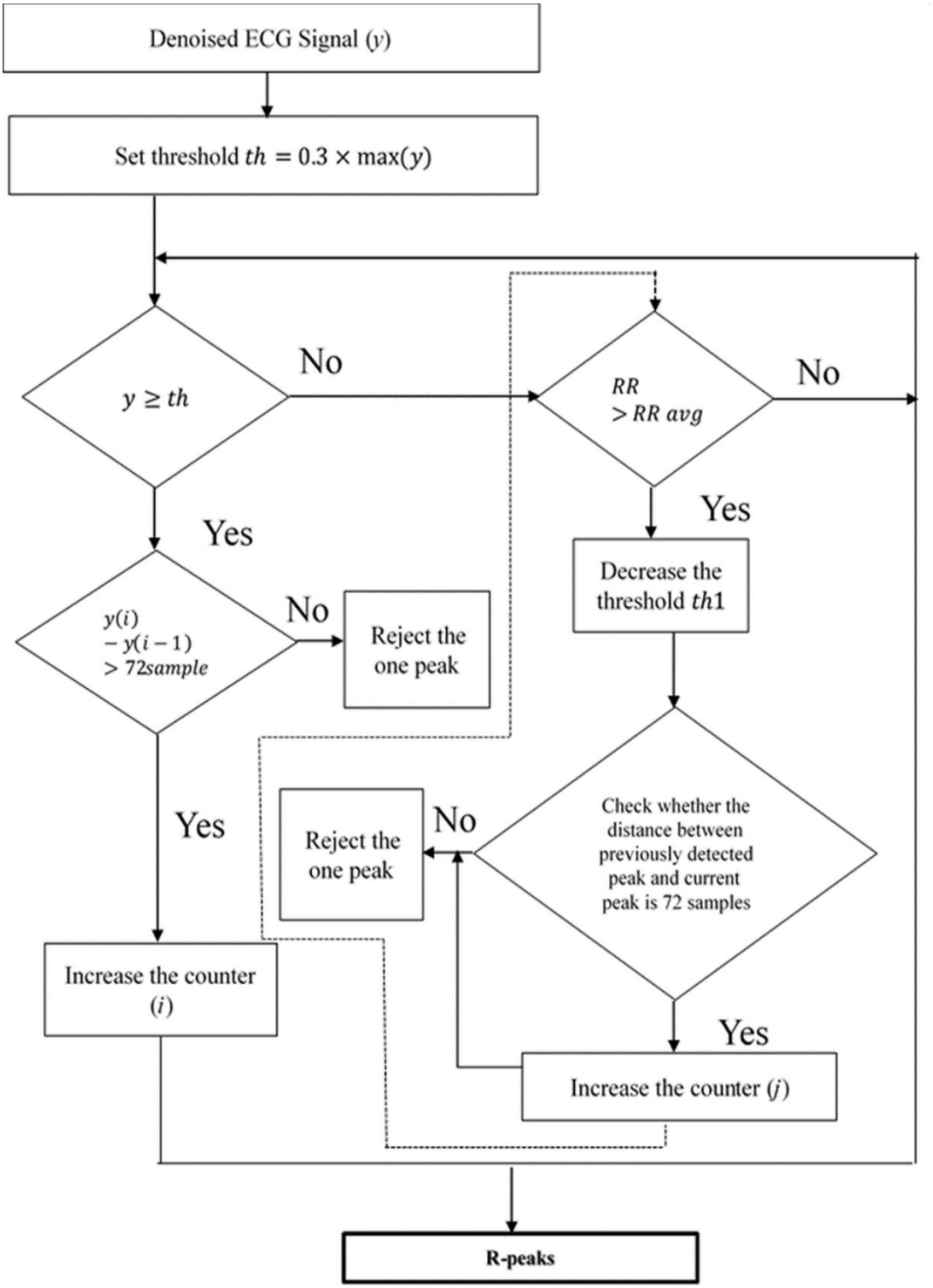

Figure 4.2 Flow chart of the *proposed* threshold technique for R-peak detection.

4.3.1 Selection of optimal fractional-order parameter

ECG records are obtained from the MIT-BIH-AD. In the pre-processing, band-pass filtering maintains 5-25 Hz frequency components in ECG waveform only (as mentioned in section 4.3). A differentiation operation based on Riesz fractional order is performed following this step. The high-frequency components and the low-frequency components of the signal are magnified and attenuated, respectively, by the differentiation operation. ECG waveform is examined on various fractional order (p), $(p = 0.1, 0.2, 0.3, 0.4, 0.5, 0.6, 0.7, 0.8, 0.9)$ to select the best optimal fractional order.

By varying the fractional order of RFODD as depicted in Figure 4.3. The visual interpretation supports the conclusion that fractional-orders RFODD like $(p = 0.1, 0.2, 0.3, 0.4)$ are less effective than fractional-orders RFODD $(p = 0.5, 0.6, 0.7, 0.8, 0.9)$ at attenuating the lower frequency components of the signal. In comparison to integer-order calculus, fractional-order calculus better captures the details of the signal [10, 16]. Some details tend to lose when the fractional order (p) approaches unity $(p \to 1)$ — the case of integer order calculus.

A small section of the ECG waveform is circled in Figure 4.3 for analyzing ECG at different fractional orders (p). It is obvious from the visual analysis that lower fractional orders $(p = 0.1, 0.2, 0.3, 0.4)$ of RFODD are ineffective at attenuating the lower frequency components, whereas higher fractional orders (p=0.5, 0.6, 0.7, 0.8, 0.9) can do so. The visual interpretation reveals that some information is lost when the fractional order (p) approaches unity.

The circled portion of Figure 4.3 is zoomed into Figure 4.4, which demonstrates that the lower fractional-order (p) fails to effectively remove the artifacts, leading to multiple peaks. As the fractional-order (p) increases, artifacts are eliminated effectively and as (p) gets closer to unity, some information is lost (as in the case of integer-order calculus) and a smooth curve with one peak is acquired. The fractional order $(p = 0.6)$ is responsible for giving the lower frequency components proper attenuations while retaining the crucial information. Therefore, to better preserve the signal's information, the fractional-order value $p = 0.6$ is selected. In terms of sensitivity (Sen), positive predictivity (PPe), and error rate (Err) (defined in chapter 3), the quantitative analysis has achieved better findings at $p = 0.6$.

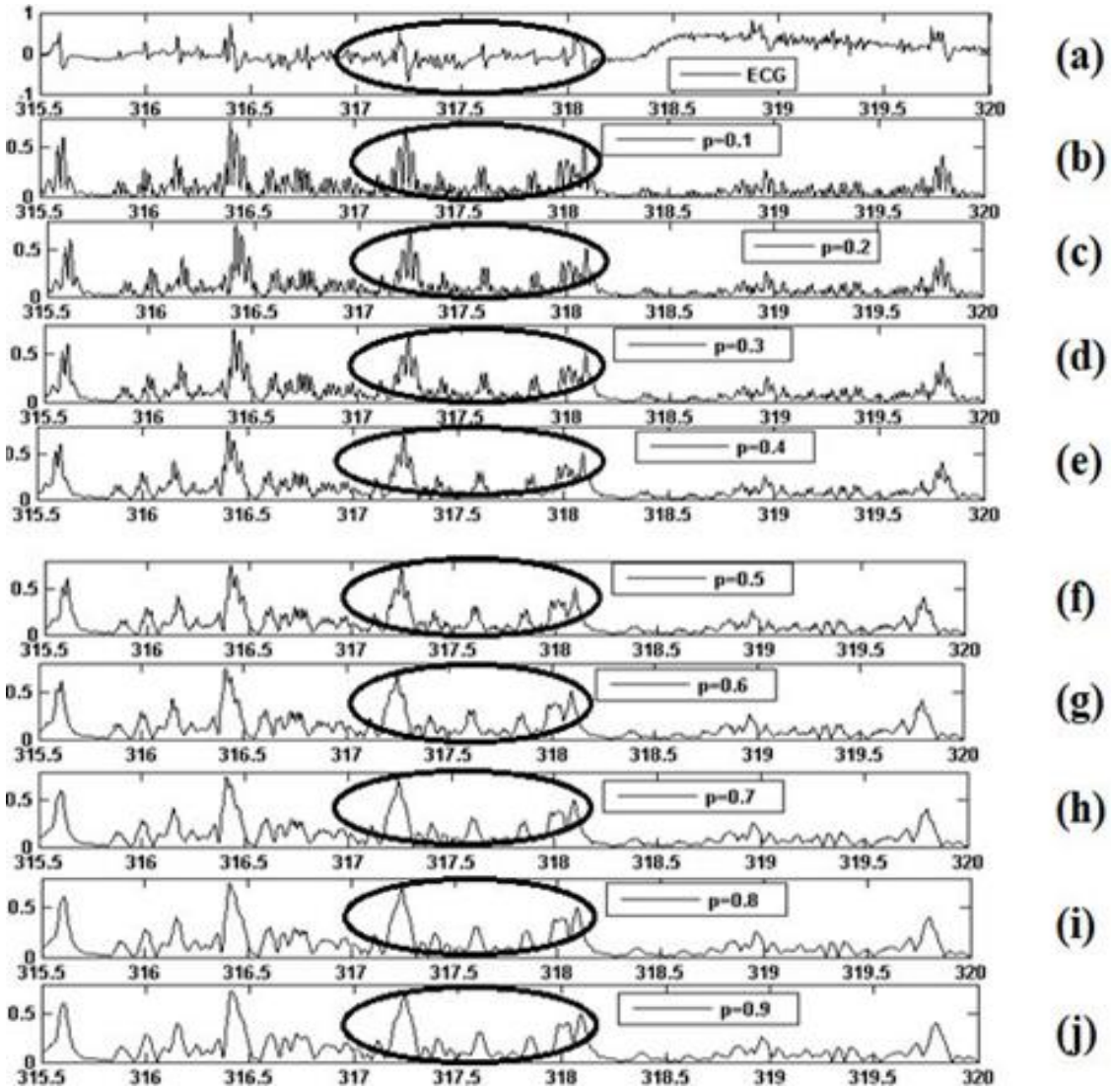

Figure 4.3 ECG **Record no. 104** with burst noise at various fractional orders (p)

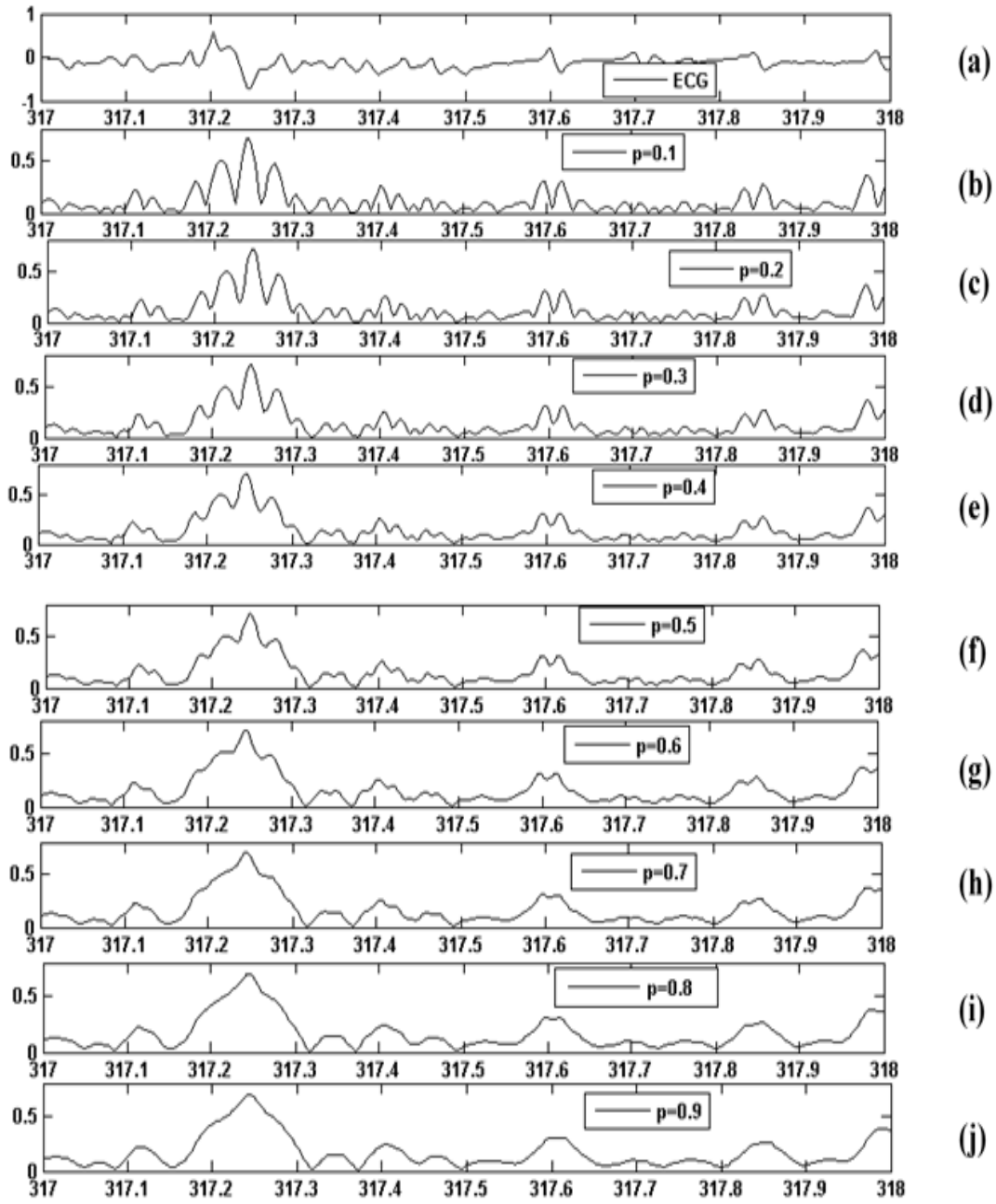

Figure 4.4 Zoomed plot of the encircled section of Figure 4.3

For quantitative analysis, the different fractional orders of the RFODD are used to calculate statistical metrics like sensitivity (Sen), positive predictivity (PPe), and error rate (Err). The performance evaluation metrics Sen, PPe, and Err are assessed at various fractional orders (p) of RFODD using few records of ECG. Table 4.1 presents the experimental findings of ECG records. The fractional orders, p=0.1, 0.2, 0.3, 0.4 of RFODD have lesser values of Sen, PPe and high values of Err, while the fractional-order 0.6 has given better results like increased Sen, PPe, and lower Err, as compared to the other fractional-orders, supporting the assertion of visual interpretation. As the

fractional order of RFODD is increased from 0.6 to 1, *Sen* and *PPe* have worsened and *Err* has increased.

Table 4.1 Various parameter performances of different ECG records at different fractional orders (p)

Record Nos. / Parameters	104	107	116	210
$\boldsymbol{p = 0.1}$				
$\boldsymbol{Sen}$	99.73	100	99.95	99.92
$\boldsymbol{PPe}$	99.91	100	100	99.96
$\boldsymbol{Err}$	0.358	0	0.041	0.075
$\boldsymbol{p = 0.2}$				
$\boldsymbol{Sen}$	99.73	100	99.95	99.92
$\boldsymbol{PPe}$	99.91	100	100	99.96
$\boldsymbol{Err}$	0.358	0	0.041	0.075
$\boldsymbol{p = 0.3}$				
$\boldsymbol{Sen}$	99.82	100	99.95	99.92
$\boldsymbol{PPe}$	99.86	100	100	99.96
$\boldsymbol{Err}$	0.314	0	0.041	0.075
$\boldsymbol{p = 0.4}$				
$\boldsymbol{Sen}$	99.86	100	99.95	99.92
$\boldsymbol{PPe}$	99.86	100	100	99.96
$\boldsymbol{Err}$	0.269	0	0.041	0.075
$\boldsymbol{p = 0.5}$				
$\boldsymbol{Sen}$	99.91	100	99.95	99.96
$\boldsymbol{PP}$e	99.86	100	100	99.96
$\boldsymbol{Err}$	0.224	0	0.041	0.075
$\boldsymbol{p = 0.6}$				
$\boldsymbol{Sen}$	99.95	100	100	99.96
$\boldsymbol{PP}$e	99.86	100	100	100
$\boldsymbol{Err}$	0.179	0	0	0.037
$\boldsymbol{p = 0.7}$				
$\boldsymbol{Sen}$	99.91	100	100	99.96
$\boldsymbol{PPe}$	99.86	100	100	100
$\boldsymbol{Err}$	0.224	0	0	0.037
$\boldsymbol{p = 0.8}$				
$\boldsymbol{Sen}$	99.91	100	100	99.96
$\boldsymbol{PPe}$	99.86	100	100	100
$\boldsymbol{Err}$	0.224	0	0	0.037
$\boldsymbol{p = 0.9}$				
$\boldsymbol{Sen}$	99.91	100	99.95	99.96
$\boldsymbol{PPe}$	99.86	100	100	100
$\boldsymbol{Err}$	0.224	0	0.041	0.037

At $p = 0.6$, the **record no. 104** has attained the highest Sen of 99.95% and lower Err of 0.179% and at all other values of p $(0.1, 0.2, 0.3, 0.4, 0.5, 0.7, 0.8, 0.9)$ of RFODD, it has a lower Sen values and higher Err.

R**ecord no. 116** has achieved the highest Sen of 100% and the lower 0% ER at $p = 0.6, 0.7,$ and 0.8. Similarly, the maximum values of *Sen* and PPe in **record no. 210 are** 99.96% and 100% respectively, and the lowest value of Err is 0.037% at $p = 0.6, 0.7, 0.8$ and 0.9. As indicated, RFODD at fractional orders, $p = 0.1, 0.2, 0.3, 0.4,$ and 0.5 artifacts are not eliminated properly, occasionally leading to multiple peaks (as mentioned earlier). Hence, increasing R-peaks' false detection in ECG and therefore increasing *Err* as a consequence and deteriorating *Sen* and *PPe*. Here, the results and quantitative analysis yield better outcomes for the fractional-order, $p = 0.6$, in terms of enhanced Sen, PPe and reduced Err for records 104, 210, and 116. In comparison to earlier methods suggested in the literature [31, 51, 52, 99, 106], it also produces better results for the same records.

4.3.2 Illustration of R-peak detection from MIT-BIH-AD

The list of MIT-BIH-AD records of studies are:

Test 1: A complete heart block situation is indicated in **record no. 107**. It is challenging to identify the R-peak detection in this record as the amplitude of its T-peaks succeeded the R-peak amplitudes. A brief section of the record ranging from 0 to 14 seconds is seen in Figure 4.5 (a). By suppressing high amplitude T-peaks, the proposed approach has correctly detected the R-peaks. The 5-25 Hz frequency components of the ECG wave are retained by band-pass filtering, the Riesz derivative suppresses the low-frequency T-waves, enhances the high-frequency QRS complex, and the ECG waveform is smoothed by the averaging filter. Figure 4.5(b), Figure 4.5(c), and Figure 4.5(d) demonstrate the band-pass filtering, Riesz derivative operation, and smoothen ECG signal respectively.

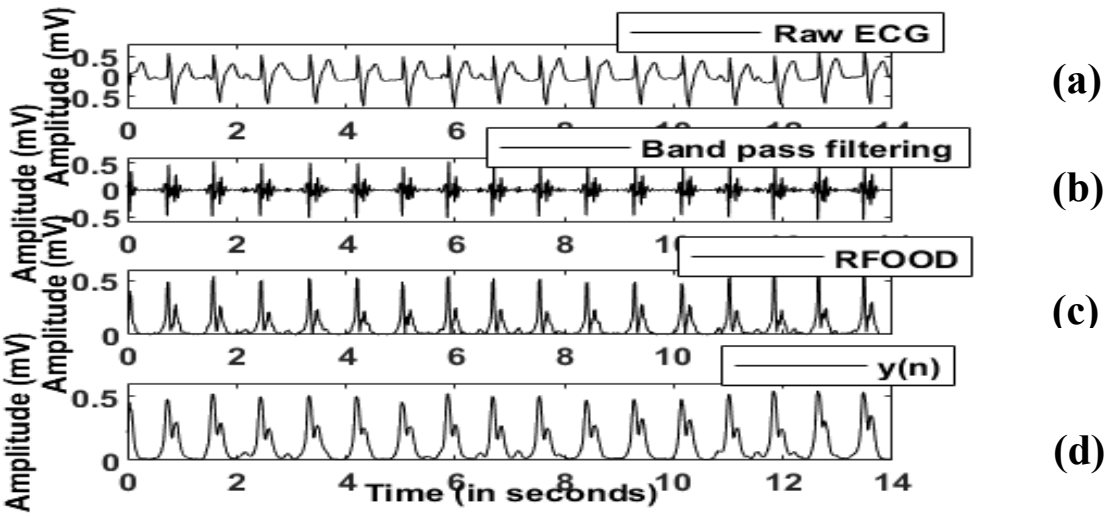

Figure 4.5 (a) ECG **record no. 107** indicating high T-peak amplitude **(b)** band-pass filtering **(c)** Riesz derivative **(d)** smooth ECG waveform

Test 2: The **record no. 200** aged 66 years has many bursts of muscle noise, therefore, making the R-peak detection a tough task. To demonstrate the effectiveness of the proposed approach at suppressing the burst noise and detecting R-peaks, a segment from 304 to 316 seconds is selected. Figure 4.6(a) depicts the segment of record no. 200, Figure 4.6(b) depicts the Riesz derivative of the signal therefore, emphasizing the high-frequency QRS complex, and Figure 4.6(c) indicates a smooth ECG signal by using a moving average filter. The proposed approach successfully identified R-peaks in presence of burst muscle.

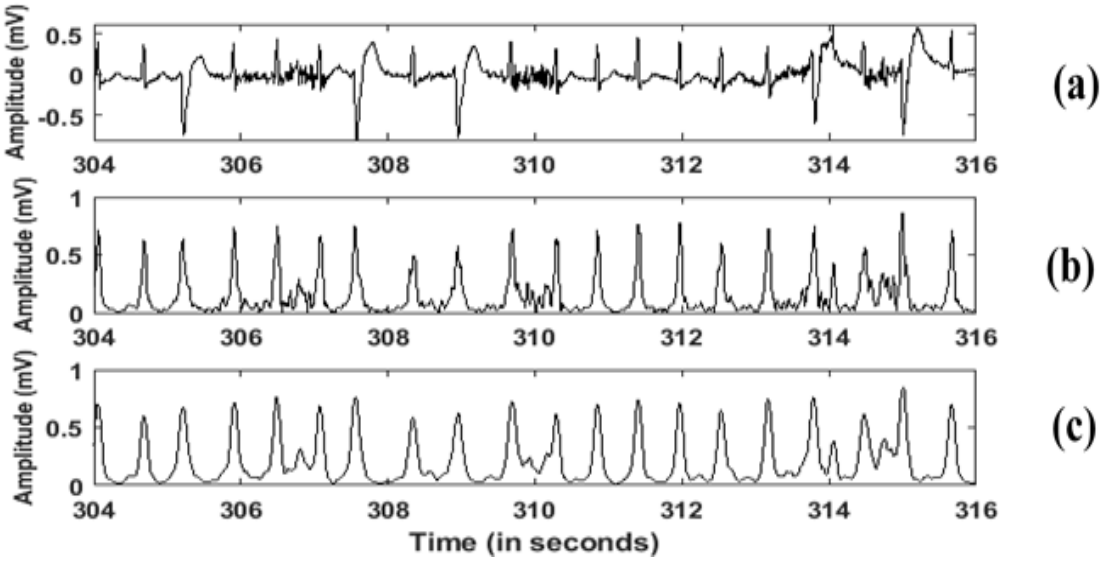

Figure 4.6 (a) depicts burst noise in **record no. 200 (b)** Riesz derivative of the signal enhancing high-frequency QRS complex **(c)** smooth ECG waveform for R-peak detection

Test 3: The MIT-BIH-AD **record no. 116** has an inverted R-peak in the ECG waveform as depicted in Figure 4.7(a). A segment from 20 to 30 seconds is selected for demonstrating the successful delineation of R-peak enhancement. The Riesz derivative of the same and magnified high-frequency component i.e., the QRS complex is shown in Figure 4.7(b). The smooth ECG waveform for R-peak detection is represented in Figure 4.7(c).

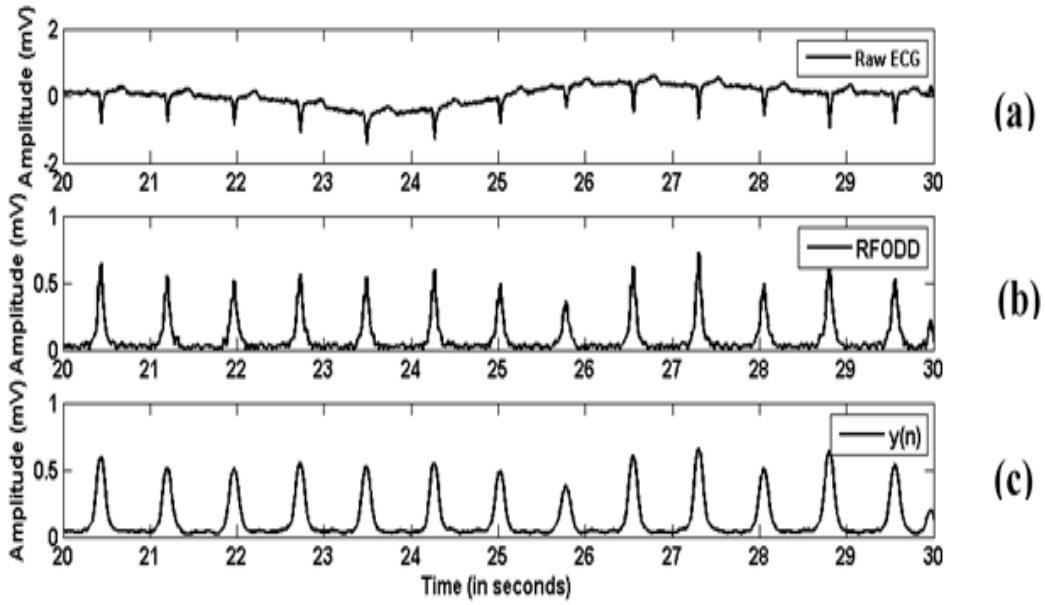

Figure 4.7 (a) Plot of ECG waveform of **record 116** depicting inverted R-peaks **(b)** Riesz derivative of the same waveform attenuating the low-frequency T peaks while enhancing the high-frequency inverted R-waves and **(c)** The averaging filter smooths the ECG waveform for detection of R-peaks

Test 4: The ECG records occasionally consist of varying RR intervals and changing QRS morphology. Therefore, two sections from **record no. 203** are selected ranging from 0 to 27 seconds and 600 to 608 seconds representing varying RR intervals and changing QRS morphology, respectively. Figure 4.8(a) is indicating the varying RR interval segment which spans 0 to 27 seconds. Riesz derivative elevating the R-peak and diminishing other frequency components in ECG is represented in Figure 4.8(b) and for the correct detection of R-peak, smoothing of ECG by an averaging filter is indicated in Figure 4.8(c).

Figure 4.9(a) indicates the segment from 600 to 608 seconds that has changing QRS morphology. The proposed approach based on the Riesz derivative enhances the R-peak in this situation too and the plot is depicted in Figure 4.9(b) and the smoothing of

the same wave is represented in Figure 4.9(c). The R-peaks are identified using the thresholding method on the smoothened ECG wave.

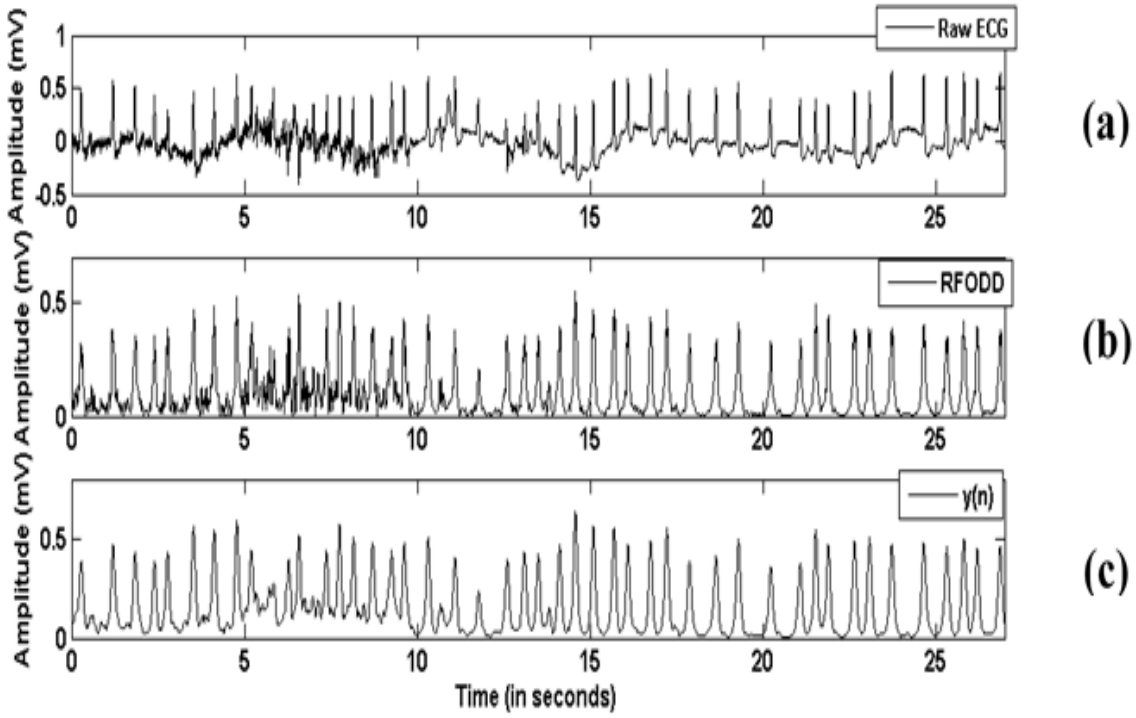

Figure 4.8 (a) Record no. 203 representing the varying RR interval **(b)** Riesz-based derivative magnifying high-frequency QRS complex **(c)** The even ECG wave smoothened by a moving average filter for correct R-peaks delineation

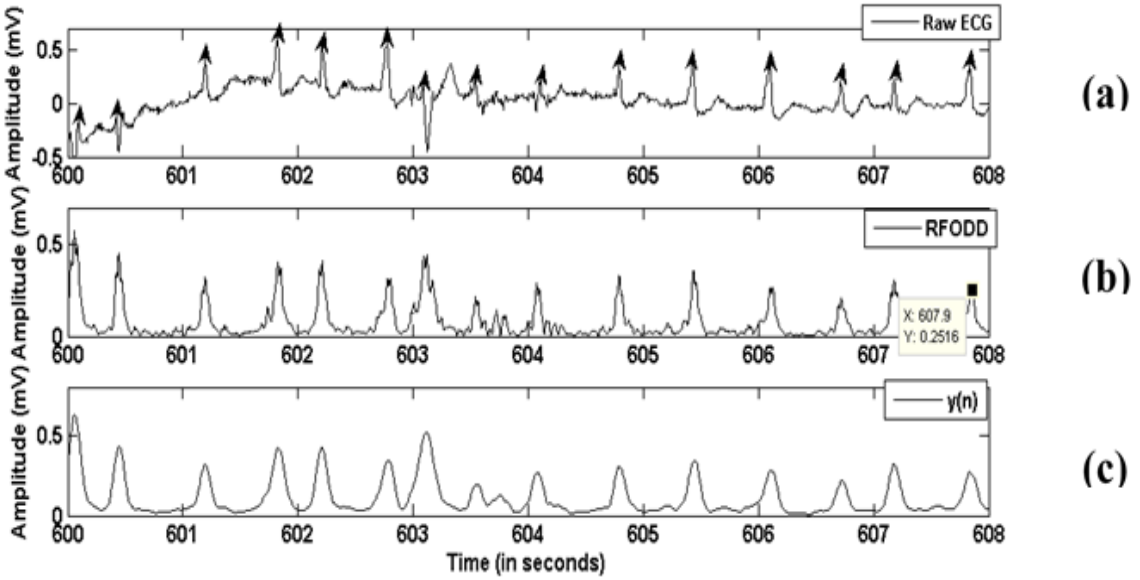

Figure 4.9 (a) The other plot of **record no. 203** exhibits changing QRS morphology **(b)** Riesz derivative amplifies the high-frequency component irrespective of the morphology **(c)** smooth ECG beat of the same segment for efficient QRS detection

4.3.3 Quantitative analysis of MIT-BIH-AD

The quantitative analysis of 48 records of the MIT-BIH-AD is performed to demonstrate the superiority of the proposed approach. The performance parameters Sen, PPe, and Err for the proposed method are 99.95%, 99.949%, and 0.095, respectively. Table 4.2 lists the test findings of various ECG records.

Table 4.2 Test findings of the proposed approach

Record No.	**Actual Beats**	**Total Detected beats (TB)**	**True Positive (TP)**	**False Negative (FN)**	**False Positive (FP)**	**Sensitivity, Sen (%)**	**Positive Predictivity, PPe (%)**	**Error Rate Err (%)**
100	2273	2273	2273	0	0	100	100	0
101	1865	1866	1864	1	2	99.99	99.89	0.16
102	2187	2187	2187	0	0	100	100	0
103	2084	2084	2084	0	0	100	100	0
104	2229	2231	2229	1	3	99.95	99.86	0.17
105	2572	2578	2571	4	7	99.84	99.72	0.42
106	2027	2028	2026	0	1	100	99.95	0.04
107	2137	2137	2137	0	0	100	100	0
108	1763	1763	1763	0	0	100	100	0
109	2532	2532	2532	0	0	100	100	0
111	2124	2124	2124	0	0	100	100	0
112	2539	2539	2538	0	1	100	99.96	0.03
113	1795	1795	1795	0	0	100	100	0
114	1879	1879	1879	0	0	100	100	0
115	1953	1953	1953	0	0	100	100	0
116	2412	2412	2412	0	0	100	100	0
117	1535	1535	1535	0	0	100	100	0
118	2278	2278	2278	0	0	100	100	0
119	1987	1987	1987	0	0	100	100	0
121	1863	1863	1863	0	0	100	100	0
122	2476	2475	2475	0	0	100	100	0
123	1518	1517	1516	0	1	100	99.93	0.06
124	1619	1619	1619	0	0	100	100	0
200	2601	2601	2601	0	0	100	100	0
201	1963	1969	1959	8	10	99.59	99.49	0.91
202	2136	2136	2134	3	2	99.85	99.90	0.23
203	2980	2980	2972	10	8	99.66	99.73	0.60
205	2656	2656	2652	0	4	100	99.84	0.15
207	1862	1862	1862	0	0	100	100	0
208	2955	2954	2950	9	4	99.69	99.86	0.44
209	3005	3005	3005	0	0	100	100	0
210	2650	2650	2650	0	0	100	100	0
212	2748	2747	2747	0	0	100	100	0
213	3251	3251	3250	0	1	100	99.96	0.03
214	2262	2262	2260	3	2	99.86	99.91	0.22
215	3363	3361	3361	2	0	99.94	100	0.05
217	2208	2208	2206	2	2	99.90	99.90	0.18
219	2154	2154	2154	0	0	100	100	0
220	2048	2048	2048	0	0	100	100	0

221	2427	2425	2425	2	0	99.91	100	0.08
222	2483	2483	2483	0	0	100	100	0
223	2605	2605	2605	0	0	100	100	0
228	2053	2052	2047	6	5	99.70	99.75	0.53
230	2256	2256	2256	0	0	100	100	0
231	1573	1572	1572	0	1	100	99.93	0.06
232	1780	1778	1777	3	1	99.83	99.94	0.22
233	3079	3079	3079	0	0	100	100	0
234	2753	2753	2753	0	0	100	100	0
Total	**1,09,498**	**1,09,503**	**1,09,448**	**54**	**55**	**99.95**	**99.949**	**0.095**

Comparing the suggested technique to the state-of-art methods [31, 51, 52, 99], it has yielded a few numbers of FN and FP as 54 and 55, respectively, and the least number of FP than [106]. All the records have obtained an error rate of less than 1%. The following records have a 0% error rate: 100, 102, 103, 107, 108, 109, 111, 113, 114, 115, 116, 117, 118, 119, 121, 122, 124, 200, 207, 209, 210, 212, 219, 220, 222, 223, 230, 233 and 234. The sensitivity of 35 records out of 48 is 100%, while the positive predictivity of 31 records out of 48 is 100%.

4.4 Performance of Proposed Method when EMG noise is added

This method is also effective when ECG data is corrupted with EMG noise, five records from MIT-BIH-AD are corrupted with EMG noise from the MIT-BIH Noise Stress database, and the sensitivity, positive predictivity, and error rate of five records are calculated and displayed in Table 4.3. The EMG noise from the MIT-BIH Noise Stress database (say, n) is combined with ECG record no. 100 (say, x) (depicted in Figure 4.10(a)) to acquire a record 100 noisy ECG (say, $y = x + n$) as represented in Figure 4.10(b), to demonstrate the efficacy of the proposed approach on EMG. The proposed method is used to filter the noisy ECG data (y), and the R-peak is detected as indicated in Figure 4.10(c). The visual interpretation confirms that all the R-peaks are accurately detected despite the presence of EMG artifacts in the ECG record. Five ECG records are used to determine the performance measures like sensitivity (Sen), positive predictivity (PPe), and error rate (Err). Table 4.3 shows the results.

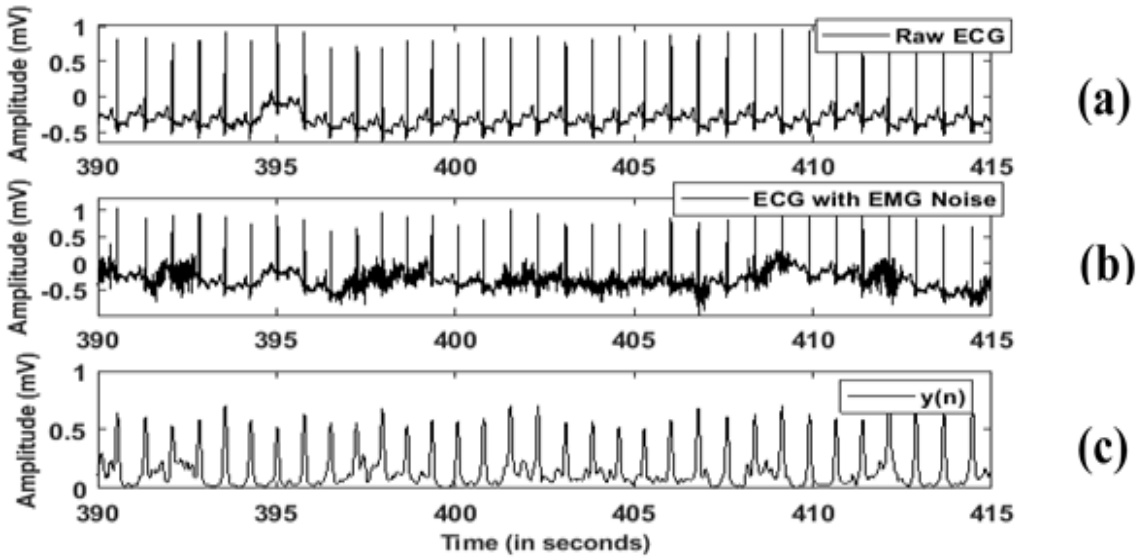

Figure 4.10 (a) ECG record number 100 from MIT-BIH-AD **(b)** ECG record number 100 corrupted with EMG noise from MIT-BIH Noise Stress database **(c)** R-peak detected using the proposed method.

Table 4.3 Experimental results of EMG corrupted ECG records

Record No.	**Actual Beats**	**Total Detected beats (TB)**	**True Positive (TP)**	**False Negative (FN)**	**False Positive (FP)**	**Sensitivity (%)**	**Positive Predictivity (%)**	**Error Rate (%)**
100	2273	2273	2273	0	0	100	100	0
105	2572	2578	2571	4	7	99.84	99.72	0.42
203	2980	2980	2972	10	8	99.66	99.73	0.60
208	2955	2954	2950	9	4	99.69	99.86	0.44
234	2753	2753	2753	0	0	100	100	0

It is evident from Tables 4.2 and 4.3 that when the proposed approach based on RFODD is applied, the presence of EMG noise in ECG data does not affect the R-peak detection. When the records (100, 105, 203, 208, and 234) are distorted by EMG noise, the proposed approach yields the same results (Sen, PPe, and Err).

4.5 Comparison with state-of-the-art Methods

The comparison of the number of records having 100% sensitivity and positive predictivity is made with the well-established algorithms from the literature in the form of a bar graph as shown in Figure 4.11. The bar graph of Figure 4.12 compares the number of records with zero error rate with other well-known techniques in the literature.

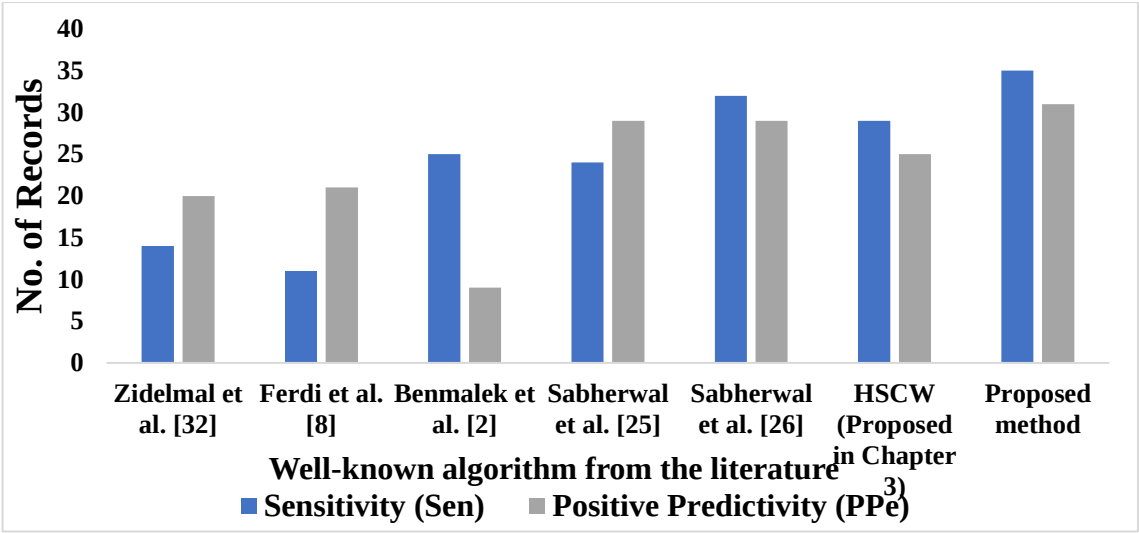

Figure 4.11 Comparison of the number of records which has 100% sensitivity (Sen) and positive predictivity (PPe) from the literature with the *proposed method*.

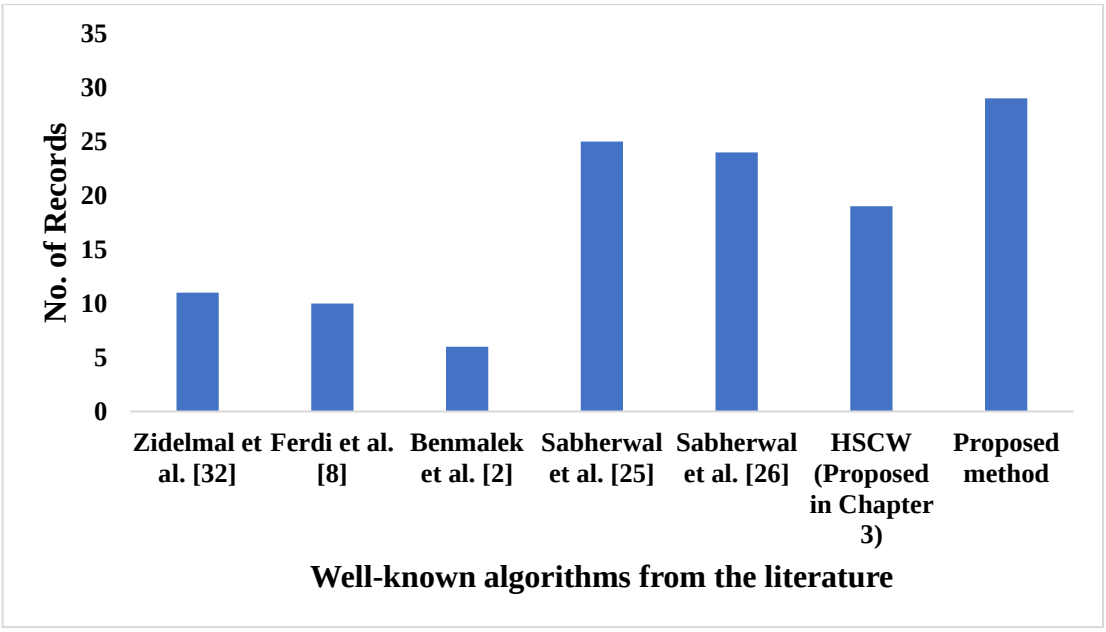

Figure 4.12 Comparison of the number of records having a zero error rate in various algorithms from the literature with the *proposed method.*

Table 4.4 compares the proposed approach to the methods described in the previous literature to validate the superiority. The test results support the claim that the proposed method outperforms all other recognised techniques in terms of greater positive predictivity and reduced error rate. Records 116 and 222, have FP and FN reported in the literature [31, 51, 52, 99, 106], but the proposed technique has reduced them to 0. Table 4.5 shows the comparison of the overall number of FP and FN.

Table 4.4 Comparison of various performance parameters results with the established algorithms

Methods	**Sensitivity, Sen (%)**	**Positive predictivity, PPe (%)**	**Error rate, Err (%)**
Ferdi *et al.*[51]	-	-	0.37
Zidelmal *et al.*[31]	99.64	99.82	0.54
Benmalek *et al.* [52]	99.86	99.86	0.28
Sabherwal *et al.* [99]	99.9	99.9	0.16
Sabherwal *et al.* [106]	99.96	99.926	0.135
HSCW (Proposed in Chapter 3)	99.93	99.95	0.117
Proposed algorithm	**99.95**	**99.949**	**0.095**

Table 4.5 Comparison of the total number of FN and FP

Methods	FN	FP
Ferdi *et al.*[51]	256	146
Zidelmal *et al.*[31]	393	193
Benmalek *et al.* [52]	156	153
Sabherwal *et al.* [99]	93	98
Sabherwal *et al.* [106]	42	80
HSCW (Proposed in Chapter 3)	76	53
Proposed algorithm	**54**	55

The proposed technique has exhibited excellent improvement in the performance metrics, such as positive predictivity and error rate for the accurate delineation of R-peaks, therefore making it the most effective R-peak detector. The approach has outperformed the state-of-the-art methods described in the literature [31, 51, 52, 99, 106] in terms of performance parameters. In diverse complex ECG patterns, the visual interpretation and quantitative findings demonstrate more effective and successful R-peak detection with good reliability in terms of the reduced FP and *Err*. The method is effective for both normal and abnormal subjects.

4.6 Conclusions

A new and innovative approach based upon fractional order is used for R-peak detection of ECG signals. Due to the inherent attributes of fractional order to eliminate noise and enhance useful information, it is employed for the successful delineation of R-peaks, which is a crucial parameter for evaluating cardiac abnormalities.

The Riesz-based fractional differentiation process authenticates to be superior to traditional methods as there is no phase delay and the R-peaks appear exactly as they did in the original waveform. Furthermore, the main benefit of fractional order over integer order is that it preserves the information in the signal, whereas the models based on integer order diminish the high-frequency contents in the signal.

All of these interpretations lead to the Riesz fractional-order derivative-based algorithm being employed for ECG filtering and R-peak detection. The proposed method successfully validates that the information is lost as the fractional-order (p) approaches unity (as in the case of integer-order calculus). The experimentation and visual interpretation confirm that fractional-order (p) 0.6 eliminates the dominant artifacts like baseline wander and power line interference in ECG beats. The proposed technique works well in ECG records with heart blocks, noisy ECG, and changing QRS morphology situations.

This approach has performed better visually and quantitatively when validated on MIT-BIH-AD and achieved sensitivity (Sen), positive predictivity (PPe), and error rate (Err) readings of 99.95%, 99.949%, and 0.095%, respectively. The proposed algorithm is robust to noise and successfully identified R-peaks in various challenging circumstances. The experimental findings are better in terms of decreased false-positive and error rates. Therefore, the proposed approach based on the Riesz fractional-order derivative appears to be advantageous and outperforms the known ones in the area.

The **main features differentiating the proposed algorithm** from other well-known techniques are described below:

- It is the first time that the concept of Riesz fractional derivative is used for the real-time biomedical signal for clinical and interpretation purposes.
- The proposed technique fits well in many complex ECG patterns, such as heart block situations with significant high T-wave amplitude, high grade noise and changing QRS morphology.
- Additionally, the proposed method behavior is also examined for the RFODD variable fractional-order (p).

CHAPTER 5

VIRTUAL INSTRUMENTATION-BASED IMPLEMENTATION OF THE PROPOSED FRACTIONAL-ORDER FILTER

THERE HAS BEEN A SIGNIFICANT amount of research on the classification of ECG arrhythmia for the MIT-BIH-AD. However, real-time ECG classification still has to be explored. The present method in literature focuses on feature extraction of ECG beats in LabVIEW and classification into normal, tachycardia, and bradycardia. Recent research focuses primarily on ECG acquisition, but it needs to be expanded to include the classification of real-time ECG beats based on cardiac ailments.

ECG signal acquisition has made significant strides to recent innovations in hardware and software technologies, making the real-time acquisition a simple task. This chapter proposes an entire classification system, which includes the acquisition and pre-processing of real-time ECG signals, feature extraction, and classification of ECG beats into normal (subjects who have never had any heart ailment history) and abnormal (subjects who have had heart ailment history) classes.

The ECG signal is obtained in real-time by utilizing the National Instruments (NI) myDAQ data acquisition device and LabVIEW. The collected signal is pre-processed with band-pass filtering and a Riesz-based fractional-order digital differentiator (RFODD) before detecting R-peak (as discussed in Chapter 4). Features are extracted after R-peak detection of the acquired data. The feature set consists of the fusion of time-domain, frequency-domain, and time-frequency domain features, and the new and novel features based on Riesz coefficients and the Fibonacci series. The research work findings achieved good results after classifying 35 real-time ECG data into normal and abnormal beats. The first time, ECG signal categorization is used to identify whether or not a subject has a history of heart disease.

5.1 Selection of Subjects

The research work focuses on extracting real-time ECG subjects. After pre-processing of the acquired signal, features are acquired in the time domain, time-frequency domain, and frequency domain, and finally classifying ECG beats into two classes, *i.e.*, normal (subjects, which never have any heart ailment history) and abnormal (subjects, which have heart ailment history). The ECG signals of 35 subjects are collected, and 25 are normal (they never have any heart ailment history). They are undergraduate, Ph.D., and university faculty members. Their age range from 19 to 79 years. The ECG signal of the remaining ten subjects is obtained from the hospital. They had a Myocardial Infarction (MI) and taking medication at the time of the data collection. As a result, they belong within the abnormal group (refer to abnormal as one who had a heart ailment history). The duration of the ECG record analysis is 10 seconds.

5.2 Proposed Virtual Instrumentation-based Design for ECG Signal Acquisition

The hardware components used in the proposed approach are ECG electrodes, NI myDAQ device, AD8232 ECG module, and LM2596 Buck converter.

5.2.1 Electrodes

The electrical signal generated by the heart and computed on the skin is extremely weak. A good quality electrode and a proper connection between the skin and the electrode are essential for stronger signal capture. Disposable self-adhesive electrodes are used. They include AgCl conducting gel to enhance signal quality. This work offers a three-lead ECG monitoring system. Electrodes are attached to the right and left arms, with the right leg acting as the body's ground [57]. Figure 5.1 shows the electrodes that are utilized.

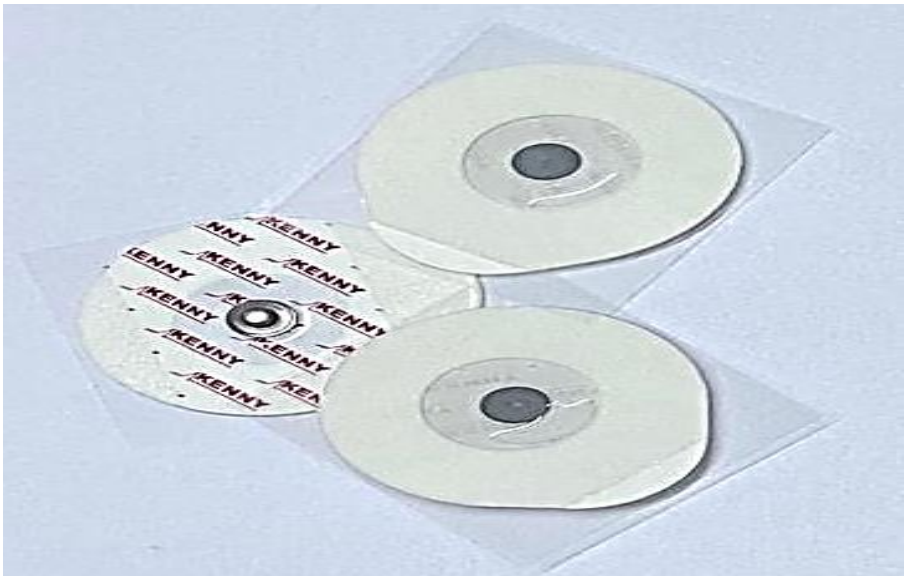

Figure 5.1 ECG Electrodes

5.2.2 AD8232 Module

AD8232 ECG module is used to acquire ECG signals from subjects due to its gain and input impedance [62]. It is an integrated signal conditioning block for ECG and other biopotential measurement applications. The main components of AD8232 are shown in Figure 5.2a.

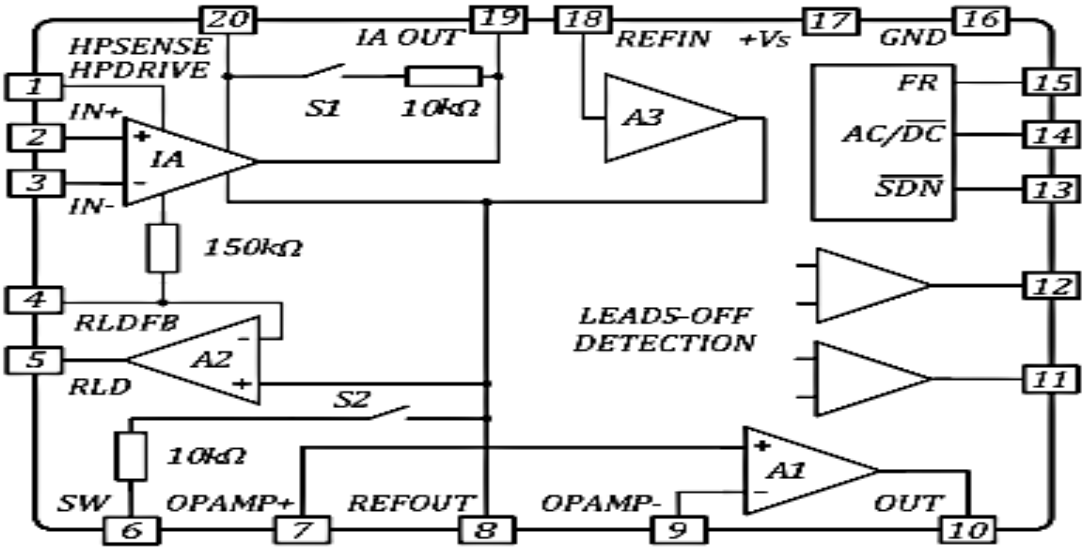

Figure 5.2a AD8232 integrated signal conditioning block [62, 107]

It also provides fast recovery of ECG signal after lead-off condition. The integrated current-feedback instrumentation amplifier, with two well-matched transconductance amplifiers, assures high common mode rejection and eliminates half-cell electrode

potential. Filtering of the acquired data is done by low-pass and high-pass filters. The two-pole high-pass filters can efficiently choose their cut-off frequency to eradicate motion artifacts and the electrode half-cell potential. The three-pole low-pass filter built around the AD8232 ECG module with external components removes the additional noise [107]. AD8232 module includes pins like SDN pin, LO+ pin, LO- pin, OUTPUT pin, 3.3V pin, and GND pin. AD8232 ECG module is in shown Figure 5.2b. This board consists of pins like the right arm, left arm, and right leg pins to connect to respective electrodes. An LED indicator is used to indicate the rhythm of the heart signal.

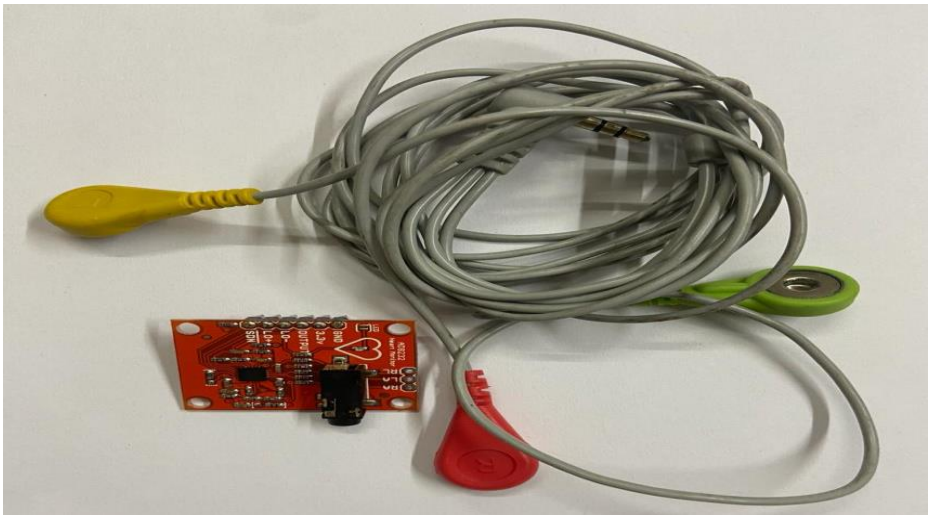

Figure 5.2b AD8232 Module

5.2.3 NI myDAQ Device

It's a hardware device that acts as an interface between the sensor module and the output device (laptop). It is a portable data acquisition device. When used with LabVIEW, it has eight plug-and-play computer-based laboratory instruments, along with a digital multimeter and oscilloscopes [57]. It acquires, computes, and analyses real-world signals using NI-LabVIEW software. The device, when integrated with NI-LabVIEW on PC, may evaluate and process obtained signals, to control simple processes at any time and from any location. This device can be used to generate or obtain analogue or digital devices. To obtain a real-world signal, it is connected to an AD8232 ECG module and an LM2596 buck converter. Figure 5.3 depicts the myDAQ gadget.

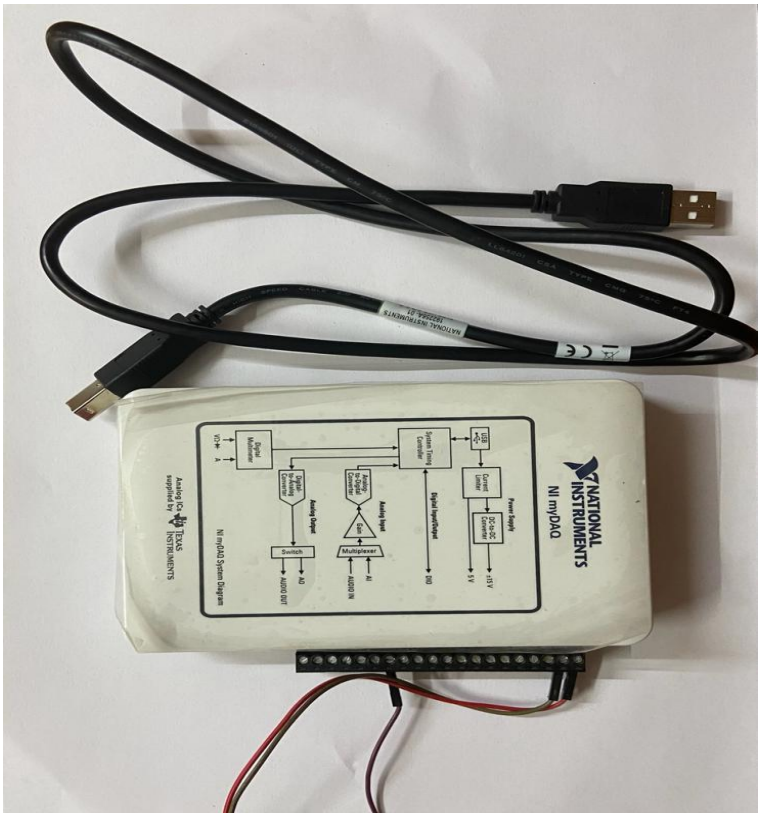

Figure 5.3 NI-myDAQ

5.2.4 LM 2596

It can provide a step-down (buck) switching regulator capable of driving 3A loads with good line and load control. It quickly steps to the required voltage by altering the potentiometer. It is depicted in Figure 5.4. It connects the AD8232 to myDAQ. AD8232 requires 3.3V power, therefore it reduces myDAQ's supply voltage from 5V to 3.3V.

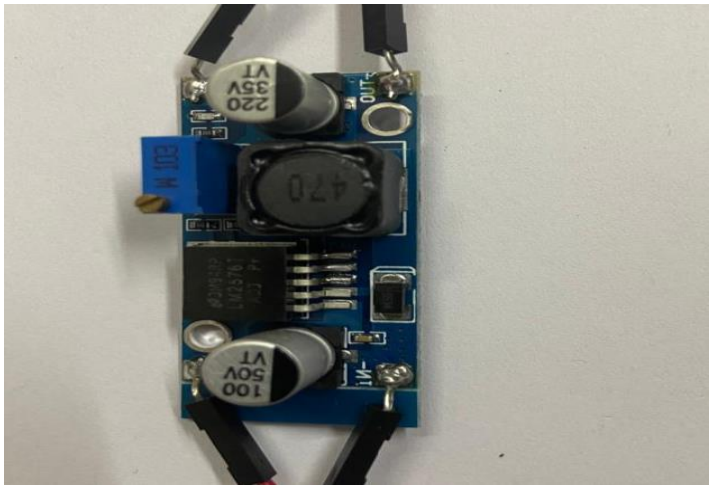

Figure 5.4 LM 2596

5.3 Data Acquisition

ECG electrodes are placed on the subject's right arm, left arm, and right leg. They are connected to the leads of the AD8232 module's right arm, left arm, and right leg. The AD8232's OUTPUT pin is connected to the analogue pin of myDAQ. MyDAQ's 5V and GND pins are connected to the input of the LM2596, while its output is connected to the 3.3V and GND pins of the AD8232. Figure 5.5a shows the overall process. The device myDAQ is shown in Figure 5.5b connected to LabVIEW on a PC.

Figure 5.5a ECG signal acquisition process in the lab

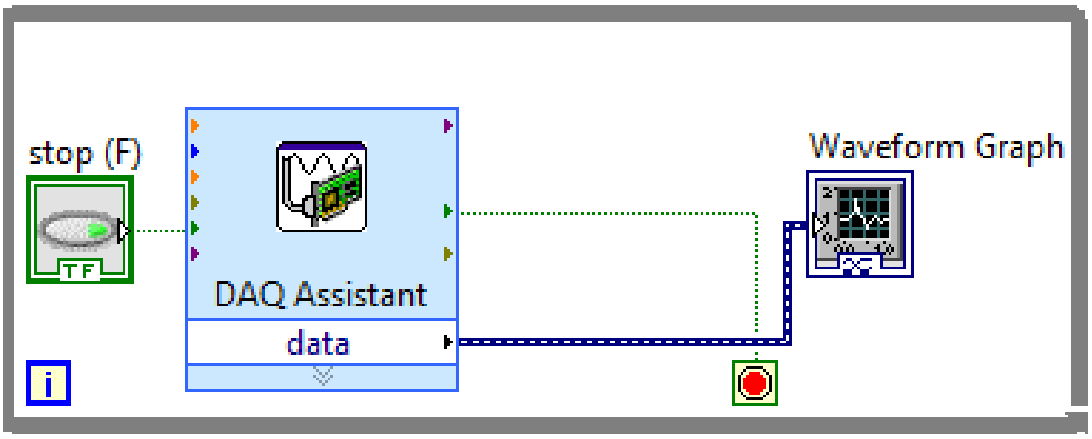

Figure 5.5b ECG signal acquisition

5.4 Feature Extraction of Real-time ECG Subjects

Figure 5.6 depicts the algorithm for real-time ECG signal acquisition and classification used in the present research work. Due to the QRS complex frequency spectrum, which ranges from 5 to 25 Hz, the acquired ECG signal is filtered using Butterworth band-pass filters with lower and higher cut-off frequencies of 5 Hz and 25 Hz respectively. [99]. The artifacts like baseline drift (1Hz) and power-line interference (50Hz) are eliminated. Each ECG record is segmented after preprocessing, and two approaches are used to extract the features to form a feature vector, as shown in Figure 5.6. After that, PCA is used to reduce the size of the feature vector [77]. The algorithm for Adaptive K Nearest Neighbors (ADkNN) receives the PCA output.

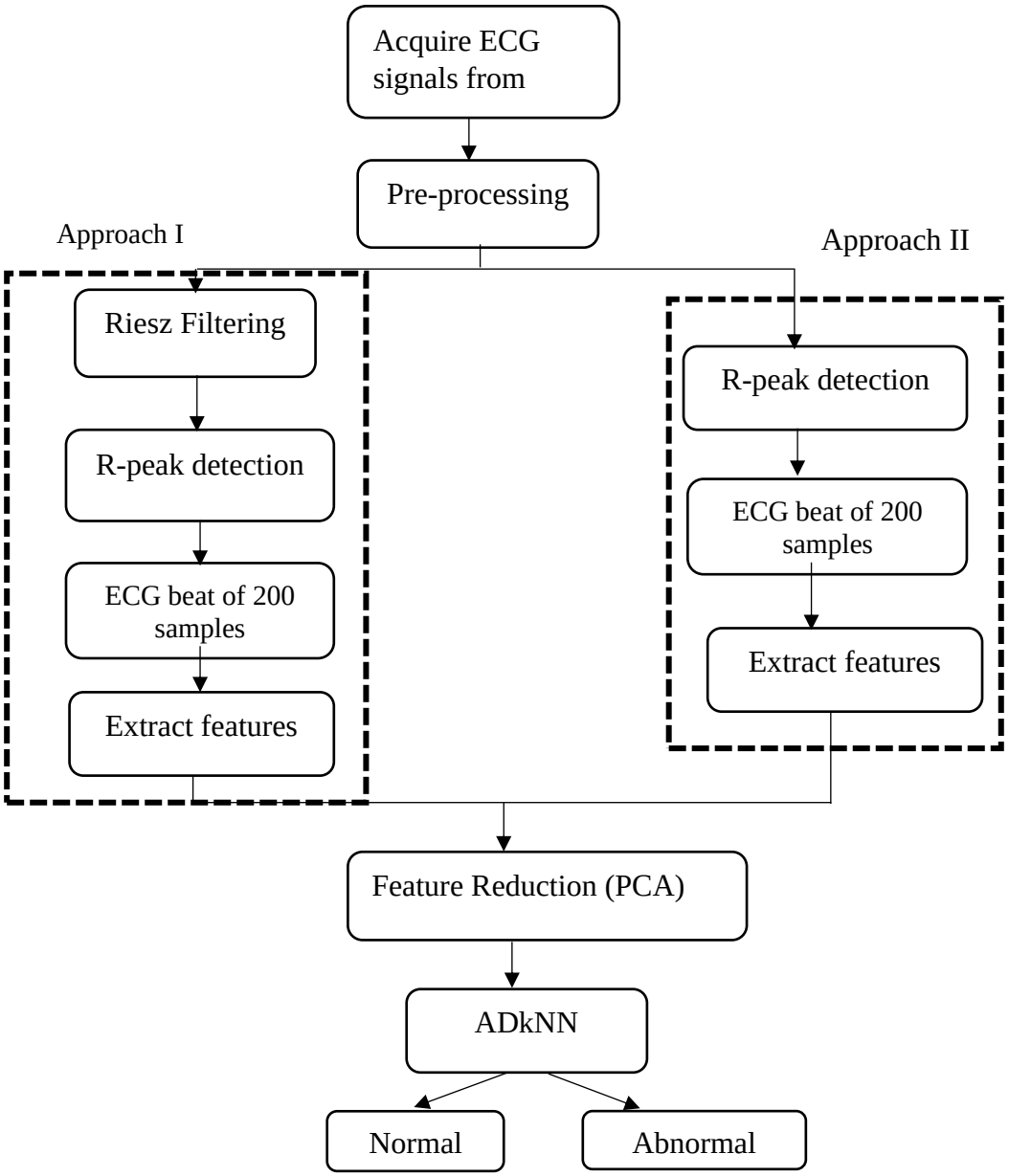

Figure 5.6 Block diagram of the proposed work

5.4.1 Approach I

Fractional-Order calculus (FOC) shows more favorable than integer order because it effectively preserves the signal's features and information, while a model based on integer order eliminates the signal's high-frequency content [10]. Riesz fractional-order digital differentiator (RFODD) was shown to be more effective than literature-based approaches in our previous Chapter in terms of decreased error rate and enhanced sensitivity for detecting R-peak. The R-peaks have been successfully delineated using fractional-order p=0.6 of RFODD while maintaining the signal's information (demonstrated in Chapter 4). The useful features that interpret the signal's underlying characteristics were extracted, which further enhancing the classifiers' effectiveness.

After pre-processing the real-time ECG data to enhance the QRS component, which is the primary characteristic of the ECG signal, a Riesz-based derivative is obtained. The ECG data is then divided into 200-sample beats, with 99 samples taken before the R peaks and 100 samples taken following the R peak. As a result, Figure 5.7 shows the 200-sample beat of two classes of real-time ECG. The features from approach I are the mean, standard deviation, peak values, and the coefficients of ECG's Riesz-based fractional-order derivative signal.

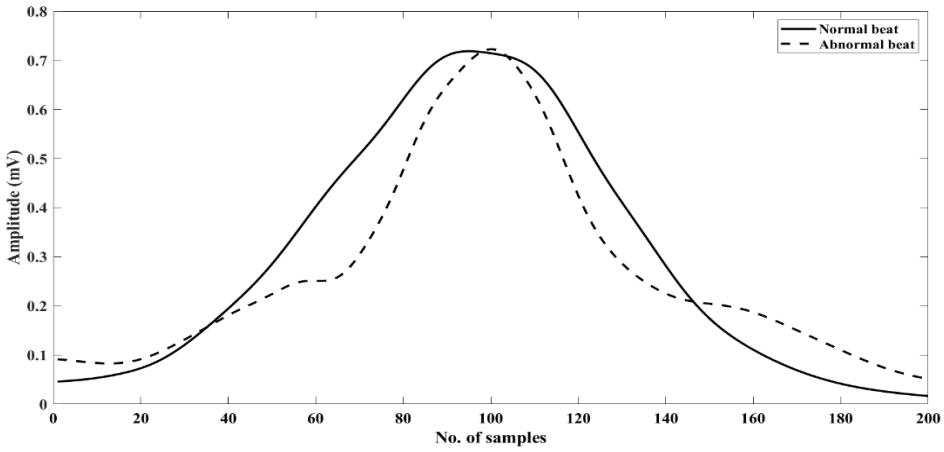

Figure 5.7 Riesz derivative of two distinct ECG beats

5.4.2 Approach II

Since ECG rhythm provides important information, it is a primary diagnostic tool for physicians in diagnosing cardiac ailments. We need thorough information on ECG rhythm for an effective computer-based automatic diagnostic tool for a physician, therefore features are extracted such that they reflect the most information about ECG

beats. The features from the time domain and time-frequency domain are retrieved. Time-Domain Features (TD Features) include the height, duration, and shape of P, QRS, and T waves, among other things. Wavelet transform (WT), S-transform (ST), and other Time-Frequency Domain Features (TFD features) of an ECG beat are described by its coefficients. In the proposed approach, the new and novel Shannon energy of Fibonacci series signal is used as one of the TD features which is described beneath in addition to TD and TFD features.

5.4.2.1 Fibonacci series (FS)

The number itself is equal to the sum of the prior two consecutive numbers. 0, 1, 1, 2, 3, 5, 8, 13, 21… are Fibonacci series number sequences. Mathematically, it is expressed as:

$$fb_a = \begin{cases} 0, & if\ a = 0 \\ 1, & if\ a = 1 \\ fb_{a-1} + fb_{a-2} & if\ a > 1 \end{cases} \tag{5.1}$$

where fb_a depicts the array element. The Fibonacci series' index was determined by 200 sample ECG beats obtained after pre-processing (as shown in Figure 5.8a), and a newly generated Fibonacci series signal is depicted in Figure 5.8b. The visual interpretation of Figure 5.8a shows that different classes of ECG beats may be distinguished, hence the Fibonacci series signal obtained in Figure 5.8b will be different for each class. As a result, the signal's energy will differ. The newly acquired Fibonacci series' Shannon energy (SE) [108] is calculated and used as a feature. Mathematically, SE is represented by:

$$SE = -|y[a]|\log(|y[a]|) \tag{5.2}$$

where $y[a]$ is normalized amplitude of the Fibonacci series signal generated.

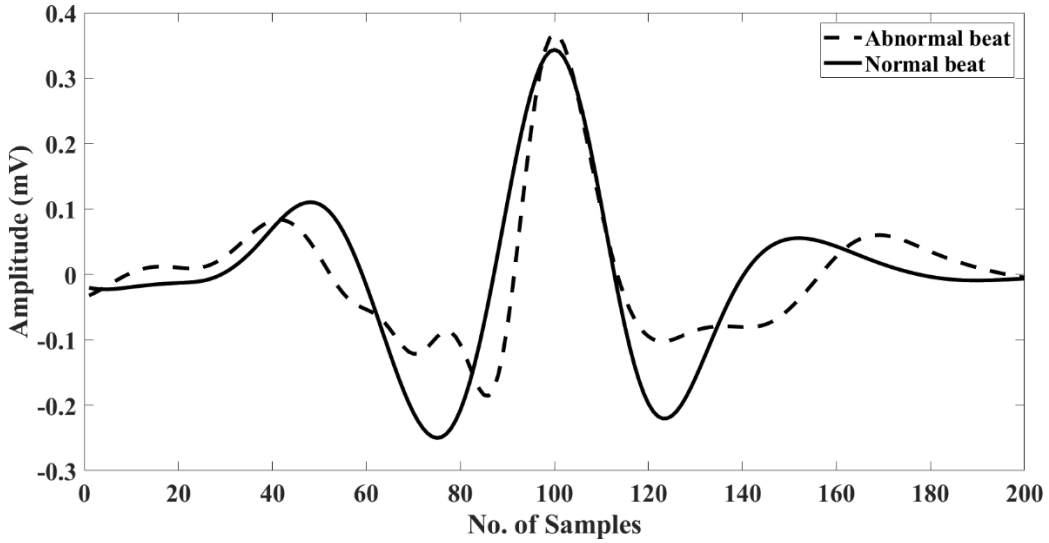

Figure 5.8a ECG beat belonging to two class type

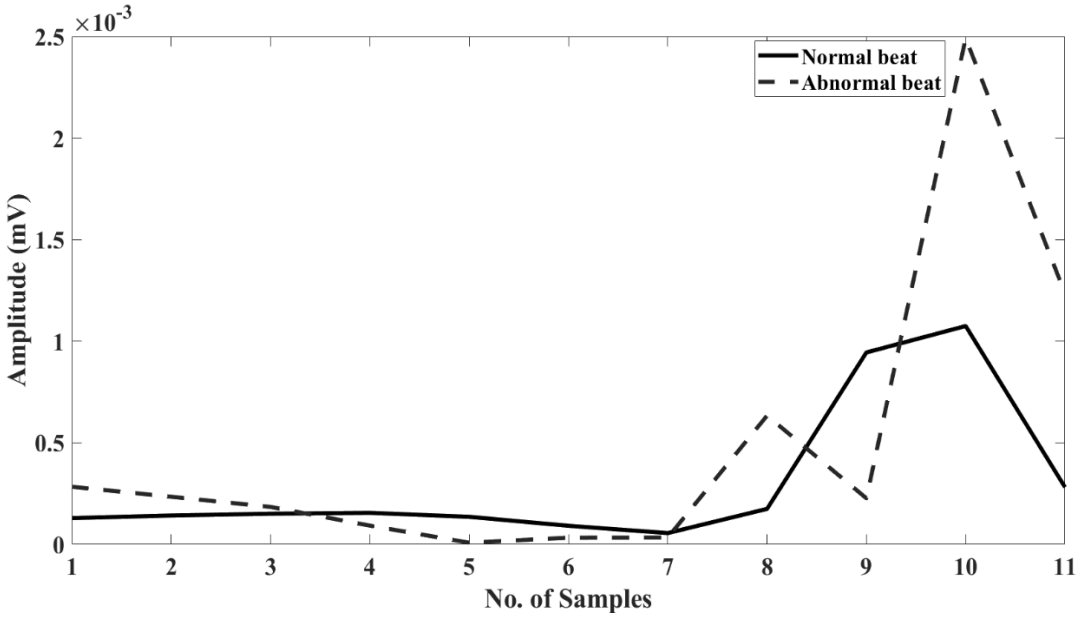

Figure 5.8b Fibonacci series signal generated from Figure 5.8a

5.4.2.2 Additional time-domain Features (Additional TD Features)

It is evident from Figure 5.8a that the morphology of ECG beats of the two classes is different. The highest and lowest values of ECG beats are regarded as features. They have dissimilar shapes and emulate different cardiac rhythms and information. ECG features include the maximal and least values of ECG beats. It is obvious from Figure 5.8a that the ECG beats of the two classes vary in PQ and ST segments mostly. ST and PQ segment maximum, minimum, and slope are regarded as characteristics. The RR interval is the most used TD feature. Therefore, the RR interval [7, 70] of two subsequent beats and the whole ECG record are taken into consideration in this study. Ten time-domain traits are considered features.

5.4.2.3 Time-frequency domain features (TFD features)

The hidden attributes of ECG beat can be effectively deciphered by the coefficients of WT [78, 109] and ST [108, 109]. ST maintains a close relationship with the Fourier Spectrum and offers frequency-dependent resolution [108]. When it is used to analyze an ECG beat, an ST matrix is produced. The SE, standard deviation, and mean are obtained as three features from the ST output. In WT, the energy of the fourth and fifth levels of decomposition is used as a trait. The time-frequency domain uses a total of five characteristic features. Figure 5.9 lists all the features that were used in this study.

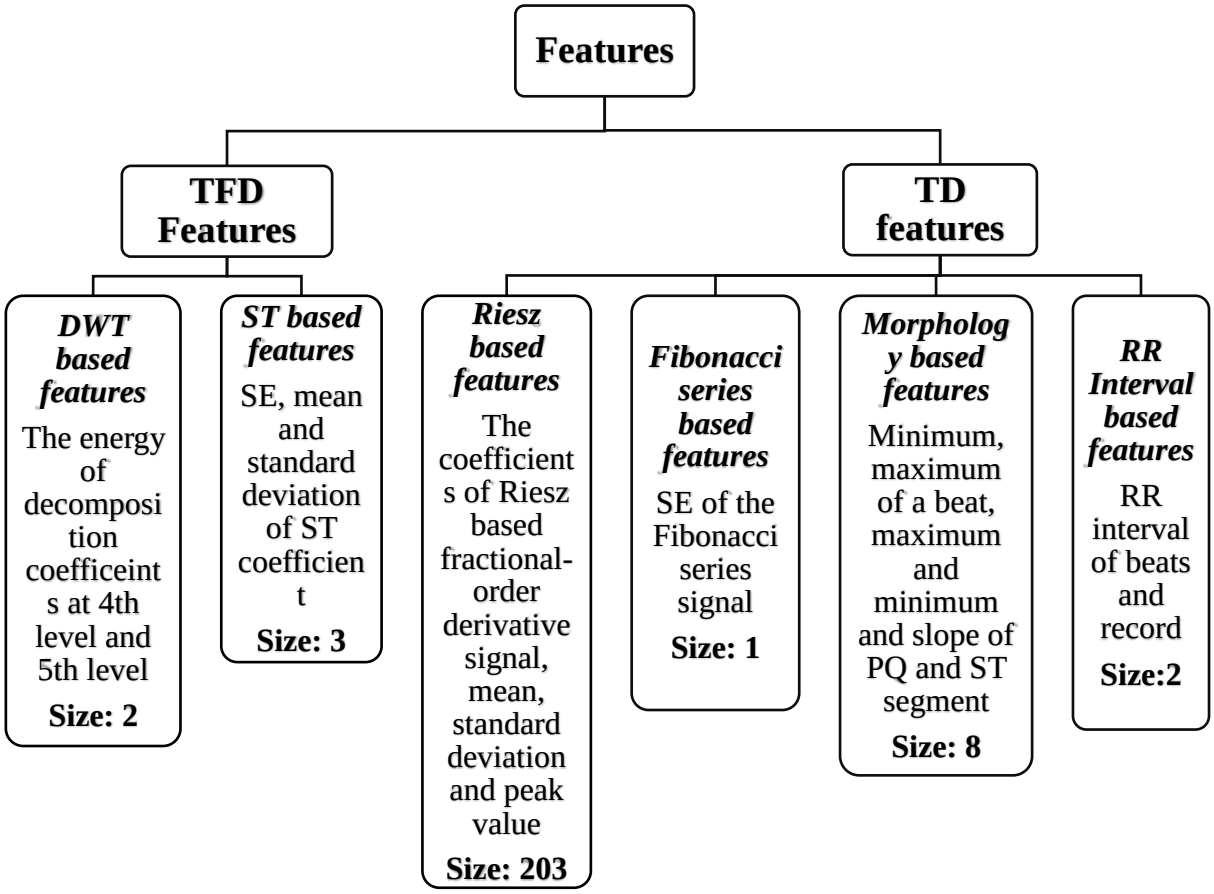

Figure 5.9 Features used for classification

Figure 5.9 shows the 219 features used in the present research work. The classification's computation time will increase as there are more features. Principal component analysis (PCA) is used to reduce the dimensions of features without hampering the classification accuracy.

5.4.3 Principal Component Analysis (PCA)

PCA is a regularly employed technique for dimensionality reduction and feature extraction. It transforms data of possibly correlated variables into principal components, which are linearly uncorrelated variables (PCs). The direction of the greatest variability in this transformation is indicated by a basis vector provided by the first PC [77]. The second PC, which is orthogonal to the first PC, yields the basis vector for the following

direction for which the condition is being used. In [77], the PCA procedure is explained. The earliest PCs have a high contribution ratio, which declines from the first PC to the last PC. The PCA method is described as:

- Compute the covariance matrix of the feature vector
  $A = (X - x)(X - x)^T$ (5.3)
  where X is the feature matrix, x represents mean vector of X.
- Calculate the matrix of eigenvectors B and diagonal matrix of eigen values C as
  $B^{-1}AB = C$ (5.4)
- The eigenvectors in B are arranged in the descending order of eigen values in Cand the projected data is calculated as
  $Projected\ data = [B^T(X - x)^T]^T$ (5.5)

The contributory ratio of the first few PCs is high and it decreases from first PC to last PC. The various PC values have been plotted against the classifier's accuracy, sensitivity, and positive predictivity (specified in section 5.5.2).

5.4.4 Adaptive K-Nearest Neighbor (ADkNN)

K-Nearest Neighbor (KNN) is very simple and easy to implement classifier. It does not depend on any specific models, tune several parameters. It is a potential analytical classification algorithm employed to classify objects or patterns based on grouping of nearest training samples or instances in the feature space. The grouping is done by the majority of voting to the nearest points. It constructs inferences directly from the training instances themselves by comparing new problem or test instances with instances present in training that is saved in memory. It is an instance-based learning method rather than performing explicit generalization [110].

It assigns test samples to the class its nearest *k* neighbors generally belong. It proves efficient in minimizing misclassification errors when there is a large number of samples in the training dataset. In this research, ADkNN is used for achieving higher accuracy. ACKER algorithm developed in [111] is employed in this work. For a given test point, *p* this algorithm approximates the expected accuracy(*e_acc*) for various values of *k* and finds the value of *k* for which it gives the highest *e_acc*.

Algorithm I

Input: query point *p*, function *f*, set *range*, integer *a*

Output: class of query point *p*

bestl_k=0

1. *maximum_accuracy=-1*
2. *for k in range do*
3. *point_accuracy=e_acc(p,k,f,a)*
4. *If point_accuracy>maximum_accuracy then*
5. *best_k=k*
6. *max_accuracy=point_accuracy*
7. *end*
8. *end*
9. *predicted_class=kNN(p,best_k)*
10. *return(predicted_class)*

Similarity function $sm: P \times P \times N \rightarrow R$ states the similar *k* environment between two considered instances. It is defined as $sm: P \times P \rightarrow R$. Imagine a function $f: P \times N \rightarrow R$ which specifies an instance and its k environment. So, a similarity function based on *f* is [111, 112]:

$$sm_f = P \times P \times N \rightarrow R\ (p, p', k) \rightarrow -dist(f(p.k), f(p', k)) \tag{5.6}$$

Here, $dist(x, y)$ is the Euclidean distance (ED) of two instances. It is used to calculate the distance of the nearest neighbors of a point. Suppose the feature vector is $(a_1(x), a_2(x) \cdots a_n(x))$ of any arbitrary point *x*. So, the ED of two given points *x* and *y* is:

$$d(x, y) = \sqrt{\sum_{i=1}^{n}(x_i - y_i)^2} \tag{5.7}$$

The more the value of similarity of two given instances with their *k* environment, the more is sm_f value. $P_{sim,a}(p, k)$ consists of *a* point whose *k* environment is very alike to the *k* environment of *p* instance with context to the considered similarity function [111, 112] which is denoted as:

$$P_{sim,a}(p, k) = argmax_p^a, (sim(p, p', k)) \tag{5.8}$$

Here, the average distance similarity function (sm_{a_d}) is used and it is defined as the average distance to the *k* closest neighbors of test point *p* [111, 112]. Average distance is written as:

$$a\_d_{(p,k)} = \frac{\sum_{i=1}^{k} dist(p,p_i)}{k} \tag{5.9}$$

Here p_i is the *ith* nearest neighbor of *p*. The similarity function based on a_d is written as:

$$sm_{a\_d}(p,p',k) = -dist(a\_d_{(p,k)}, a\_d(p',k)) \tag{5.10}$$

The next, step is to calculate the expected accuracy (e_acc). For a test point *p* with its *k* environment, a set of points $P_{sm,a}(p,k)$ which has identical *k* environments found from the training set. Since the k environments are alike, there exists a correlation between the accuracy of kNN classification function for a given instance p $acc(c'_p(p),\{p\})$ and the accuracy of kNN classifier for $P_{sm,a}(p,k)$ [112]. So, the e_acc is given below:

$$e\_acc_a(p,k) = acc(c'_k, P_{sm,a}(p,k)) \tag{5.11}$$

It is assumed that statistically different regions are identical. It is found that e_acc is a good indicator for real accuracy.

Algorithm II

Expected accuracy

Input: point *p*, integer *k*, function *f*, integer *a*

Result: *e_acc* for kNN(*p*,*k*)

1. *find set* $P_{sm,l}(p,k)$ *of l different points* p' *with minimal difference to reference function based on f.*
   $sm(p,p') = |f(p,k) - f(p',k)|$
   $P_{sm,l}(p,k) = argmax(\sum sim(p,p',k))$ *as in (8)*
2. *Correctly predicted=number of correct predictions of kNN*(p',k)*, here* $p' \epsilon P_{sm,a}(p,k)$
3. *e_acc=*$\frac{correctly\ predicted}{a}$
4. *return e_acc*

5.5 Results and Discussion

The suggested method was tested using MATLAB 2021a and LabVIEW 2016 on a PC with an Intel Core i7 CPU running at 3.40 GHz and 8 GB of RAM.

This work focuses on developing an entire system for classification starting from the acquisition of real-time ECG signals, pre-processing, R-peak detection, feature extraction, and then classification.

5.5.1 R-peak Detection

A few real-time ECG signal simulation results for R-peak detection are shown below:

Subject1:

Subject 1 is a 30-year-old female who has never had a history of cardiac disease. She doesn't smoke. As illustrated in Figure 5.10(a), a brief real-time signal slice from 0 to 8 seconds is chosen. The suggested method successfully identified R-peaks. The ECG wave's 5–25 Hz frequency components are kept after band-pass filtering, and the QRS complex is improved using the Riesz derivative. The band-pass filtering and Riesz derivative operation are shown in Figure 5.10(b) and 10(c) respectively.

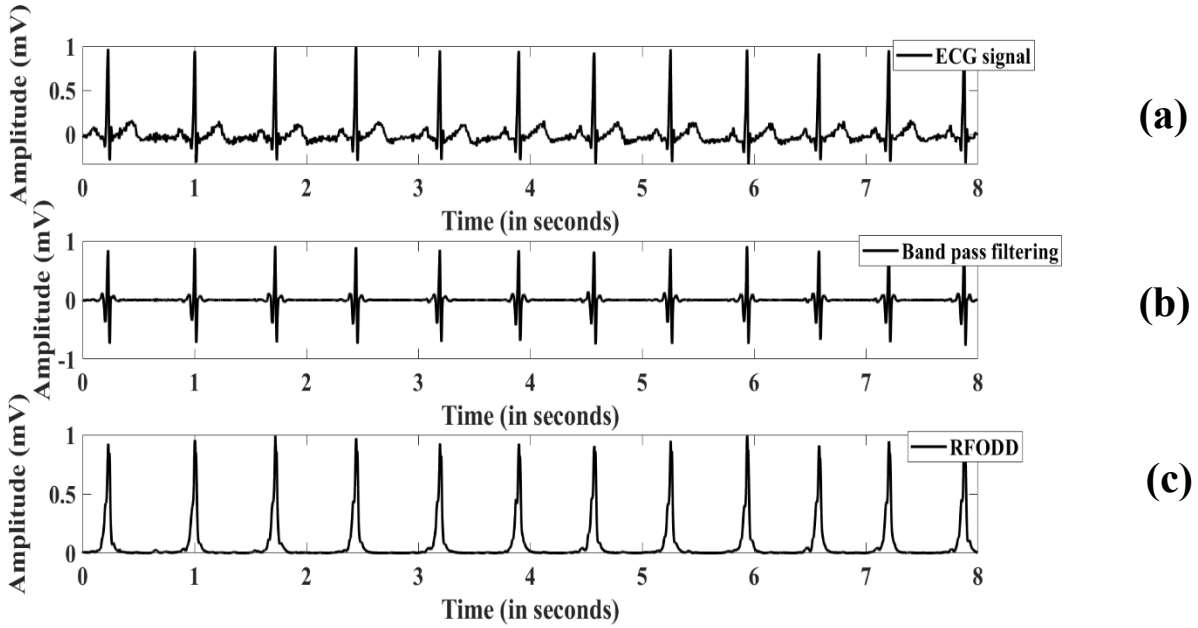

Figure 5.10 (a) Real-time ECG waveform of subject 1 (b) band-pass filtering (c) Riesz-based derivative signal.

Subject 2

Subject 2 is female aged 29 years. A fragment of 0 to 7 seconds is shown in Figure 5.11 (a). There is successful enhancement and delineation of R-peak detection using the proposed method as shown in Figure 5.11 (b). Thus, R-peak is easily detected using the proposed approach.

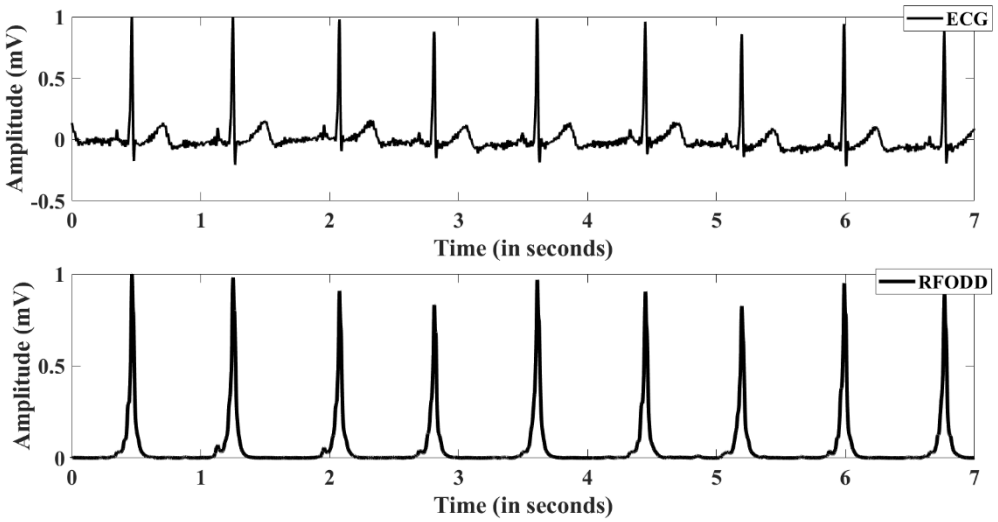

Figure 5.11 (a) Real-time ECG signal of subject 2 (b) Riesz-based derivative signal.

Subject 3

Subject 3 is aged 79 years male. He has varying RR intervals and has to change QRS morphology as depicted in Figure 5.12 (a). The suggested method successfully amplifies the high-frequency R-peak in this scenario as shown in Figure 5.12 (b). Therefore, R-peak can be easily detected in varying QRS morphology also.

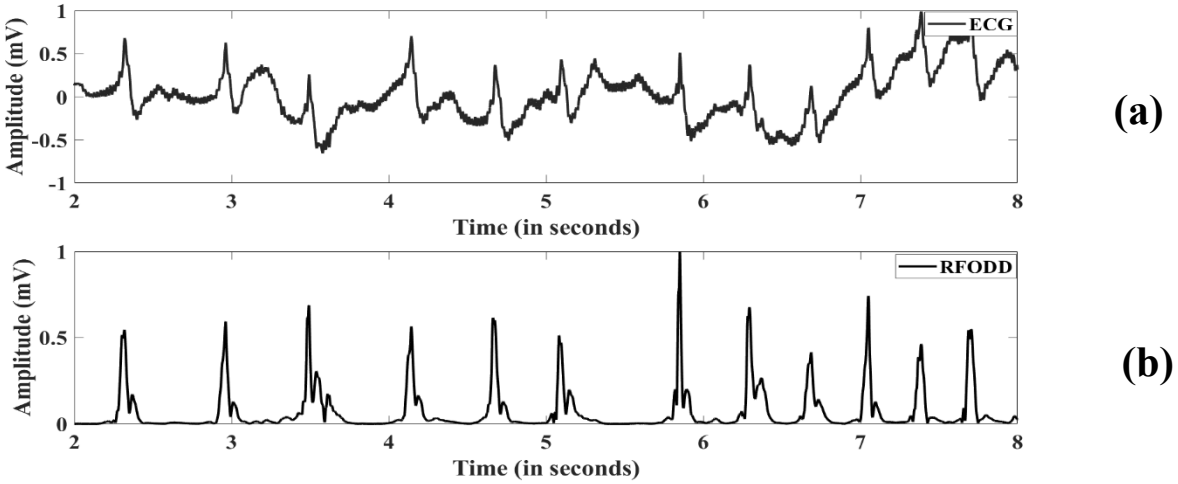

Figure 5.12 (a) ECG waveform of subject 3 (b) Riesz-based derivative signal.

Subject 4

Subject 4 is male aged 33 years. A fragment ranging from 0 to 7 seconds is selected. It has burst noise as depicted in Figure 5.13 (a), thus making R-peak detection difficult. But the proposed approach has enhanced high-frequency R-peaks in the signal very efficiently and attenuated the artifacts successfully as shown in Figure 5.13 (b). This way R-peak can be easily detected using the proposed approach.

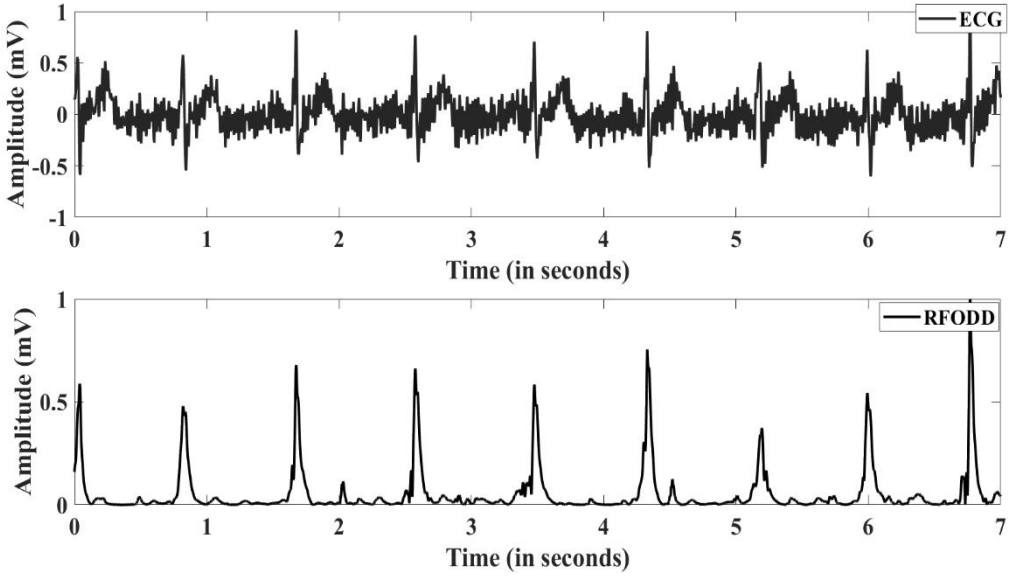

Figure 5.13 (a) ECG waveform of subject 3 (b) Riesz-based derivative signal.

The proposed approach is effective in detecting R-peaks in varying QRS morphology and burst noise situations also.

5.5.2 Classification of real-time ECG subjects

This work focuses on building the system more authentic in a real application. Therefore, it employs real-time ECG signals for research. After the signal acquisition, the focus is to extract relevant, non-redundant, and informative features that prove advantageous in detecting or classifying ECG beats into two classes i.e. normal (subjects never have heart ailment history) and abnormal (subjects have heart ailment history) effectively.

The features used in this work are tabulated in Figure 5.9. Time-domain and time-frequency domain characteristics are combined to form a feature vector. The result demonstrates that this feature set is successful in categorizing data and obtained good classification results.

The main motive behind feature extraction is to select or extract features that reflect complete and distinguish information about two classes of ECG beats. In this approach, one feature is represented as a boxplot diagram to indicate how distinct it is between two groups. The Shannon energy feature of two ECG classes is shown in the boxplot in Figure 5.14

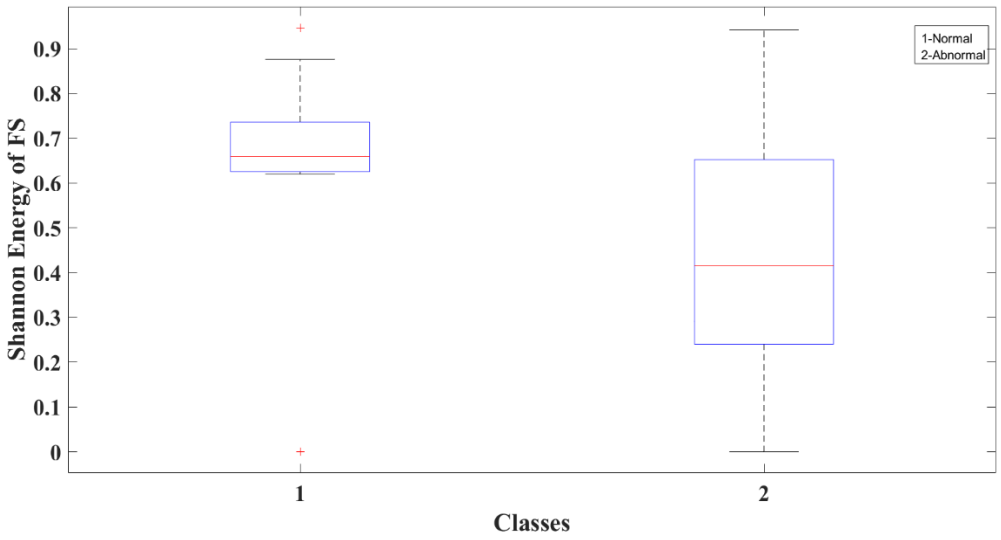

Figure 5.14 Two classes' FS Shannon energy in a boxplot diagram

The performance metrics such as sensitivity, positive predictivity, and accuracy are mostly used to evaluate the performance of the model. The quantitative and qualitative analysis is performed to prove the superiority of this method as compared to methods available in the literature, some common performance evaluation parameters are used, that is defined as:

$$\text{Sensitivity, } Sen = \frac{TP}{TP+FN} \tag{5.12}$$

$$\text{Positive Predictivity, } PPe = \frac{TP}{TP+FP} \tag{5.13}$$

$$\text{Accuracy, } acc = \frac{TN+TP}{TN+TP+FN+FP} \tag{5.14}$$

where TN is negative which indicates the abnormal beats are classified accurately. TP stands for true positive which shows that the number of normal beats is predicted as normal accurately. FP stands for false positive which is the number of actual abnormal samples predicted as normal. FN is false negative i.e. number of actual normal beats classified incorrectly. Table 5.1 shows the confusion matrix for the classifier.

Table 5.1 Confusion Matrix

Actual ~~Predicted~~	**Negative**	**Positive**
Abnormal	TN	FP
Normal	FN	TP

5.5.2.1 Feature selection using PCA

Figure 5.9 shows 219 features used in this work. Feature set dimensionality is reduced by using PCA. Figure. 5.15 makes it graphically obvious that the classifier's accuracy rises from 5 PC to 12 PC and then stays constant for more than 12 PC.

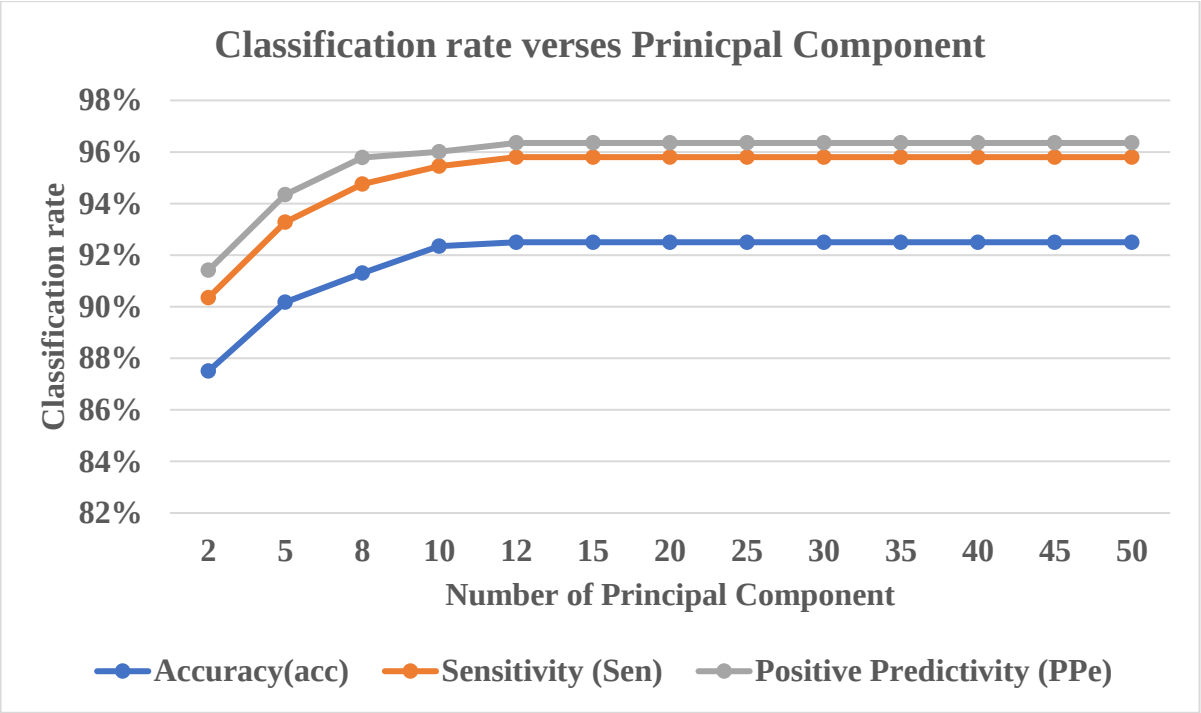

Figure 5.15 Plot of classification rate verse number of principal Component

5.5.2.2 Classification results

The set of 12 features is fed to the classifier ADkNN. The classification or misclassification is measured in terms of TP (true positive), FN (false negative), FP (false positive), and TN (true negative. For classification, ADkNN is used, along with the 10-fold cross-validation technique. Figure 5.16 shows the outcomes of the 10-fold cross-validation approach. The values of sensitivity, positive predictivity, and accuracy of two classes of ECG signals are represented in Table 5.2.

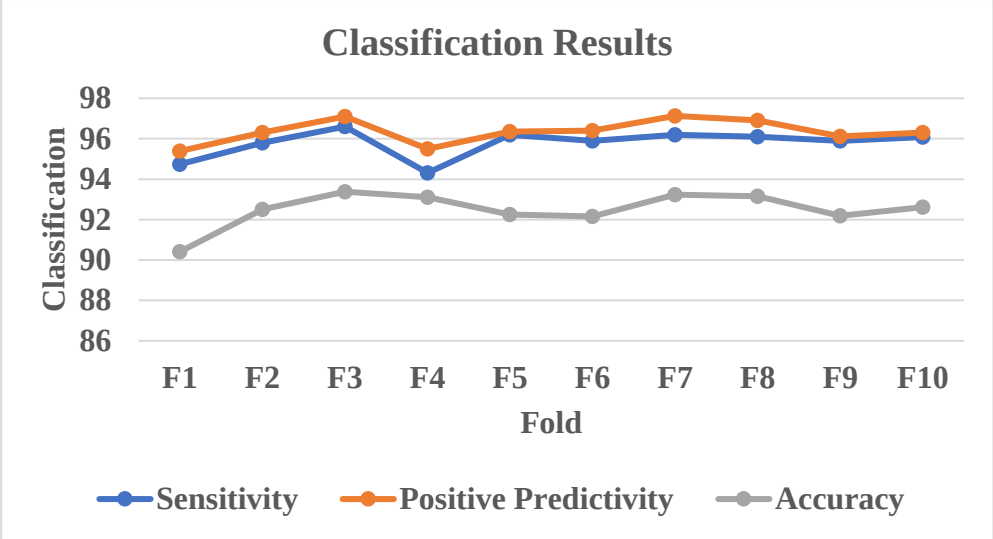

Figure 5.16 Classification Results

Table 5.2 ECG classification results for two classes

	Accuracy	Sensitivity	Positive Predictivity
Class Normal	95.39	97.9	98.55
Class Abnormal	89.61	93.7	94.15
	92.5	95.8	96.35

According to Figure 5.16, each fold has values for all three assessment parameters that are greater than 90%. 92.5%, 95.8%, and 96.35%, respectively, are the final values for accuracy, sensitivity, and positive predictivity. The results are compared with the state-of-the-art methods in Table 5.3.

Table 5.3 Comparison with the literature

Methods	**Real-Time Data Acquisition**	**ECG Feature Extracted**	**Statistics Calculated**	**Classification**
Ay *et al.* [68]	Yes	Yes	No	No
Kaya *et al.* [113]	-	Yes	No	No
Jain *et al.* [114]	No	Yes	No	No
Sharma *et al.* [57]	Yes	Yes	Yes	No
Proposed Method	Yes	Yes	Yes	Yes

Table 5.3, shows that it is the first time in the literature that classification is performed on a real-time ECG signal. The acquired real-time data is classified into two classes i.e. Normal (subjects who never have cardiac ailment history) and abnormal (subjects who have cardiac ailment history). The signal is acquired using the hardware system which consists of NI-myDAQ, LM2596, AD8232 ECG modules to acquire real-time ECG signal. R-peaks are detected efficiently with a 0% error rate even in changing

QRS morphology and burst muscle noise cases. The classification model uses an adaptive kNN neighbor for the classification.

5.6 Conclusions

The work presents a realistic model for acquiring real-time ECG data and its classification into two groups: normal (subjects with no history of cardiac disease) and abnormal (subjects who have a heart ailment history). The proposed technique uses NI-myDAQ, an AD8232 ECG module, and an LM2596 to acquire real-time ECG signals. The suggested work detected R-peaks in 35 real-time ECG signals with a 0% error rate. It has successfully recognized R-peaks in changing QRS morphology and burst muscle noise. The method combines the Fibonacci series's Shannon energy, Riesz fractional-order derivative signal coefficients, and other time-domain features and time-frequency domain features. The adaptive kNN classification performance on the proposed method yielded 92.5% accuracy, 95.8% sensitivity, and 96.35% positive predictivity. The first time the classification of real-time ECG data is performed to investigate whether the subject has cardiac ailment history or not, thus making the proposed approach reliable beneficial, and outstanding in the field.

The ***vital distinguishing attributes of the proposed classification method*** from the literature available are:

- The hardware system is developed using NI-myDAQ, LM2596, AD8232 ECG module to acquire real-time ECG signal.
- The method proposed is real and robust as it is the first time in literature that classification is performed on a real-time ECG signal.
- The acquired real-time data is classified into two classes i.e. Normal (subjects who never have cardiac ailment history) and abnormal (subjects who have cardiac ailment history)

CHAPTER 6

ECG BEAT CLASSIFICATION USING MIT-BIH-AD

AN IRREGULAR HEARTBEAT, or arrhythmia, alters the ECG signal normal cardiac cycle. Arrhythmia classification automatically is a difficult but highly desirable endeavor. The intra-patient criterion is typically used to evaluate traditional techniques of classifying arrhythmias, which may not be appropriate for the inter-patient criterion. A comprehensive classification technique has been proposed in the research, and it is successful for the minority class of the MIT-BIH arrhythmia database (MIT-BIH-AD) and performs well in intra-patient and inter-patient criteria.

The proposed approach in this chapter includes preliminary pre-processing of ECG signal based on Riesz fractional-order digital differentiator and R-peak detection (as proposed in Chapter 4), and various features are extracted from ECG beats. The feature set proposed in Chapter 5 is used which is a fusion of time-frequency, time domain traits, and features based on the Fibonacci series and the coefficients of fractional-order Riesz-based derivative. In this chapter, the proposed model classification is extended to MIT-BIH-AD to include more classes. The classification of MIT-BIH-AD is performed into six ECG classes.

The performance parameters like sensitivity, accuracy, and positive predictivity are calculated for both the intra and inter-patient schemes. The approach has achieved overall accuracy, positive predictivity, and sensitivity values for the intra-patient scheme are 99.85%, 99.93%, and 99.16% respectively, and for the inter-patient criterion of 89.89%, 92.5%, and 95.54% an average value of sensitivity, accuracy and positive predictivity of six ECG classes. The suggested method has performed well for the minority class in both criteria and the obtained results outperform the results of previous methods available in the literature in both schemes.

6.1 Overview of Classification

The classification of ECG arrhythmia has been the subject of extensive study. However, further investigation is still needed in this area because:

a) Although current research has achieved high accuracy values, it primarily focuses on an intra-patient criterion or beat-based scheme (which uses the same subject's ECG beats for training and testing), whereas in real-world applications, the training set would come from different subjects, and the testing set would come from completely different subjects (this is referred as an inter-patient scheme or record-based criterion) [7]
b) The methods available in the literature perform poorly for unbalanced datasets since they achieved low values for positive predictivity and sensitivity for small-size classes in the dataset. For instance, the MIT-BIH-AD [115] class atrial premature contraction (A), accounts for 2.37% of the entire dataset.

The key goal of this chapter is to overcome the aforementioned issues. The study focuses on extracting useful and non-redundant features. As indicated in chapters 4 and 5 and the literature [10], fractional-order calculus (FOC) secures signal information more successfully than integer-order calculus. So, in this research, the emphasis is on identifying ECG features that indicate deeper information and inherent beat characteristics. To achieve it, pre-processing of ECG signal is done using Riesz fractional-order digital differentiator. The coefficients of Riesz derivative signal are considered to be a part of the feature vector. The feature set proposed in Chapter 5 is used on MIT-BIH-AD. Therefore, the purpose of this work is to address this important and challenging topic and verify the results with previously published methods.

6.2 Selection of ECG Beats of MIT-BIH-AD for various Classes

Various ECG databases are accessible to verify the developed methods. The usage of verified databases is strongly advised because the results procured are identical to real-world signals. The MIT-BIH-AD is one of the most popular and frequently recommended for testing automatic arrhythmia classification. The MIT-BIH-AD contains ECG beats with rapidly changing QRS shape, inverted R-peaks, inverted T-

peaks, T-peak amplitude greater than R-peaks, broader R-waves, abrupt change in beat morphology, *etc*. Up to 16 different forms of arrhythmias exist.

This research work uses A (Atrial Premature Contraction Beats), L (Left Bundle Branch Block Beats), N (Normal Beats), P (Paced Beats), R (Right Bundle Branch Block Beats), and V (Premature Ventricular Contraction)] beats. There are 1,09,966 total beats in MIT-BIH-AD, and the considerate beats are 1,07,049, therefore they occupy the majority of the database [115].

Both the intra and inter-patient criterion is employed to allow a fair comparison with the approaches available in the literature. The 10-Fold Cross-Validation (10-FCV) method is applied to both schemes. The cross-validation method is commonly utilized in the literature for beat-based criteria for arrhythmia classification. We would use it for both the criterion in this research. Data profiles are shown in Table 6 for the intra and inter-patient schemes (1a and 6.1b). The split of ECG records during the training and testing phases is illustrated In Table 6.1c for the inter-patient-based 10-FCV method [18].

The MIT-BIH-AD is very imbalanced, 75,022 (70%) of ECG beats correspond to N, 2546 (2.37%) belong to A and 7129 (6.65%) correspond to V. Likewise, the L class consists of 8072 beats (7.54%), R contains 7255 (6.77%) and P class has 7025 beats (6.56%) [18]. Table 6.1c shows that only a few records are repeated in the cross-validation test set because some beats are present in some records only. For instance 4 ECG records have L type beats and 6 ECG records have R type beats [115].

Table 6.1a Dissection of beats for 10-FCV approach for intra-patient criterion [115]

Fold	Total training beats						No. of training beats	Total testing beats						No. of test beats
	N	L	R	V	A	P		N	L	R	V	A	P	
1	67520	7265	6530	6417	2292	6323	96347	7502	807	725	712	254	702	10702
2	67520	7265	6530	6416	2292	6323	96346	7502	807	725	713	254	702	10703
3	67520	7265	6530	6416	2292	6323	96346	7502	807	725	713	254	702	10703
4	67520	7265	6530	6416	2292	6323	96346	7502	807	725	713	254	702	10703
5	67520	7265	6530	6416	2291	6323	96345	7502	807	725	713	255	702	10704
6	67520	7265	6529	6416	2291	6322	96343	7502	807	726	713	255	703	10706
7	67520	7265	6529	6416	2291	6322	96343	7502	807	726	713	255	703	10706
8	67520	7265	6529	6416	2291	6322	96343	7502	807	726	713	255	703	10706
9	67519	7264	6529	6416	2291	6322	96341	7503	808	726	713	255	703	10708
10	67519	7264	6529	6416	2291	6322	96341	7503	808	726	713	255	703	10708

Table 6.1b Dissection of beats based on 10-FCV approach for the inter-patient criterion [115]

Fold	Total training beats						No. of training beats	Total testing beats						No. of test beats
	N	L	R	V	A	P		N	L	R	V	A	P	
1	70682	5581	5090	6912	2414	5483	96162	4340	2491	2165	217	132	1542	10887
2	70989	5949	5725	6461	2544	4947	96615	4033	2123	1530	668	2	2078	10434
3	68715	6615	7170	6979	2427	5647	97553	6307	1457	85	150	119	1378	9496
4	70167	6071	5430	6760	2544	4998	95970	4855	2001	1825	369	2	2027	11079
5	70719	5581	6002	7027	2545	4947	96821	4303	2491	1253	102	1	2078	10228
6	70189	5949	6858	6503	1128	5483	96110	4833	2123	397	626	1418	1542	10939
7	69882	6615	5005	6809	1960	4998	95269	5140	1457	2250	320	586	2027	11780
8	69583	6071	5725	6596	2534	5647	96156	5439	2001	1530	533	12	1378	10893
9	72718	4124	7170	6824	2231	5483	98550	2304	3948	85	305	315	1542	8499
10	71772	5949	5430	6294	2539	4998	96982	3250	2123	1825	835	7	2027	10067

Table 6.1c Dissection of ECG record for inter-patient criterion based on10-FCV approach for the training and testing set [115]

Fold	Training set records	Test set records	Fold	Training set records	Test set records
1	Remaining records	100,101, 109, 118, 217	6	Remaining records	111, 202, 203, 217, 232
2	Remaining records	105,106, 107, 111, 124	7	Remaining records	102, 118, 207, 209, 210
3	Remaining records	104,112, 113, 114, 207	8	Remaining records	104, 124, 214, 215, 219
4	Remaining records	102,116, 117, 212, 214	9	Remaining records	109, 207, 217, 222
5	Remaining records	107,109, 122, 123, 231	10	Remaining records	102, 111, 212, 233

6.3 Feature Extraction of ECG beat of MIT-BIH-AD

Figure 6.1 depicts the algorithm for classifying ECG arrhythmias. The raw ECG is procured from MIT-BIH-AD. Every classification model shares a usual framework which includes pre-processing, extraction of features, and data classification. The ECG signal pre-processing is a crucial step as it enables the extraction of useful and non-redundant features that best describe the ECG beat. Noises and artifacts such as Baseline Wander (BW) and Power Line Interference (PLI), occur in every ECG record [116]. These noises can sometimes alter the ECG wave shape significantly, therefore making its scrutiny a tough job while examining it with computer-aided approaches.

The QRS complex has a frequency range of 5-25 Hz, and the Butterworth band-pass filters with lower and higher cut-off frequencies: 5Hz and 25Hz respectively are used to process the ECG waveform [99]. The artifacts like PLI (50Hz) and BW (1Hz) are eliminated. Following pre-processing, each ECG beat is segmented, and two techniques are used to extract the features to build a feature vector (as presented in Figure 6.1). Then,

principal component analysis (PCA) is applied to the feature vector to minimize the feature's dimensions [77]. Classifier uses the PCA output as its input.

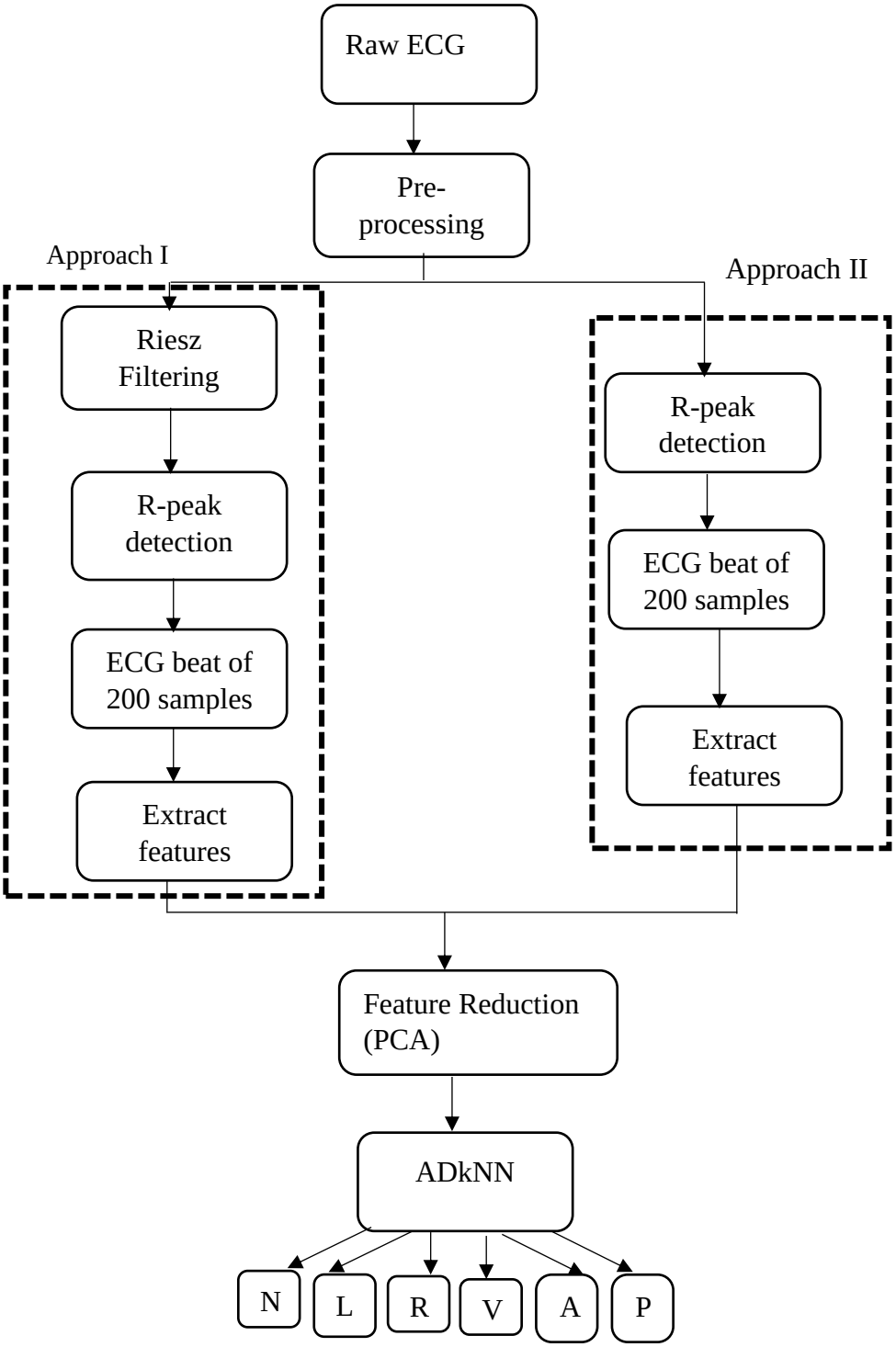

Figure 6.1 Block diagram for MIT-BIH-AD classification

6.3.1 Approach I

Due to the inherited abilities of fractional order to remove artifacts and amplify useful information in signals, fractional-order calculus (FOC) has proven to offer unique details in signal processing [10, 16]. While models developed directly or indirectly on integer order tend to remove the high-frequency components from the signal as fractional-order has the benefit over the integer order that it preserves the signal's features. In recent decades, FOC has received a lot of attention in signal processing, particularly ECG signal processing. Because of its emphasis on the capacity to remove artifacts, elevate important information and produce fractal signals, FOC is applied to ECG signals [10, 16].

It is mentioned in Chapter 4, the Riesz fractional-order digital differentiator (RFODD) was found to have higher sensitivity and reduced error rate for R-peak detection than the other approaches in the literature. The efficiency with which RFODD at fractional-order p=0.6 has recognized the R-peaks while retaining the signal's information (as mentioned in Chapter 4). This characteristic enables the extraction of informative features that reflect the ECG signal's underlying characteristics, enhancing the classifier's effectiveness.

In Approach, I, the Riesz-based derivative [discussed in Chapter 4] is acquired following the pre-processing of the ECG waveform to magnify the high-frequency QRS complex that is characteristic of the signal [99]. Then ECG record is divided into 200 samples beat, with 99 samples taken just before and 100 samples just after the R-peak [78]. Figure 6.2 displays the 200 sample beats of six different types of ECG. The features from Approach I are the coefficients of the Riesz-based fractional-order derivative signal as well as the peak values, mean, and standard deviation of the ECG derivative signal.

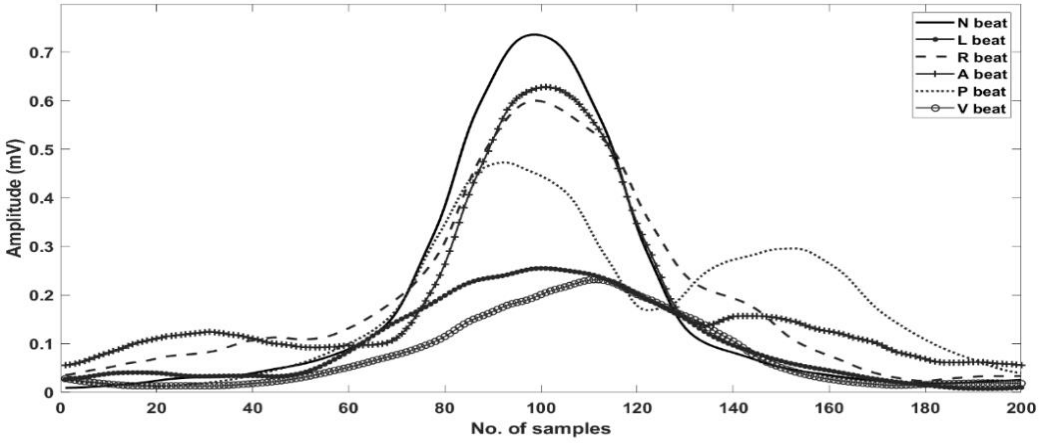

Figure 6.2 Riesz derivative of six different type of ECG beats

6.3.2 Approach II

The ECG signal rhythm has important information, therefore making it an efficient tool for the physician in diagnosing cardiac abnormalities. To have complete information about non-stationary ECG signals, features are extracted from the Time Domain (TD) and Time-Frequency Domain (TFD), so that they reflect the most information about the beat. Morphological or TD and TFD are two frequently used ECG features in arrhythmia classification. TD characteristics or fiducial features typically include the shape, height, and duration of QRS, P and T wave, and so on [117]. TFD characteristics include coefficients of Wavelet Transform (WT) and S-transform (ST) in the ECG beat.

In this research, the Fibonacci series is used as one of the TD features which is explained below along with other TD and TFD traits.

6.3.2.1 Fibonacci series

The Fibonacci series is defined below:

$$f_b = \begin{cases} 0, & if\ b = 0 \\ 1, & if\ b = 1 \\ f_{b-1} + f_{b-2} & if\ b > 1 \end{cases} \tag{6.1}$$

where f_b represents the array element. FS is used as an index for acquiring features from the ECG beat. The FS's index is used by 200 sample ECG beats (as depicted in Figure 6.3a) obtained after the pre-processing, and a Fibonacci series signal is generated from it (as shown in Figure 6.3b). The visual interpretation of Figure 6.3a indicates that beats belonging to different classes are discernible from each other, thus the acquired Fibonacci signals in Figure 6.3b are distinguishable from each other. Therefore, the energy contained in the signals will also vary. The newly acquired Fibonacci signal's (FS) Shannon energy (SE) is computed and used as the feature. It determines the energy per sample of the local spectrum. It's outlined as:

$$SE = -|y[n]|\log\left(|y[n]|\right) \tag{6.2}$$

where $y[n]$ is the amplitude of the Fibonacci series signal generated.

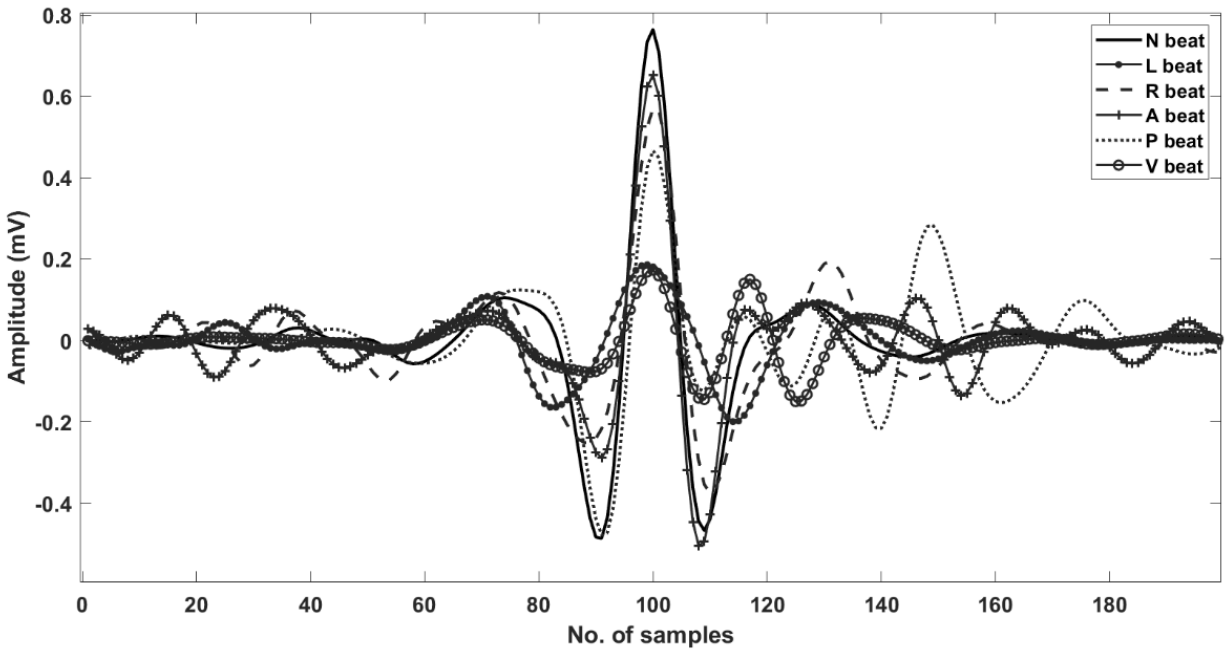

Figure 6.3a Six different type of ECG beats.

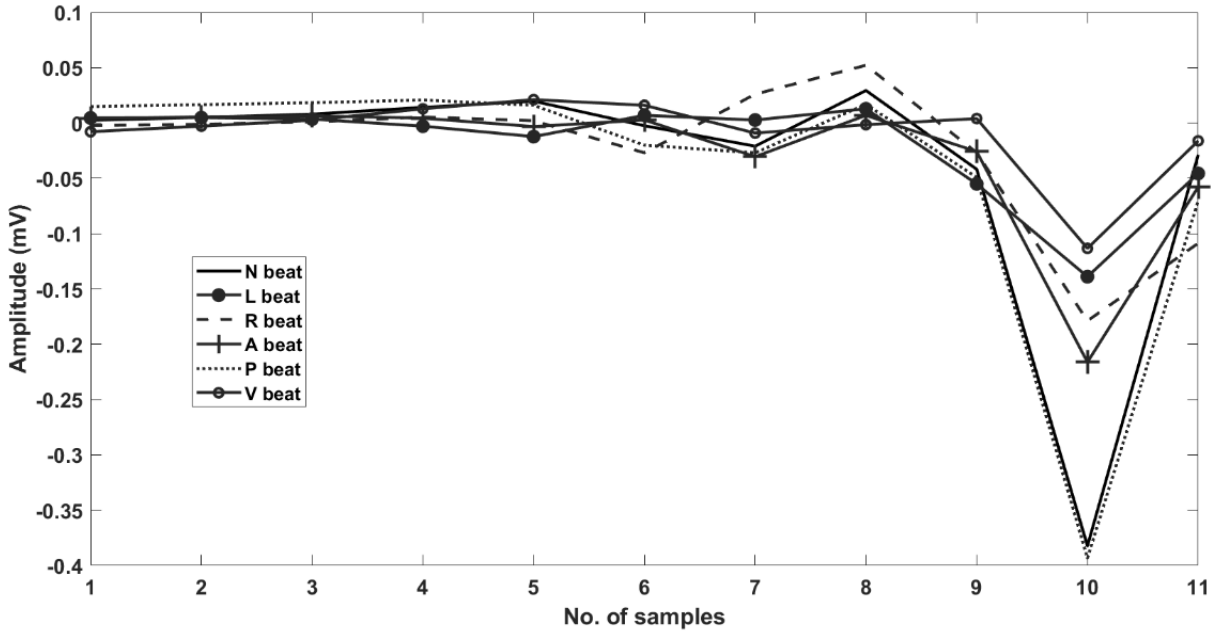

Figure 6.3b FS signal acquired from Figure 6.3a.

6.3.2.2 Additional time-domain (TD) characteristics

Figure 6.3a shows that ECG beats of different classes have distinct morphology. ECG beat belonging to different classes have distinct shapes and reflect different cardiovascular information. The careful analysis of six different types of ECG beats as depicted in Figure 6.3a, confirms that the morphology of ECG beats varies mainly in ST

and PQ segments. As a consequence, the maximum, and minimum, slope of ST and PQ segments, and the maximum and minimum of ECG beat are regarded as features. RR interval is the most used TD feature [7, 70]. Therefore, two RR intervals are employed in this work: (i) RR interval of two consecutive beats and (ii) RR interval of the record. A total of ten TD features are considered.

6.3.2.3 Time-Frequency Domain (TFD) characteristics

The hidden traits of ECG beat can be effectively interpreted by the coefficients of WT [78, 109] and ST [109]. These coefficients are large in number, and using them directly as features is complex. Therefore, other high-level features like entropy or Shannon energy, energy are derived from these coefficients for better classification results. These characteristics are widely used in image processing, signal processing, and pattern recognition.

ST maintains a close relationship with the Fourier Spectrum and offers frequency-dependent resolution [108]. When it is used to analyze an ECG beat, an ST matrix is produced. The SE, standard deviation, and mean are obtained as three features from the ST output.

The energy content for N and V type ECG beat are plotted in [31] for 4^{th} and 5^{th} level decomposition. It was indicated that the energy of the QRS complex reaches its peak at the fourth level for N beats, meanwhile at the fifth level for V beats. As a result, these bands' energy is employed as features. Seven features in total are used in the TFD. Table 6.2 lists all the features extracted for the study.

Table 6.2 Features employed for arrhythmia classification.

	Feature Name	Description	Size	Total
Novel Features	Riesz based features	The coefficients of Riesz based fractional-order derivative signal + peak value, mean, and standard deviation of Riesz based derivative signal.	203	204
	Fibonacci series	Shannon energy of the Fibonacci series signal	1	
Time-domain	Morphology	Maximum, minimum of a beat, maximum, minimum	8	10

features		and slope of ST and RQ segment		
	RR-Interval	RR interval between beats +RR interval of record.	2	
Time-frequency domain features	DWT	The energy of 4^{th} and 5^{th} level decomposition coefficients	4	7
	ST	Shannon energy, mean and standard deviation of ST coefficient	3	

Table 6.2 shows that there is a total of 221 traits in all. The classification process will take longer to compute as the number of features increases. Therefore, the dimensionality reduction technique principal component analysis (PCA) is utilized to decrease the number of features in the feature vector without impacting the classifier's accuracy. The details are provided below.

6.3.3 Principal Component Analysis (PCA)

It is a well-known and often-used technique for dimensionality reduction and feature extraction. Data of correlated variables are transformed into principal components (PCs), which are linearly uncorrelated variables. The 1^{st} PC provides a basis vector for the direction of greatest variability in this transformation [92, 109]. The 2^{nd} PC, which is orthogonal to the 1^{st} PC, provides the basis vector for the subsequent direction for the condition that is being applied. The PCA procedure is explained in detail in Chapter 5. In this study, various PC values are compared to the classifier's accuracy rate, and the details are given in Section 6.4.1.

6.3.4 Adaptive K nearest neighbor (ADkNN)

It designates test samples to the class that typically includes its closest k neighbors. When the training dataset contains a high number of samples, it works well at reducing misclassification errors. ADkNN is utilized in this study to get improved accuracy (more detail is explained in Chapter 5). For different values of k, this algorithm identifies the k value at which it provides the highest expected accuracy (e acc) for a specific test point, p.

6.4 Results and Discussion

The suggested work was tested using a MATLAB 2021a system with an Intel Core i7 CPU with having 3.40 GHz processor with 8 GB of RAM.

The suggested method aims on extracting features that manifest favorably in detecting, classifying, and quantifying relevant ECG beat parameters, and making the system more realistic in a real scenario. The focus is mainly to boost the classification performance of the minority class. Thus, features are selected so that they exhibit discernibility among six different classes so that the issue of class imbalance is resolved. The proposed method is tested on the MIT-BIH-AD.

The significant features of ECG beat are derived (depicted in Table 6.2) from the TD, TFD, Fibonacci series signal, and coefficients of the Riesz-based derivative signal. The methodology is to fuse all the features. This feature set is also used for the classification of real-time ECG subjects and yielded good results in Chapter 5. In this chapter, it is used on MIT-BIH-AD. The result demonstrates that the suggested feature fusion is highly effective in terms of accuracy for the classification of ECG arrhythmia both in inter-patient and intra-patient criterion, as well as in achieving better classification performance for the minority class of MIT-BIH-AD.

The key to create an efficient diagnostic system for identifying and classifying arrhythmias is to choose outstanding feature information that provides comprehensive knowledge of ECG signal while at the same time is discernible from other class features. One of the features is depicted as a boxplot to demonstrate the distinguishability of the features. In Figure 6.5, the Shannon energy of FS of six classes is represented in the form of the boxplot.

The performance measures like sensitivity, and positive predictivity are generally the best ones for assessing the system's performance. To demonstrate the superiority of this strategy over well-established approaches, quantitative and qualitative analysis is carried out, and some widespread performance evaluation parameters which are defined below are used.

Sensitivity, $Sen = \frac{\sum_{M=1}^{N} TP_M}{\sum_{M=1}^{N} TP_M + \sum_{M=1}^{N} FN_M}$ (6.3)

Positive Predictivity, $PPe = \frac{\sum_{M=1}^{N} TP_M}{\sum_{M=1}^{N} TP_M + \sum_{M=1}^{N} FP_M}$ (6.4)

$$\text{Accuracy, } acc = \frac{\sum_{M=1}^{N} TP_M + \sum_{M=1}^{N} TN_M}{\sum_{M=1}^{N} TP_M + \sum_{M=1}^{N} TN_M + \sum_{M=1}^{N} FN_N + \sum_{M=1}^{N} FP_N} \quad (6.5)$$

where N is the total number of beats, TP_M (true positives) which is described as the number of M types that are accurately predicted. TN_M is the true negative and is calculated as the number of not-M types that are accurately predicted. FP_M (false positive) and is calculated as the number of not M-types that are inaccurately classified as M types. FN_M (false negative) and it is defined as the number of M types that are inaccurately classified as not M-types. The four indices of the N class (TP_M, TN_M, FN_M, FP_M) are mentioned in Table 6.3a. Similarly, TP, TN, FP, and FN are calculated for other classes. The confusion matrix for performance evaluation parameters for the classifier is tabulated in Table 6.3a. The subscript n, l, r, v, a, and p in Table 6.3b stands for class N, L, R, V, A, and P respectively in Table 6.3b.

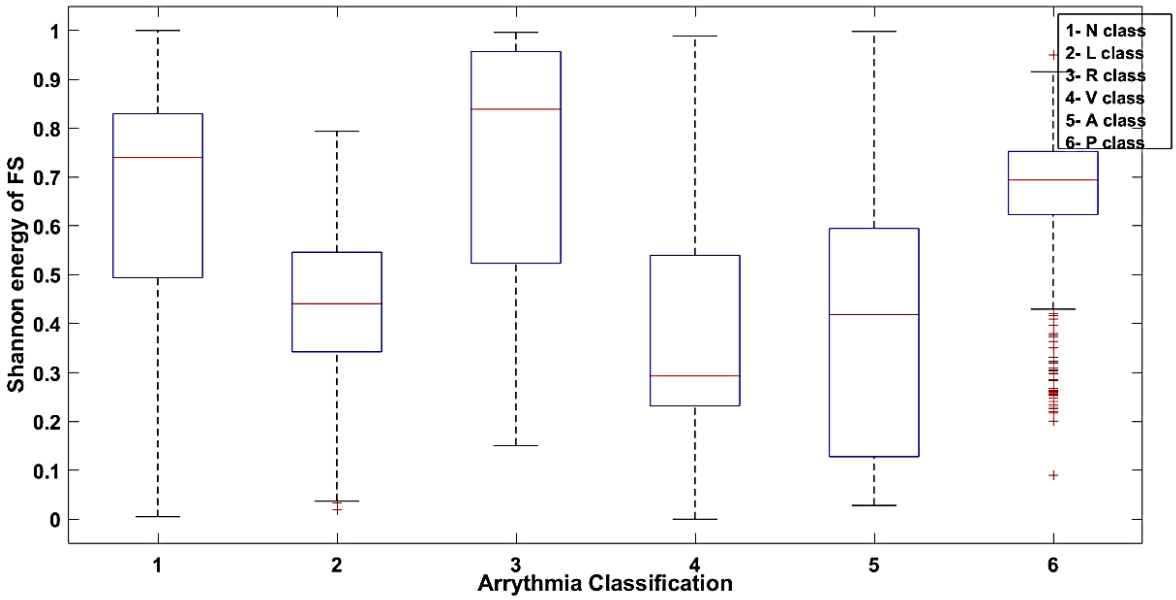

Figure 6.4 Boxplot representation of the Shannon energy of FS of six classes.

Table 6.3a Calculation guide for N beat class's TP, TN, FN, and FP.

	N	**L**	**R**	**V**	**A**	**P**
N	TP_N	FN_N	FN_N	FN_N	FN_N	FN_N
L	FP_N	TN_N	TN_N	TN_N	TN_N	TN_N
R	FP_N	TN_N	TN_N	TN_N	TN_N	TN_N
V	FP_N	TN_N	TN_N	TN_N	TN_N	TN_N
A	FP_N	TN_N	TN_N	TN_N	TN_N	TN_N
P	FP_N	TN_N	TN_N	TN_N	TN_N	TN_N

Table 6.3b Performance evaluation parameters for Classifier.

				Algorithm				
Reference		**n**	**l**	**r**	**V**	**a**	**p**	**Sum**
	N	Nn	Nl	Nr	Nv	Na	Np	∑**N**
	L	Ln	Ll	Lr	Lv	La	Lp	∑**L**
	R	Rn	Rl	Rr	Rv	Ra	Rp	∑**R**
	V	Vn	Vl	Vr	Vv	Va	Vp	∑**V**
	A	An	Al	Ar	Av	Aa	Ap	∑**A**
	P	Pn	Pl	Pr	Pv	Pa	Pp	∑**P**
								∑

A sensitivity (*Sen*) metric can be used to convey a false alarm diagnosis. A low value of *Sen* indicates that the cardiac arrhythmia is being misclassified by the classifier, thus leading to a false diagnosis. A false alarm may have an impact on the psychological state of a subject leading to unwanted stress and trauma. Sensitivity is a crucial metric to consider while making a decision.

The proposed method proposes a technique that fits well into a real scenario and addresses the aforementioned issues with a minority class, *i.e.*, a class of MIT-BIH-AD. This research work, therefore suggests a beneficial approach for automatic arrhythmia classification and it is evaluated for intra-patient and inter-patient schemes and attained good results.

6.4.1 Feature selection using PCA

Table 6.2 shows that there are 221 traits in all. To decrease the dimensionality of a feature vector while maintaining the accuracy of the classifier, PCA is applied. The different PC count is considered and *acc*, *Sen*, and *PPe* of the classifier are plotted. It has been discovered that for the intra-patient scheme, the accuracy grows quickly as the number of PC increases and then it stays constant for 15 PC and more PCs. The classifier's accuracy rate is stable for 15 PC or more in the inter-patient scheme as well. The plots of the number of PCs versus the classifier accuracy rate for intra and inter-patient schemes respectively are shown in Figures 6.5 and 6.6.

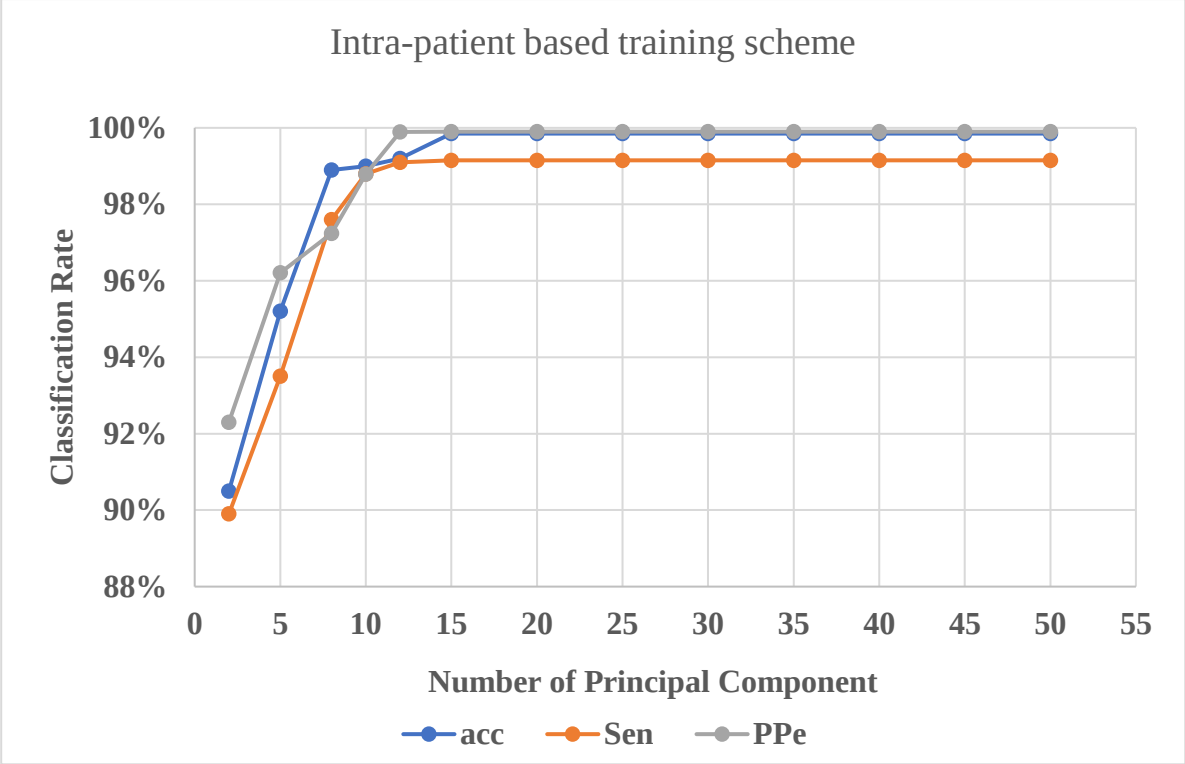

Figure 6.5 Plot indicating classification for intra-patient scheme versus the number of PC

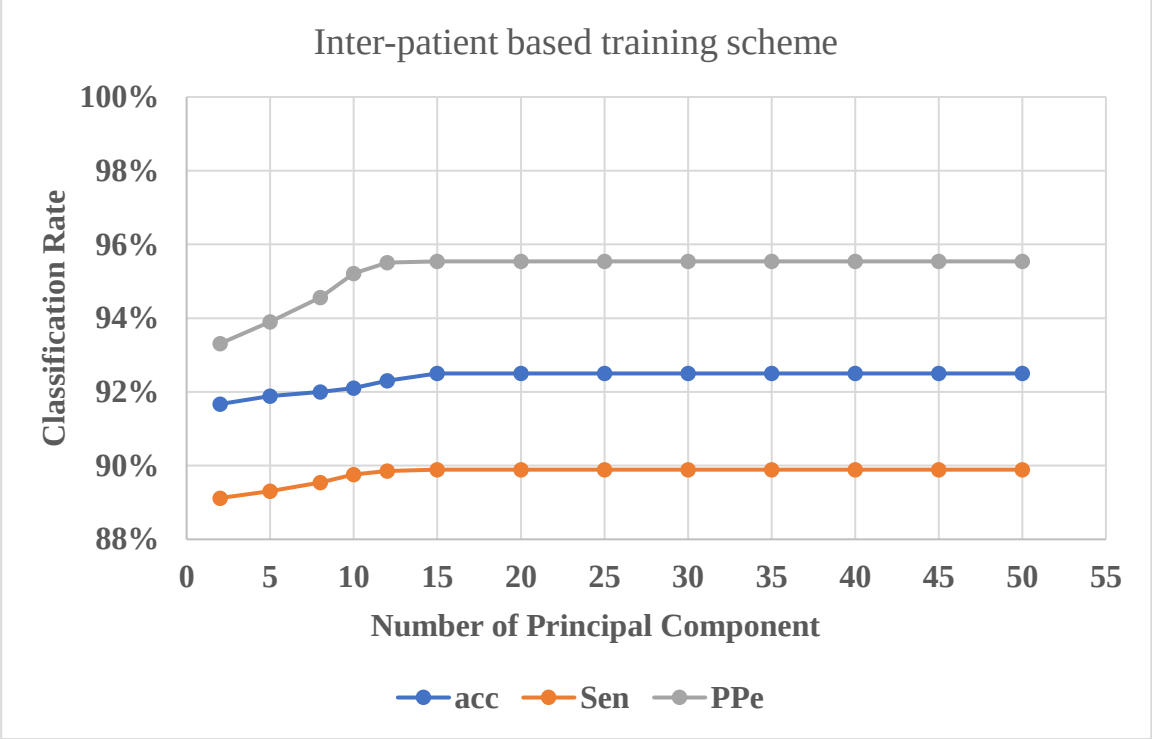

Figure 6.6 Plot indicating classification rate for inter-patient scheme versus the number of PC

6.4.2 Simulation results for the intra-patient scheme

The intra-patient criterion or beat-based scheme uses a set of 15 features. For classification, ADkNN and the 10-FCV technique are used. Table 6.4 contains the results of *Sen*, *acc*, and *PPe* for six classes and Figure 6.7 displays the results for the 10-FCV technique. In all, 107049 beats are employed in this study and the distribution of the beats for the 10-FCV method is tabulated in Table 6.1a.

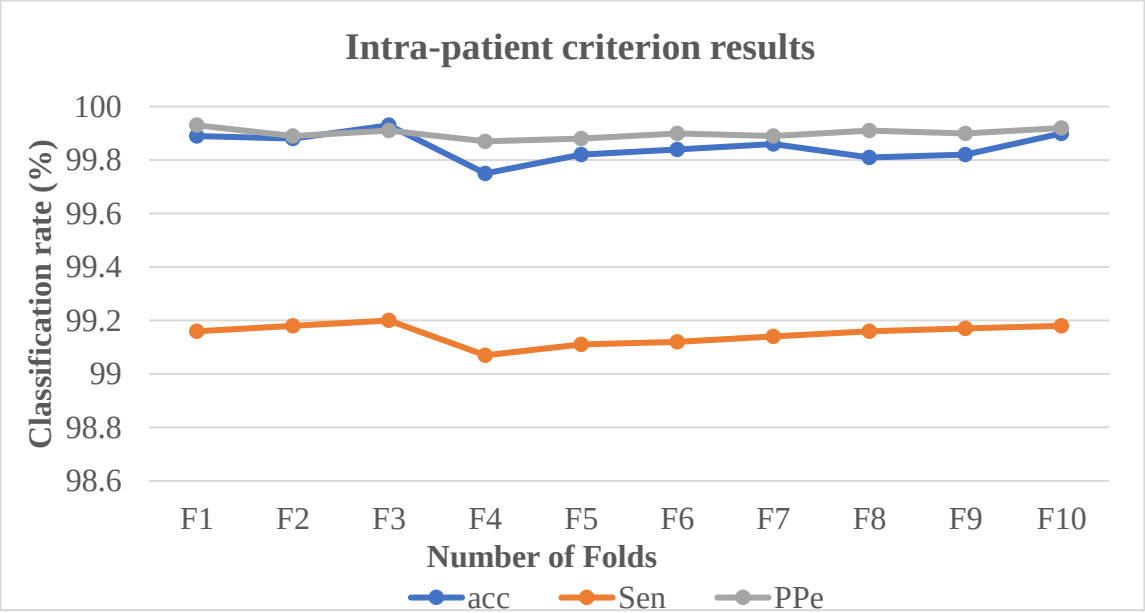

Figure 6.7 Classification evaluation parameters for intra-patient criterion.

Table 6.4 ECG arrhythmia classification results for six classes for intra-patient criterion.

	Accuracy	**Sensitivity**	**Positive Predictivity**
Class N	99.99	99.99	99.99
Class L	99.94	99.24	99.95
Class R	99.95	99.29	99.96
Class V	99.92	99.31	99.97
Class A	99.39	98.1	99.75
Class P	99.91	99.03	99.96
	99.85	**99.16**	**99.93**

The intra-patient criterion has attained outstanding outcomes using the suggested methodology. Figure 6.7 makes it evident that all three assessment parameters have values of more than 99% for each fold. ADkNN's total *acc* is 99.85%, while *Sen* and *PPe* are 99.16% and 99.93% respectively. The minority class also did well with the suggested method, achieving 99.39% *acc*, 98.1% *Se*, and 99.75% *PP*. of the six classes, Class N has the highest values of *acc*, *Sen*, and *PP*e.

6.4.3 Simulation results for the inter-patient scheme

The inter-patient criterion is taken into consideration as described in [115] to make the proposed work more practical. To improve classification rates, an ADkNN classifier is used, along with 10-FCV. Tables 6.1c and Table 6.1b respectively show the distribution of the data for the inter-patient criterion and the number of beats in the training and testing set for the 10 folds. In this dataset, class A is the minority class. Table 6.5 contains the results of *Sen*, *acc*, and *PPe* findings for six classes and Figure 6.8 displays the results for 10-FCV.

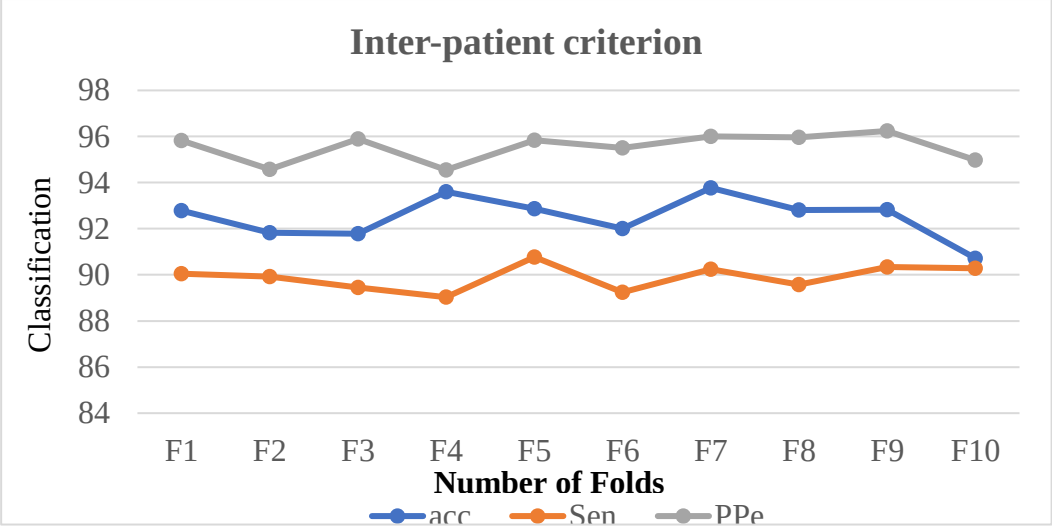

Figure 6.8 Classification evaluation parameters for inter-patient criterion.

Table 6.5 ECG arrhythmia classification results for six classes for inter-patient criterion.

	acc	**Se**	**PP**
Class N	99.99	99.79	99.99
Class L	92.57	88.67	96.17
Class R	92.63	89.59	96.48
Class V	93.71	90.01	97.74
Class A	85.41	83.23	89.81
Class P	90.69	88.05	93.05
	92.5	**89.89**	**95.54**

The proposed work has outperformed the inter-patient criterion also. The overall accuracy for ADkNN is 92.5%, and *Sen* and *PPe* are 89.89% and 95.54% respectively. The highest classification rates were attained by class N with *acc*, *Sen*, and *PPe* are 99.99%, 99.79%, and 99.99% respectively. In terms of *acc*, *Sen*, and *PPe*, the minority class A likewise did quite well, scoring 85.41%, 83.23%, and 89.81% respectively.

6.5 Comparison with state-of-the-art Methods

The outcomes of the proposed study are compared with those of state-of-the-art methods and they are shown in Table 6.6. The achieved results demonstrate that the suggested approach is superior to that described in the literature [91, 115, 118-124] in the intra-patient criterion achieving 99.85% *acc*, 99.16% *Sen,* and 99.93% *PPe* as well as in inter-patient attaining 92.5% *acc*, 89.89% *Se* and 95.54% *PP* of six ECG beats. Table 6.6 makes it evident that various approaches in the literature have used different numbers of beats, records and pre-processing techniques. Therefore, the classification rates may be impacted by all of these techniques. Numerous methods have attained more than 90% results for classification in literature. Many of them have used only the intra-patient scheme (beat-based criterion) or evaluated their result over a smaller dataset. However, the proposed approach has used 1,07,049 beats from MIT-BIH-AD, taking into account all the effective beats in the dataset, and has achieved high values for evaluation parameters. The proposed strategy, which outperformed methods described in the literature [91, 115, 121], took into account the inter-patient scheme as well. Thus, the comparison shows that the proposed approach is very promising for classifying ECG signal beats and can be a useful tool for automatic ECG beat classification.

6.6 Conclusions

This research work proposes a new and innovative method for classifying ECG arrhythmias. This approach amalgamated time-frequency features, the Riesz-based fractional-order derivative signal coefficients, and the Shannon energy of the Fibonacci signal obtained from the beat with other time-domain features.

The suggested strategy outperforms the other methods in literature since it has attained promising performances in issues faced in the literature: (i) it performed well for the minority class, *i.e.,* A of MIT-BIH-AD, achieving better performance parameters for it; (ii) the algorithm is more realistic as it is evaluated on the inter-patient scheme also. When evaluated on the MIT-BIH-AD, the performance of the proposed algorithm outperformed the state-of-the-art approaches. For six types of ECG beat classification, the findings for the intra-patients criterion attained an average value of accuracy, sensitivity, and positive predictivity of 99.85%, 99.15%, and 99.9% respectively, and for

Table 6.6 Comparison of the ECG arrhythmia classification.

Methods	**Feature selection (dimension)**	**Inter/ Intra scheme**	**Beat Type**	**Training/ Test beat**	**Classifiers**	**K-fold cross validation**	**acc**	**Se**	**PP**
Garcia *et al*. [91]	Yes	Inter	3		SVM	Unknown	92.4	-	-
Qin *et al.* [115]	Yes	Intra	6	107049	SVM	10-fold	99.7	99.09	99.7
		Inter				10-fold	81.47	44.40	81.47
Acharya *et al.* [118]	No	Intra	5	109449	Deep convolutional NN	10-fold	Set A: 93.47	96.01	97.87
							Set B: 94.03	96.71	97.86
Yu *et al.* [119]	-	Intra	8	9800	BPNN, PNN	-	98.7	-	-
Lin *et al.* [120]	Yes	Intra	3	99827	Linear Discriminant	Unknown	Set A: 93	83.5	67.6
							Set B: 90.8	86.4	68.2
Lu *et al.* [121]	-	Intra	3	-	RF	Unknown	99.9	-	-
		Inter					99.53		
Jha *et al.* [122]	Yes	Intra	8	41097	SVM	-	99.27	96.22	-
Kutlu *et al.* [123]	Yes	Intra	16	5887	kNN	No	93.56	85.59	-
Kutlu *et al*. [124]	Yes	Intra	5	5887	kNN	No	-	89.8	-
Proposed Method	Yes	Intra	6	107049	ADkNN	10-fold	99.99	99.99	99.99
		Inter					92.5	89.89	95.54

the inter-patient criterion, an average value of accuracy, sensitivity and positive predictivity of 92.5%, 89.89%, and 95.65% respectively.

The proposed method has demonstrated its viability in a real-world scenario by outperforming state-of-the-art methods in the inter-patient scheme. The results are better in performance evaluating parameters such as sensitivity, positive predictivity, and accuracy. The approach works well for minority class A of MIT-BIH-AD as it produces better outcomes for both inter and intra-patient criteria.

The ***major distinguishing characteristics of the suggested work*** from other methods in literature are as enlisted:

- Following the interpretation of fractional-order to eliminate noise effectively and strengthen the important details of the signal, it is the first time that the Riesz based fractional-order derivative signal coefficients are used as feature to preserve the information better.
- The proposed method has performed well for minority class. It yielded superior performance in terms of *Se*, *PP* for class A of MIT-BIH-AD in both inter-patient and intra-patient criterion
- The method is robust and real, as it is evaluated on the inter-patient scheme or record based scheme.

CHAPTER 7

CONCLUSIONS AND FUTURE WORK

ELECTROCARDIOGRAM (ECG) signal conveys crucial diagnostic details regarding the functioning of the heart. Its processing and analysis are crucial and critical in the diagnosis of heart problems. The QRS complex detection is the main focus of almost all automatic computer-based approaches. The accurate detection of the QRS complex is extremely important in clinical and in wearable. Any dysfunction in normal ECG sinus rhythm due to premature or delay depolarization or repolarization of atria and ventricles results in the change of morphology of QRS which is further related to one or other heart diseases. Raw ECG has artifacts like baseline wander, power line interference, and muscle noise. Thus, for appropriate evaluation of cardiovascular diseases, a general framework is followed: (i) de-noising, (ii) QRS complex detection (iii) feature extraction and (iv) classification.

This study focuses on proposing a real-time and robust method for ECG classification as this approach includes real-time ECG data acquisition, pre-processing, R-peak detection, feature extraction and classification. This method is also tested on MIT-BIH-AD to evaluate its performance with state-of-the-art methods. The main contributions of this dissertation are summarized in Section 7.1 and a few tracks for future research are presented in Section 7.2.

7.1 Conclusion

The main contribution of the thesis is to propose a real-time and robust method for ECG classification. The contribution of the research work reported in this dissertation can be concluded as follows:

- Design of Hamming self-convolution window (HSCW) based band-pass filter approach in contrast to conventional window-based filter.

- Establishment of an efficient method for R-peak detection based on Riesz fractional-order digital differentiator (RFODD).
- Design of method to acquire real-time ECG data acquisition, perform pre-processing, feature extraction and classification of beat into normal (subjects which never had cardiac ailment history) and abnormal (subjects who have cardiac ailment history).
- Design of robust ECG classification method, which tests ECG beat of MIT-BIH-AD. This method has performed well for both intra and inter-patient criterion and has given good results for minority class.

The initial work in this thesis focused on the development of HSCW band-pass filter which has narrow main lobe width and lower side lobe level as compared to conventional Hamming window-based filter. Since the researcher has extensively studied the FIR filters in context of ECG pre-processing, this work offered an improved window function which has narrow main lobe width and lower side lobe level for designing new filter. The analytical and simulation investigations shows that the suggested method, when compared to traditional window-based filters and other well-known techniques in literature yields much better results for R-peak detection.

Furthermore, considering the remarkable performance of fractional-order calculus (FOC) in engineering and science domains, it has been the centre of attention in research communities. The inquisitiveness for the introduction of fractional derivatives in ECG signal processing field is stimulated by its astonishing performance and robustness attained in control theory. In-depth research on FOC has been published in the literature, where it has been proved that FOC outperforms its integer-order counterparts in terms of both noise reduction and signal information preservation. Therefore, further research work carried out in the thesis is to develop an efficient method for R-peak detection using fractional-order digital differentiator (FODD). The Riesz FODD is used (RFODD) as it has no phase delay in its response to accurately delineate the R-peak in ECG signal. The FOC method provides an extra degree of freedom which helps in optimizing the performance of the methods. RFODD method is analysed on ECG waveform by varying the fractional-order and optimum value is chosen. From the simulation studies conducted, it is demonstrated that the suggested technique can successfully identify the R-peak in various complex situation like changing QRS morphology, inverted T-wave, T-wave has more amplitude than R-peak,

etc. The proposed method is also compared to state-of-the-art method and it has outperformed them in terms of performance metrics.

After establishing an efficient method for R-peak detection using RFODD which eliminates various artifacts and preserves the signal information better than integer-order model, further research focuses on developing real-time classification method to classify real subject ECG beats. The virtual instrumentation method based on National Instruments LabVIEW platform is designed for acquiring real-time ECG data. Thus, a complete classification method is proposed which comprises data acquisition, pre-processing, feature extraction, and classification of ECG beats into normal (subjects who have never had any heart ailment history) and abnormal (subjects who have had heart ailment history) classes. The experimental studies have achieved excellent results for real-time ECG subjects. In this research, new and novel features are used based on coefficients of signal obtained after differentiation operation by RFODD and the Shannon energy of Fibonacci series signal generated. The adaptive k nearest neighbor (ADkNN) is explored for the classification.

Then, after performing classification on real subject ECG beats, the proposed method is extended on MIT-BIH-AD to make a system more robust and to include more classes of ECG beat. It is used to classify ECG beats of MIT-BIH-AD into six categories. In the proposed method, both intra and inter-patient criteria for classification are used. The suggested work also performs well for the minority class of MIT-BIH-AD.

7.2 Future Work

A few tracks for future research out of the present work are outlined below:

- The preliminary results obtained by the proposed HSCW filter approach for R-peak detection in ECG signals are promising and hence, it can be concluded that the suggested method may be useful for several signal filtering, image enhancement, and biomedical signal/image processing applications. Consequently, the possible application of HSCW filter approach for diverse signal and image application and its detailed comparison analysis with existing techniques are still subject to further future exploration.

- The performance of the proposed method based on RFODD in real-time is dependent on the fractional-order selection, which is chosen based upon the conducted experimental studies. As a result, the future work can be extended to an adaptive fractional-order so that fractional-order is adjusted according to the dynamic gradient aspects of real-time ECG signals and images.
- Furthermore, the proposed method for classification of real-time ECG subjects can be extended into more number of classes.

REFERENCES

[1] R. M. Rangayyan, *Biomedical signal analysis*. John Wiley & Sons, 2015.

[2] P. Sabherwal, M. Agrawal, L. Singh, "Automatic detection of the R peaks in single-lead ECG signal," *Circuits, Systems and Signal Processing*, vol.36, no**.** 11, pp. 4637–4652, 2017.

[3] R. E. Rushmer, *Cardiovascular Dynamics.* WB Saunders, Philadelphia, PA, 4th edition, 1976.

[4] M. V. G Miranda, I. P. V. Espinosa and M. J. F. Calero, "ECG signal features extraction," *IEEE Eucador Technical Chapters Meetings*, pp.1-6, 2016.

[5] E. Merdjanovska, E. and A. Rashkovska, "Comprehensive survey of computational ECG analysis: Databases, methods and applications," *Expert Systems with Applications*, vol. 203, 2022.

[6] E. J. D. S Luz, W.R Schwartz, G. Cámara-Chávez, G. and D. Menotti, "ECG-based heartbeat classification for arrhythmia detection: A survey," *Computer Methods and Programs in Biomedicine*, vol. 127, pp.144-164, 2016.

[7] T. K. Rawat, *Digital Signal Processing*, Oxford University Press India, 2015.

[8] K. M. M. Prabhu, *Window Functions and their Applications in Signal Processing*. CRC Press, Boca Raton, 2013.

[9] H. Wen, Z. Teng and S. Guo, "Triangular self-convolution window with desirable sidelobe behaviors for harmonic analysis of power system*," IEEE Transactions Instrumentation and Measuremen*t, vol. 59, no. 3, pp. 543–552, 2010.

[10] J. Wang, Y. Ye, Y. Gao, S. Qian and X. Gao, Fractional compound integral with application to ECG signal denoising. Circuits, Systems and Signal Processing, vol. 34, no**.** 6, pp. 1915–1930, 2015.

[11] B. T. Krishna, "Studies on fractional order differentiators and integrators: A survey," *Signal Processing*, vol. 91, no. 3, pp. 386-426, 2011.

[12] M. D. Ortigueira and J. T.Machado, "Fractional calculus applications in signals and systems," *Signal Processing*, vol. 86, no. 10, pp. 2503-2504, 2006.

[13] V. L. Roger, M. P. H Faha and M. B Turner, Heart Disease and Stroke Statistics: 2012 Update.Circulation, vol. 125, no. 1, 2012.

[14] C. Nayak, S. K. Saha, R. Kar and D. Mandal, "An efficient and robust digital fractional order differentiator based ECG pre-processor design for QRS detection," *IEEE Transactions on Biomedical Circuits and Systems*, vol. 13, no. 4, pp. 682-696, 2019.

[15] S. Kumar, K. Singh and R. Saxena, Analysis and design of non-recursive digital differentiators in fractional domain for signal processing applications, Doctoral dissertation 2014.

[16] R. Pachauri, R. Saxena, and S. N. Sharma, "Design of FIR filters with better performance using Z-window," *International Conference on Communications, Computing and Control Applications (CCCA)*, pp. 1-5, 2011.

[17] N. V. Thakor and Y. S. Zhu, "Application of adaptive filtering to ECG analysis: noise cancellation and arrhythmia detection," *IEEE Transactions on Biomedical Engineering*, vol. 38, no. 8, pp. 785-794, 1991.

[18] N. Razzaq, S. S. A. Sheikh, M. Salman and T. Zaidi, "An Intelligent Adaptive Filter for Elimination of Power Line Interference from High Resolution Electrocardiogram," *IEEE Access*, vol. 4, pp. 1676-1688, 2016.

[19] P. Phukpattaranont, "QRS detection algorithm based on the quadratic filter," *Expert Systems with Applications*, vol. 42, no. 11, pp. 4867-4877, 2015.

[20] R. Vullings, B. D. Vries and J. W. M. Bergmans, "An adaptive Kalman filter for ECG signal enhancement," *IEEE Transactions on Biomedical Engineering*, vol. 58, no. 4, pp. 1094–1103, 2011.

[21] F. H. Harris, "On the use of windows for harmonic analysis with the discrete Fourier transform," *IEEE Proceedings*, vol. 66, no. 1, pp. 51-83, 1978.

[22] I. S. Reljin, B. D. Reljin and V. D. Papic, "Extremely flat-top windows for harmonic analysis," *IEEE Transactions Instrumentation and Measurement*, vol 56, no. 3, pp. 1025–1041, 2007.

[23] I. Reljin and B. Reljin, "Signal processing by using new window functions generated by means of convolution," *Proceedings of 9th ISTET*, pp. 232–234, 1997.

[24] D. Xianzhong and R. Gretsch, "Quasi-synchronous sampling algorithm and its applications," *IEEE Transactions and Instrumentation and Measurement*, vol. 43, no. 2, pp. 204–209, 1994.

[25] J. Zhang, C. Liang and Y. Chen, "A new family of windows–convolution windows and their applications," *Science in China Series E Engineering and Material Science*, vol. 48, no. 4, pp. 468–481, 2005.

[26] B. T. Krishna and P. Chandrasekhar, "Reduction of sidelobe level using convolutional windows," *Proceedings of 1st International Conference in Emerging Technology Trends in Electronics, Communication and Networking (ET2ECN)*, pp. 1–5, 2012.

[27] P. Rai, O. V. S. R. Varaprasad and D. S. Sarma, "An overview of power harmonic analysis based on triangular self convolution window," *IEEE Conference on Power Systems*, pp. 1–5, 2016.

[28] L. Smital, M. Vítek, J. Kozumplík and I. Provazník, "Adaptive wavelet Wiener filtering of ECG signals," *IEEE Transactions on Biomedical Engineering*, vol. 60, no. 2, pp. 437–445, 2013.

[29] M. Merah, T. A. Abdelmalik and B. H. Larbi, "R-peaks detection based on stationary wavelet transform," *Computer Methods and Programs in Biomedicine*, vol. 121. no. 3, pp. 149–160, 2015.

[30] M. Rakshit and S. Das, "An efficient wavelet-based automated R-peaks detection method using Hilbert transform," *Biocybernetics and Biomedical Engineering*, vol. 37, no. 3, pp. 566–577, 2017.

[31] Z. Zidelmal, A. Amirou, M. Adnane and A. Belouchrani, "QRS detection based on wavelet coefficients," *Computer Methods and Programs in Biomedicine*, vol. 107, no. 3, pp. 490–496, 2012.

[32] E. Castillo, D. P. Morales, G. Botella, A. García, L. Parrilla and A. J. Palma, "Efficient wavelet-based ECG processing for single-lead FHR extraction," *Digital Signal Processing*, vol. 23, no. 6, pp.1897-1909, 2013.

[33] C. K. Jha and M. H. Kolekar, "Empirical mode decomposition and wavelet transform based ECG data compression scheme," *IRBM*, vol. 42, no. 1, pp.65-72, 2021.

[34] M. Arora, S. Bashani, K. K. Gupta and A. M. Mohammed, "Wavelet denoising: Comparative analysis and optimization using machine learning," *9th International Conference on Industrial and Information Systems (ICIIS)*, pp. 1-6, 2014.

[35] D. H. Chae, Y. F. Alem, S. Durrani and R. A. Kennedy, "Performance study of compressive sampling for ECG signal compression in noisy and varying sparsity acquisition," *IEEE International Conference on Acoustics, Speech and Signal Processing*, pp. 1306-1309, 2013.

[36] S. Ari, M. K. Das and A. Chacko, "ECG signal enhancement using S-transform," *Computers in Biology and Medicine*, vol. 43, no. 6, pp. 649–660, 2013.

[37] B. Biswal, "ECG signal analysis using modified S-transform," *Healthcare Technology Letters*, vol. 4, no. 2, pp. 68, 2017.

[38] M. K. Das and S. Ari, "Analysis of ECG signal denoising method based on S-transform," *IRBM,* vol. 34, no. 6, pp. 362–370, 2013.

[39] Z. Zidelmal, A. Amirou, D. Ould-Abdeslam, A. Moukadem and A. Dieterlen, "QRS detection using S-Transform and Shannon energy*," Computer Methods and Programs in Biomedicine,* vol. 116, no. 1, pp. 1–9, 2014.

[40] M. D. Ortigueira, "Fractional Calculus for Scientists and Engineers*," Lecture Notes in Electrical Engineering* (Springer, Berlin), pp. 84, 2011.

[41] I. Podlubny, "Geometric and physical interpretation of fractional integration and fractional differentiation," *Fractional Calculus and Applied Analysis*, vol. 5, no. 4, pp. 367–386, 2002.

[42] S. Kumar, R. Saxena and K. Singh, "Fractional Fourier transform and fractional-order calculus-based image edge detection," *Circuits, Systems, and Signal Processing*, vol. 36, no. 4, pp. 1493–1513 2017.

[43] Y. Pu, J. Zhou and X. Yuan, "Fractional differential mask: a fractional differential-based approach for multiscale texture enhancement," *IEEE Transactions on Image Processing*, vol. 19, no. 2, pp. 491–511, 2010.

[44] Y. Luo, Y. Q. Chen, H. S. Ahn and Y. Pi, "Fractional-order periodic adaptive learning compensation for state-dependent periodic disturbance," *IEEE Transactions on Control Systems Technology*, vol. 20, no. 2, pp. 465–472, 2012.

[45] S. Kumar and R. Saxena, "ϕFrMF: fractional Fourier matched filter," *Circuits, Systems, and Signal Processing*, vol. 37, no. 1, pp. 49–80, 2018.

[46] S. Kumar, K. Singh and R. Saxena, "Caputo-based fractional derivative in fractional Fourier transform domain," *IEEE Journal on Emerging and Selected Topics in Circuits and Systems*, vol. 3, no. 3, pp. 300–307, 2013.

[47] S. Kumar, K. Singh and R. Saxena, "Closed-form analytical expression of fractional order differentiation in fractional Fourier transform domain," *Circuits, Systems, and Signal Processing*, vol. 32, no. 4, pp. 1875–1889, 2013.

[48] Y. Ferdi, "Some applications of fractional order calculus to design digital filters for biomedical signal processing," *Journal of Mechanics in Medicine and Biology*, vol. 12, no. 2, 2012.

[49] Y. Ferdi, "Fractional order calculus-based filters for biomedical signal processing," *IEEE 1st Conference on Biomedical Engineering (MECBME),* pp. 73–76, 2011.

[50] Y. Ferdi, "Improved lowpass differentiator for physiological signal processing," *IEEE 7th International Symposium on Communication Systems Networks and Digital Signal Processing (CSNDSP)*, pp. 747–750, 2010.

[51] Y. Ferdi, J.P. Herbeuval, A. Charef and B. Boucheham, "R wave detection using

fractional digital differentiation," *ITBM-RBM*, vol. 24, pp. 273–280, 2013.

[52] M. Benmalek and A. Charef, "Digital fractional-order operators for *R*-wave detection in electrocardiogram signal," *IET Signal Processing*, vol. 3, no. 5, pp. 381–390, 2009.

[53] S. Jain, V. Bajaj and A. Kumar, "Riemann Liouvelle fractional integral based empirical mode decomposition for ECG denoising," *IEEE Journal of Biomedical and Health Informatics*, vol. 22, no. 4, pp. 1133–1139, 2018.

[54] J. Wang, Y. Ye, X. Pan and X. Gao, "Parallel-type fractional zero-phase filtering for ECG signal denoising," *Biomedical Signal Processing and Control*, vol. 18, pp. 36–41, 2015.

[55] C. C. Tseng and S. L. Lee, "Design of digital Riesz fractional-order differentiator," *Signal Processing*, vol. 102, pp. 32–45, 2014.

[56] M. Lascu and D. Lascu, "LabVIEW based biomedical signal acquisition and processing," *Proceedings of the 7th WSEAS International Conference on Signal, Speech and Image Processing*, pp. 38-43, 2007.

[57] A. K. Sharma and K. K. Kim, "Real-time ECG signal acquisition and processing using LabVIEW," *Journal of Sensor Science and Technology*, vol. 29, no. 3, pp. 162-171, 2020.

[58] S. Jain, S. Pathak and B. Kumar, "A robust design and analysis of analog front end for portable ECG acquisition system," *IEEE Region 10 Humanitarian Technology Conference (R10-HTC)*, pp. 1-5, 2016.

[59] O. P. Singh, D. Mekonnen and M. B. Malarvili, "LabVIEW based ECG patient monitoring system for cardiovascular patient using SMTP Technology," *Journal of Medical Engineering*, 2015.

[60] P. O. Bobbie, C Z Arif, H Chaudhari and S Pujari, "Electrocardiogram (EKG) Data Acquisition and Wireless transmission," *Proceedings of WSEAS International Conference on System Engineering*, pp. 1-7, 2004.

[61] F. El-Hamad and M. Baumert, "Comparison of single-lead and multi-lead ECG for QT variability assessment using autoregressive modelling," *Physiological Measurement*, vol. 43, pp. 105002, 2022.

[62] S. Dhande, "LabVIEW Based ECG Signal Acquisition and Analysis," *International Journal of Engineering Applied Sciences and Technology*," vol. 5, no. 9, pp. 2455-2143, 2021.

[63] D. Paul and R. A. Jaswal, **"**Comparison of Features Extraction and Parameters of Different ECG Signals Using LabVIEW," *International Research Journal of Engineering and Technology*, vol. 3, no. 7, 2016.

[64] A. M. A Zaidi, M. J. Ahmed and A. S. M. Bakibillah, "Feature extraction and

characterization of cardiovascular arrhythmia and normal sinus rhythm from ECG signals using LabVIEW," *IEEE International Conference on Imaging, Vision & Pattern Recognition*, pp. 1-6, 2017.

[65] C. Bhyri and A. M. N. Bhanu, "ECG Signal Based Heart Disease Detection System for Telemedicine Application Using LabVIEW," *International Journal of Research and Scientific Innovation*, vol. 4, no. 9, ISSN: 2321-2705, 2017.

[66] S. Shafi, S. Harish, S. Tej and P. Raj, "An efficient and low cost real time heart rate monitoring and alerting system using virtual instrumentation," *International Journal of Recent Technology and Engineering*, vol. 8, no. 1, pp. 325-328, 2019.

[67] A. Deshmukh and Y. Gandole, "ECG Feature Extraction Using NI LabVIEW Biomedical Workbench," *International Journal of Recent Scientific Research*, vol. 6, no. 8, pp. 5603-5607, 2015.

[68] A. N. Ay, M. Z. Yildiz and B Boru. "Real-time feature extraction of ECG signals using NI LabVIEW," *Sakarya University Journal of Science*, vol. 21, no. 4, pp. 576-583, 2017.

[69] S. M. Anwar, M. Gul, M. Majid and M. Alnowami, "Arrhythmia classification of ECG signals using hybrid features," *Computational and Mathematical Methods in Medicine*, vol. 2018, 2018.

[70] P. deChazal, M. O'Dwyer and R. B. Reilly, "Automatic classification of heartbeats using ECG morphology and heartbeat interval features," *IEEE Transactions on Biomedical Engineering*, vol. 51, no. 7, pp. 1196–1206, 2004.

[71] P. Laguna, R. Jan´e and P. Caminal, "Automatic detection of wave boundaries in multilead ECG signals: validation with the CSE database," *Computers and Biomedical Research*, vol. 27, no. 1, pp. 45–60, 1994.

[72] S. Sahoo, B. Kanungo, S. Behera and S. Sabut, "Multiresolution wavelet transform based feature extraction and ECG classification to detect cardiac abnormalities," *Measurement*, vol. 108, pp. 55–66, 2017.

[73] S. Yu and K. Chou, "Integration of independent component analysis and neural networks for ECG beat classification," *Expert Systems with Applications*, vol. 34, no. 4, pp. 2841–2846, 2008.

[74] M. Sarfraz, A. A. Khan and F.F. Li, "Using independent component analysis to obtain feature space for reliable ECG arrhythmia classification," *IEEE International Conference on Bioinformatics and Biomedicine*, pp. 62–67, 2014.

[75] U. Satija, B. Ramkumar and M. S. Manikandan, "A new automated signal quality-aware ECG beat classification method for unsupervised ECG diagnosis environments," *IEEE Sensors Journal*, vol. 19, no. 1, pp. 277-286, 2018.

[76] V. Vijean, G. R. Pavinthiran, Y. F. Chong, C. C. Lim, S. A. Awang, and H. Muthusamy, "False Arrhythmia Alarm Detection Through ECG Signals," *Proceedings of the International e-Conference on Intelligent Systems and Signal*

Processing, pp. 305-319, 2022.

[77] R. J. Martis, U. R. Acharya, and L. C. Min, "ECG beat classification using PCA, LDA, ICA and Discrete Wavelet Transform," *Biomedical Signal Processing and Control*, vol. 8, no. 5, pp. 437–448, 2013.

[78] M. K. Das and S. Ari, "ECG beats classification using mixture of features," *International Scholarly Research Notices*, pp. 1–12, 2014.

[79] K. N. Rajesh and R. Dhuli, "Classification of ECG Heartbeats using nonlinear Decomposition Methods and Support Vector Machine," *Computer Biology and Medicine*, vol. 87, pp. 271–284, 2017.

[80] V. N. Vapnik, "An overview of statistical learning theory," *IEEE Transactions on Neural Networks*, vol. 10, no. 5, pp. 988–999, 1999.

[81] V. Mond´ ejar-Guerra, J. Novo, J. Rouco, M.G. Penedo and M. Ortega, "Heartbeat classification fusing temporal and morphological information of ECGs via ensemble of classifiers," *Biomedical Signal Processing and Control*, vol. 47, pp. 41–48, 2019.

[82] F. Y. Abdalla, L. Wu, H. Ullah, G. Ren, A. Noor and Y. Zhao, "ECG arrhythmia classification using artificial intelligence and nonlinear and nonstationary decomposition," *Signal, Image and Video Processing*, vol. 13, no. 7, pp. 1283–1291, 2019.

[83] J. Chromik, L. Pirl, J. Beilharz, B. Arnrich and A. Polze, "Certainty in QRS detection with artificial neural networks," *Biomedical Signal Processing and Control*, vol. 68, pp.102628, 2021.

[84] M. Barni, P. Failla, R. Lazzeretti, A. R. Sadeghi and T. Schneider, "Privacy-preserving ECG classification with branching programs and neural networks," *IEEE Transactions on Information Forensics and Security*, vol. 6, no. 2, pp.452-468, 2011.

[85] R. Pandey, "Feedforward neural network for blind equalization with PSK signals," *Neural Computing & Applications*, vol. 14, no. 4, pp.290-298, 2005.

[86] H. D. M. Ribeiro, A. Arnold, J. P. Howard, M. J. Shun-Shin, Y. Zhang, D. P. Francis, P. B. Lim, Z. Whinnett and M. Zolgharni, "ECG-based real-time arrhythmia monitoring using quantized deep neural networks: A feasibility study," *Computers in Biology and Medicine*, vol. 143, pp.105249, 2022.

[87] A. Jain and I. Sreedevi, "An Improved Deep Neural Network for Multiclass Classification of Diabetic Foot Thermogram" *2nd International Conference on Intelligent Technologies (CONIT)*, pp. 1-6, 2022.

[88] L. Xiaolin, B. Cardiff, B. and D. John, "A 1d convolutional neural network for heartbeat classification from single lead ECG," *27th IEEE International Conference on Electronics, Circuits and Systems (ICECS)*, pp. 1-2, 2020.

[89] K. Gupta, A. Bhavsar and A. K. Sao, "Detection of mitotic HEp-2 cell images: role of feature representation and classification framework under class skew," *Medical & Biological Engineering & Computing*, vol. 60, no. 8, pp. 2405-2421, 2022.

[90] M. Holmer, J. P. Martínez, E. Gil, F. Sandberg, B. Olde and L. Sörnmo, "Detection of ventricular premature beats based on the pressure signals of a hemodialysis machine," *Medical Engineering & Physics*, vol. 51, pp.49-55, 2018.

[91] G. Garcia, G. Moreira, D. Menotti and E. Luz, "Inter-patient ECG heartbeat classification with temporal VCG optimized by PSO," *Scientific Reports*, vol. 7, no. 1, article no. 10543, 2017.

[92] A. K. Sangaiah, M. Arumugam and G. B. Bian, "An intelligent learning approach for improving ECG signal classification and arrhythmia analysis," *Artificial Intelligence in Medicine*, vol. 103, 2020.

[93] P. Pławiak, "Novel methodology of cardiac health recognition based on ECG signals and evolutionary-neural system," *Expert Systems with Applications*, vol. 92, pp. 334-349, 2018.

[94] G. Bortolan, and W. Pedrycz, "An interactive framework for an analysis of ECG signals," *Artificial Intelligence in Medicine*, vol. 24, no. 2, pp.109-132, 2002.

[95] T. Li and M. Zhou, "ECG classification using wavelet packet entropy and random forests," *Entropy*, vol. 18, no. 8, 2016.

[96] A. H. Nuttall, "Some windows with very good sidelobe behavior," *IEEE Transactions on Acoustics, Speech and Signal Processing*, vol. 29, no. 1, pp. 84-91 1981.

[97] S. Kumar, K. Singh and R. Saxena, "Analysis of Dirichlet and Generalized "Hamming" window functions in the fractional Fourier transform domains," *Signal Processing*, vol. 91, no. 3, pp. 600-606, 2011.

[98] J. G. Proakis, and D. G. Manolakis, *Digital Signal Processing*, 3rd edition, 1996.

[99] P. Sabherwal, M. Agrawal and L. Singh, "Automatic Detection of the R Peaks in Single-Lead ECG Signal," *Circuits, Systems, and Signal Processing*, vol. 36, no. 11, pp. 4637-4652, 2017.

[100] S. Z. Mahmoodabadi, A. Ahmadian and M. D. Abolhasani, "ECG feature extraction using Daubechies wavelets," *Proceedings of the 5th International conference on Visualization, Imaging and Image Processing*, pp. 343-348, 2005.

[101] C. Meyer, J. F. Gavela and M. Harris, "Combining algorithms in automatic detection of QRS complexes in ECG signals," *IEEE Transactions on Information Technology in Biomedicine*, vol. 10, no. 3, pp. 468-475, 2006.

[102] T. Sharma and K. K. Sharma, "QRS complex detection in ECG signals using locally adaptive weighted total variation denoising," *Computers in Biology and Medicine*, vol. 87, pp. 187-199, 2017.

[103] J. Pan and W. J. Tompkins, "A real-time QRS detection algorithm," *IEEE Transactions on Biomedical Engineering*, vol. 32, no. 3, pp. 230-236, 1985.

[104] MIT-BIH Arrhythmia Database (Massachusetts Institute of Technology, Biomedical Engineering Center, Cambridge, MA, 1992), www.physionet.org/physiobank

[105] G. B. Moody and R. G. Mark, "The impact of the MIT-BIH arrhythmia database," *IEEE Engineering in Medicine and Biology Magazine*, vol. 20, no. 3, pp. 45-50, 2001.

[106] P. Sabherwal, L. Singh and M. Agrawal, "Aiding the Detection of QRS Complex in ECG Signals by Detecting S Peaks Independently," *Cardiovascular Engineering and Technology*, vol. 9, no. 3, pp. 469-481, 2018.

[107] N. Djermanova, M. Marinov, B. Ganev, S. Tabakov and G. Nikolov, "LabVIEW based ECG signal acquisition and analysis," *XXV International Scientific Conference Electronics (ET)*, pp. 1-4, 2016.

[108] A. Bajaj and S. Kumar, "QRS complex detection using fractional Stockwell transform and fractional Stockwell Shannon energy," *Biomedical Signal Processing and Control*, vol. 54, 2019.

[109] K. N. Rajesh and R. Dhuli, "Classification of ECG Heartbeats using nonlinear Decomposition Methods and Support Vector Machine," *Computers in Biology and Medicine*, vol. 87, pp. 271-284, 2017.

[110] I. Saini, D. Singh and A. Khosla, "QRS detection using K-Nearest Neighbor algorithm (KNN) and evaluation on standard ECG databases," *Journal of Advanced Research*, vol. 4, no. 4, pp. 331-344, 2013.

[111] M. Kibanov, M. Becker, J. Mueller, M. Atzmueller, A. Hotho and G. Stumme, "Adaptive kNN using expected accuracy for classification of geo-spatial data," *Proceedings of the 33rd Annual ACM Symposium on Applied Computing*, pp. 857-865, 2018.

[112] A. Onyezewe, A. F. Kana, F. B. Abdullahi, and A. O. Abdulsalami, "An Enhanced Adaptive k-Nearest Neighbor Classifier Using Simulated Annealing," *International Journal of Intelligent Systems & Applications*, vol. 13, no. 1, pp. 34-44, 2013.

[113] D. Kaya, M. Türk and T. Kaya, "Wavelet-based analysis method for heart rate detection of ECG signal using LabVIEW," *40th International Convention on Information and Communication Technology, Electronics and Microelectronics (MIPRO)*, pp. 314-317, 2017.

[114] S. Jain and P. Kumar, "LABVIEW based expert system for detection of heart abnormalities," *International Conference on Advances in Electrical Engineering (ICAEE),* pp. 1-5, 2014.

[115] Q. Qin, J. Li, L. Zhang, Y. Yue, Y. and C. Liu, "Combining low-dimensional wavelet features and support vector machine for arrhythmia beat classification," *Scientific reports*, vol. 7, no. 1, pp.1-12, 2017.

[116] A. Singhal, P. Singh, B. Fatimah, and R. B. Pachori, "An efficient removal of power-line interference and baseline wander from ECG signals by employing Fourier decomposition technique," *Biomedical Signal Processing and Control*, vol. 57, 2020.

[117] M. Ingale, R. Cordeiro, S. Thentu, Y. Park, and N. Karimian, "ECG biometric authentication: A comparative analysis," *IEEE Access*, vol. 8, pp.117853-117866, 2020.

[118] U. R. Acharya, S. L. Oh, Y. Hagiwara, J. H. Tan, M. Adam, A. Gertych and R. S. Tan, A Deep Convolutional Neural Network Model to Classify Heartbeats, *Computers in Biology and Medicine*, vol. 89, pp. 389–396, 2017.

[119] S. N. Yu and K. T. Chou, "Integration of Independent Component Analysis and Neural Networks for ECG Beat Classification," *Expert Systems with Applications*, vol. 34, no. 4, pp. 2841–2846, 2008.

[120] C. C. Lin and C. M. Yang, "Heartbeat classification using normalized RR intervals and morphological features," *Mathematical Problems in Engineering*, vol. 2014, article ID. 712474, 2014.

[121] W. Lu, H. Hou and J. Chu, "Feature fusion for imbalanced ECG data analysis," *Biomedical Signal Processing and Control*, vol. 41, pp. 152-160, 2018.

[122] C. K. Jha and M. H. Kolekar, "Cardiac arrhythmia classification using tunable Q-wavelet transform based features and support vector machine classifier," *Biomedical Signal Processing and Control*, vol. 59, 2020.

[123] Y. Kutlu and D. Kuntalp, "A Multi-stage automatic arrhythmia recognition and classification system," *Computer in Biology and Medicine*, vol. 41, no. 1, pp. 37–45, 2011.

[124] Y. Kutlu and D. Kuntalp, "Feature extraction for ECG heartbeats using higher order statistics of WPD coefficients," *Computer Methods and Programs in Biomedicine*, vol. 105, no. 3, pp. 257–267, 2012.

LIST OF PUBLICATIONS

International Journals

1. **A. Kaur**, A. Agarwal, R. Agarwal, and S. Kumar, "A novel approach to ECG R-peak detection." *Arabian Journal for Science and Engineering*, vol.44, no. 8, pp. 6679-6691, 2019. DOI:10.1007/s13369-018-3557-8 (SCI Journal, **Impact Factor: 2.9, Publisher: Springer**)

2. **A. Kaur**, S. Kumar, A. Agarwal, and R. Agarwal, "An efficient R-peak detection using Riesz fractional-order digital differentiator." *Circuits, Systems, and Signal Processing*, vol. 39, no.4, pp.1965-1987, 2020. DOI:10.1007/s00034-019-01238-3 (SCI Journal, **Impact Factor: 2.3, Publisher: Springer**)

3. **A. Kaur**, S. Kumar, R. Agarwal, and A. Agarwal, "Intra and inter-patient arrhythmia classification using feature fusion with novel feature set based on fractional-order and fibonacci series." *Biomedical Signal Processing and Control*, vol. 72, 2022, DOI:10.1016/j.bspc.2021.103365 (SCI Journal, **Impact Factor: 5.1, Publisher: Elsevier**)

4. **A. Kaur**, S. Kumar, and A. Agarwal, and R. Agarwal, "A Complete Method for real-time ECG Subjects Acquisition and classification using LabVIEW and MATLAB," *Arabian Journal for Science and Engineering* (SCI Journal, **Impact Factor: 2.9, Publisher: Springer under review**)

Conferences

1. **A. Kaur**, S. Kumar, A. Agarwal, and R. Agarwal, "R-peak Detection and Classification Using Adaptive Boosting Algorithm," presented at *13th Western Pacific Conference on Acoustics (WESPAC), CSIR-NPL, New Delhi, India, Nov 11-15, 2018.*

2. **A. Kaur**, S. Kumar, A. Agarwal, and R. Agarwal, "A Novel Thresholding Technique for R-peak Detection in ECG," *2nd International Conference on Advanced Computational and Communications Paradigms, (ICACCP), SMIT, Sikkim, India, Feb 25-28th* 2019.

3. **A. Kaur**, S. Kumar, R. Agarwal, A. Agarwal, “ECG Classification using K-Nearest Neighbor and Naïve Bayes Models,” Admet 2020, CSIR-NPL, New Delhi, India, Jan, 2020.

4. **A. Kaur**, S. Kumar, A. Agarwal, R. Agarwal, “R-peak Detection in Real-time ECG Signal,” Admet 2022, CSIR-NPL, New Delhi, India, 2022.